# LABORATORY SIMULATION OF METAL DUSTING CORROSION

by

Andrew James Laburn Vaughan

A dissertation submitted to the Faculty of Engineering, University of Cape Town in partial fulfillment of the degree of Master of Science in Engineering

Department of Materials Engineering
University of Cape Town
December 1997

# Abstract

A laboratory carburising furnace in which metal dusting conditions are simulated has been designed and constructed. This furnace has been used to simulate and study the metal dusting corrosion of four iron-based alloys viz. 9Cr Mo 45 steel, Incoloy 800H, AISI 310 stainless steel and Chromanite - an experimental high-nitrogen Cr-Mn stainless steel (HNSS).

Tests conducted on the carburising furnace show that the rig is capable of heating a flowing gas environment to temperatures of 800°C in the horizontal ceramic tube. The design allows the testing of up to thirty-six test specimens in a constant-temperature test zone. Systems for the safe heating and disposal of gases such as hydrogen and carbon monoxide have been incorporated into the design.

Four twenty-four hour exposures were performed on specimens of the CrMo steel and as received samples of AISI 310. This was followed by a series of seven week-long exposures of Incoloy 800H, AISI 310 and the high nitrogen stainless steel (HNSS). These specimens were tested in an annealed and polished condition in order to increase their susceptibility to metal dusting. In a third test series, specimens of these three alloys were tested in an annealed and abraded condition in order to determine the effect of grain size and surface roughness on metal dusting resistance.

Exposures of the CrMo specimens resulted in general metal loss and massive carbon deposition after the first exposure of 24 hours. Filamentous carbon deposits containing metal particles showed that metal dusting corrosion of the specimens had taken place. The as received AISI 310 specimens showed no signs of metal dusting attack over the same exposure time. This was attributed to a protective surface chromia layer that prevented carburisation of the specimens.

During the second test series, specimens of Incoloy 800H in the sensitised condition showed a high susceptibility to metal dusting. Carburisation of the matrix carburisation was accompanied by large carbon protrusions growing from the specimens' surfaces. Large pits were observed on the specimens after five weeks. Sensitised AISI 310 specimens also showed signs of metal dusting but at a slower rate. The difference in performance between these two alloys was attributed to the difference in alloying contents, notably chromium, nickel and silicon. The HNSS specimens showed a high resistance to carburisation, carbon deposition and metal loss during the first six weeks. Small amounts of carbon deposition and pitting were observed after the seventh exposure. The good resistance to metal dusting of this alloy was attributed to its alloying contents, which included chromium, manganese, sulphur and nitrogen.

The results of the third test series showed that resistance to metal dusting was significantly improved by increasing the surface roughness and decreasing the grain size of the specimens.

A new alloy, Fe-25Cr-12Ni-9Mn-4.5Al-2Si-0.5N is proposed for fabrication and exposure to metal dusting environments to evaluate its suitability for use in industrial applications. It is also recommended that further work be carried out in evaluating the effect of increasing the nitrogen, chromium and manganese contents of the Fe-18Cr-9Mn-0.5N alloy that performed well in this project. Investigations into the effect of aluminising and nitriding components should also be carried out.

# Acknowledgements

I would like to express my appreciation and thanks for the assistance I have received in the course of this work, in particular from:

Professor A. Ball, my supervisor, for his guidance, wisdom and encouragement;

Mira Topic for her tireless assistance with the electron microscope;

the technical staff of the Department of Materials Engineering - Glen Newins, Mike Dietz, Nick Dreze, Reggie Hendriks and Dave Dean for their valuable assistance in the construction of the experimental apparatus and preparation of specimens;

Bernard Greeves and James Petersen for their help with the photographs presented in this thesis;

the staff and students of the Department of Materials Engineering for their friendship, advice and encouragement.

The financial assistance and technical help provided by Mossgas is gratefully acknowledged.

Dedicated to my family - Stuart, Brenda, Catherine and Jonathan Vaughan. Thank-you for your constant love, encouragement and guidance over the years and throughout this project.

**The fear of the Lord is the beginning of knowledge,**

**(Proverbs 1:7)**

# Table of Contents

# 1. Introduction

## 1.1 Background to the research

Metal dusting corrosion is a term used to describe the catastrophic carburisation of engineering alloys. The phenomenon of metal dusting was reported by Camp, Phillips and Gross in the mid nineteen-fifties. A few years later, similar occurrences of this new corrosion process were described by Prange [1], Eberle and Wylie [2] and Hoyt and Caughey [3]. Since then, metal dusting caused considerable damage in many industrial carburising atmospheres over the last four decades [4][5][6]. This corrosion process occurs when components are saturated with carbon by a highly carburising atmosphere. Carbon deposition on the surface of the components leads to a breakdown of the carburised matrix into a "dust" of metal particles and carbon. This corrosion product is removed by the flowing gas, revealing pitting and general wastage of the alloy [7].

High temperature austenitic stainless steels that are commonly used in high temperature environments have shown varied susceptibilities to metal dusting. Alloys that have performed well in some environments have been heavily attacked in others. The unpredictability of the occurrence of metal dusting is well documented in the literature. The composition of the carburising environment and process conditions such as temperature and pressure have a strong influence on whether or not metal dusting will occur [8].

The failure of reactor components in a secondary methane reformer at Mossgas due to metal dusting was recently reported by Holland *et al.*[6]. Disintegration of a burner liner resulted in the perforation of the reformer walls. Downstream components such as a waste heat boiler tube sheet also exhibited damage due to metal dusting.

A surprising feature was the sharp contrast in the susceptibilities of two high temperature superalloys used in the burner liner. Components made from the nickel-based Inconel 600 were heavily attacked while those made from iron-based Incoloy 800 were affected only to a small degree. This is in contrast to the poor performance of Incoloy 800 in other industrial environments [9]. Various attempts at using protective coatings and other alloys have met with some success. However, a long-term solution to the problem of metal dusting in the Mossgas environment has yet to be found.

To facilitate this process, it was decided to initiate a research project on metal dusting at the University of Cape Town. Simulation of metal dusting in a laboratory environment would enable the evaluation of particular solutions to the problem. Examples of these are coatings, environmental changes and alloying additions. The research presented in this thesis forms the first part of this project.

## 1.2 Scope and limitations of the research

The scope of this project encompasses the design and construction of a metal dusting simulation rig and the exposure of selected alloys to a metal dusting environment. A series of alloy exposures was initially done to verify the reliability with which metal dusting conditions could be simulated. This was followed by longer exposures of high temperature alloys.

The aim of these exposures was primarily to establish the effectiveness of the rig in simulating metal dusting of alloys currently used in industrial environments. To this purpose, four alloys were selected for testing. These were AISI 310 stainless steel, Incoloy 800H, a CrMo steel - BS 1501-621 - and an austenitic high nitrogen stainless steel Fe-18Cr-9Mn-0.5N also known as Chromanite.

The results of these exposures were used to compare the performances of these alloys in metal dusting environments. Analysis of the samples was done by recording mass changes and by using scanning electron and optical microscopy. These results were then compared with those described in the literature on metal dusting and conclusions were drawn.

# 2. Literature Review

A review of the literature pertaining to metal dusting is set out in the following chapter. Aspects of carburisation considered relevant to the process of metal dusting are discussed. This is followed by a brief review of industrial experiences of metal dusting, a short history of the research that has been conducted into the problem and a description of the currently accepted mechanism of metal dusting. Lastly, the effects of variables controlling resistance to metal dusting are discussed.

## 2.1 Carburisation of iron-based alloys

### 2.1.1 Introduction

The process of carburisation - in which carbon enters and diffuses through a metal matrix - can have both positive and negative effects on the performance of an alloy. For example, carburisation of some steels is used to increase the surface hardness for improved wear resistance. Carbon is introduced into the alloy at an elevated temperature from a solid, liquid or gaseous carbon source. This results in an increased carbon concentration in the surface regions of the component. When the material is quenched a transformation to martensite takes place near the surface. The high hardness of this phase, together with residual compressive stresses, improves the component's resistance to wear and fatigue while maintaining a high toughness [10].

In some situations the carburising environment is strong enough to supersaturate the component with carbon. This can result in the eventual degradation of the matrix due to excessive carbide precipitation and decomposition. Such carburising environments are found in many industrial applications and particularly in petrochemical industries [5]. Typical temperatures at which carburisation occurs are usually between 450 and

1000 °C. Carburising atmospheres contain a variety of hydrocarbon gases such as CO, $H_2$ and $CH_4$ [5]. At these temperatures and compositions the gas environments have carbon activities that are higher than the carbon activity of components such as furnace tubes, reactor linings, heat exchanger tubes and tube sheets [5]. The high carbon activity results in carbon diffusion into the alloy matrix and the precipitation of carbides along grain boundaries and within grains. Continued growth of these carbides leads to the formation of a network of brittle intergranular carbides surrounded by an alloy-depleted matrix. Failure of carburised components occurs by embrittlement or loss in creep strength at high temperatures [11]. Highly carburising environments may also lead to the phenomenon of metal dusting [7].

There are three main processes involved in the carburising of metals by gaseous environments [11]. These are:

- carbon deposition on the alloy surface
- diffusion of the carbon into the surface regions of the alloy
- the formation of carbides due to the reaction of the dissolved carbon with active elements in the alloy such as chromium and iron

A fourth process, that of carbon deposition on the surface of the alloy, occurs particularly during the catastrophic carburisation process of metal dusting [12]. These four processes are discussed in each of the following sections.

### 2.1.2 Carbon transfer to the metal surface

Four main surface reactions have been identified as being the most active in introducing carbon to the alloy surface from the carburising atmosphere [13][14]. These are:

$$2CO \Leftrightarrow CO_2 + C \quad (1)$$

$$H_2 + CO \Leftrightarrow H_2O + C \quad (2)$$

$$CH_4 \Leftrightarrow C + 2H_2 \quad (3)$$

$$M + CO \Leftrightarrow C + MO \quad (4)$$

where M represents any suitably reactive metallic element, e.g. Fe.

Hochman [12] and Richardson [8] assumed that equation (1), the Boudouard reaction, was the most active in depositing carbon into the surface of the metal. Grabke, however based his work on reaction (2), since the kinetics of this reaction are faster than the other three in some metal dusting environments [15].

Each reaction has an associated temperature-dependent equilibrium constant (k) and carbon activity ($a_c$). In general, carburisation of an alloy will take place [5] if

$$(a_c)_{\text{environment}} > (a_c)_{\text{alloy.}}$$

In environments where reaction (2) is the dominant reaction, the carbon activity can be calculated from:

$$\Delta G^{\circ} = -RT \ln\left(\frac{a_c \cdot P_{H_2O}}{P_{CO} \cdot P_{H_2}}\right) \qquad (5a)$$

or

$$a_c = e^{-\Delta G/RT}\left(\frac{P_{CO} \cdot P_{H_2}}{P_{H_2O}}\right) \qquad (5b)$$

where: $\Delta G^{\circ}$ is the standard free energy of formation for the reaction
R is the molar gas constant
T is the temperature of the environment
$P_{CO}, P_{H_2}, P_{H_2O}$ are the partial pressures of carbon-monoxide, hydrogen and steam in the mixture.

This equation can be used to plot the carbon activities of the carburising environments as a function of the $\frac{P_{CO} \cdot P_{H_2}}{P_{H_2O}}$ ratio for various temperatures. Such a plot has been constructed by Lai [5] and is shown in Figure 2-1. It is evident that the carbon activity increases as temperature decreases for a fixed gas composition. It must be remembered that these plots are valid for equilibrium mixtures only. In many industrial environments the large flow velocities of the gas streams mean that the carburising reactions do not have sufficient time to come to equilibrium. In this case these plots are used on the basis of the inlet gas composition and allow a reasonable estimate of the carbon activity at a specific location to be made [5].

It is not as simple to calculate the carbon activity in an alloy [5]. For plain carbon steels, it is assumed that the steel is in equilibrium with cementite ($Fe_3C$) and the carbon activity is found from:

$$\Delta G^\circ = -RT\ln\left(\frac{a_{Fe_3C}}{a_c \cdot a_{Fe}^3}\right) \qquad (6)$$

where $a_{Fe_3C}$ and $a_{Fe}$ are assumed to be unity

i.e. $$\Delta G^\circ = -RT\ln\left(\frac{1}{a_c}\right)$$

or $$a_c = e^{\Delta G^\circ / RT} \qquad (7)$$

This function has been superimposed on the diagram in Figure 2-1. Carbon activities for Fe-18Cr-8Ni alloys have been determined by Natesan and Kassner [16] and are also included in Figure 2-1 along with the carbon activity levels of a 2.25Cr 1Mo steel.

Plots such as these are useful in predicting whether carburisation of the alloy will occur or not. The carbon activity of the environment can be found from the y-axis of the graph for a given temperature and $\frac{P_{CO} \cdot P_{H_2}}{P_{H_2O}}$ ratio. This value is then compared with the carbon activity for the relevant alloy at the same temperature.

Carburising environments such as those in which metal dusting occurs, that have carbon activities in excess of unity have a strong tendency to transfer carbon to an alloy surface. In these situations, rapid carburisation and eventually supersaturation of the alloy with carbon will take place [17].

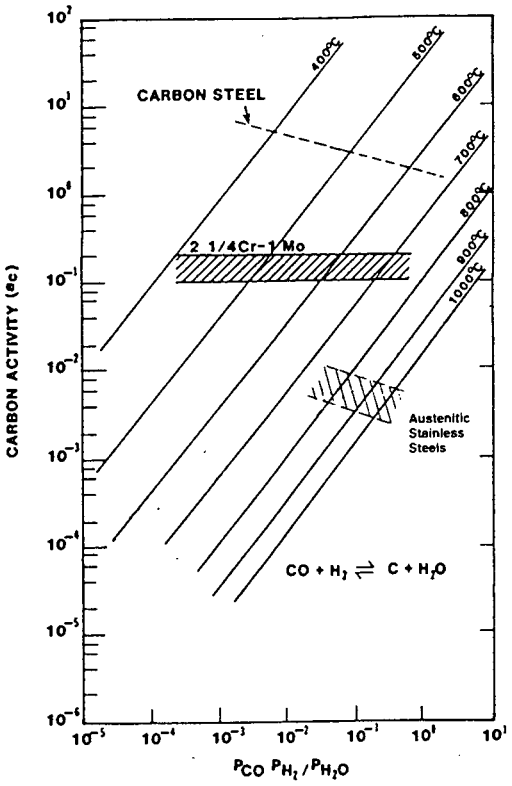


Fig. 4.1 Carbon activity of an environment based on the reaction $CO + H_2 = C + H_2O$ compared to carbon steel ($a_c$ in equilibrium with $Fe_3C$) and 2.25Cr-1Mo and austenitic stainless steels (both measured $a_c$)

**Figure 2-1 Carbon activities as a function of temperature for the reaction $H_2$+CO⇔$H_2O$+C as well as carbon activities of some alloys. For a specific environmental temperature and $\frac{P_{CO} \cdot P_{H_2}}{P_{H_2O}}$ ratio, the carbon activity of the environment can be found by reading off the right hand axis. This value is then compared with the carbon activity for a specific alloy at the same temperature (after Lai [5]).**

**Growth of carbon deposits on the alloy surface**

Carbon transfer from a carburising atmosphere to an alloy can also lead to the formation of bulk carbon deposits on the alloy surface. Carbon growths that result from interactions between hydrocarbon gases and metals have a complex structure [18]. Three forms of carbon growth that can occur are amorphous, filamentous and graphitic platelets. The deposition of carbon in filamentous form is of particular interest with regard to metal dusting corrosion and has been frequently observed in industrial and laboratory environments [12][8][19].

A number of mechanisms for the nucleation and growth of carbon filaments have been proposed. Kock, De Bokx, Boellaard, Klop and Geus [20] have found that a high carbide content is a prerequisite for the formation of carbon filaments. Decomposition of these carbides produces metal and smaller carbide particles, which then act as catalysts for the decomposition of a hydrocarbon gas.

Carbon atoms resulting from this decomposition diffuse through the metal or carbide particle to the face nearest the support surface [21][22] (Figure 2-2). The carbon is then deposited from solution at the base of the particle. As this process continues, the metal particle is lifted from the surface. An outer skin of carbon on the filament is formed by the surface diffusion of carbon around the particle. Growth of the filament stops when the metal particle is covered by carbon, preventing further decomposition of the hydrocarbon gas [18]. The effect of filamentous carbon growth is thus the gradual removal of metal from the substrate [23].

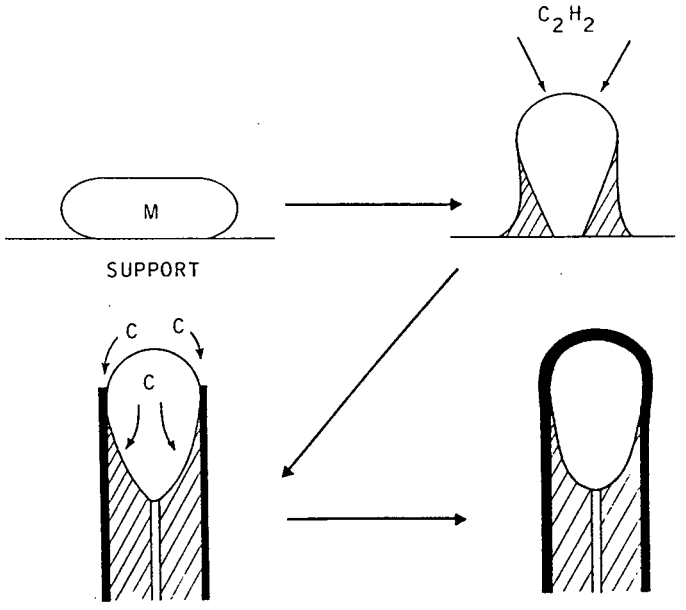


**Figure 2-2 Schematic of the proposed mechanism of carbon filament formation. A metal particle on the alloy surface (a) catalyses a carbon decomposition reaction leading to the deposition of carbon into the particle. The dissolved carbon diffuses through the particle and is deposited at the base of the particle as solid carbon (b). As this process continues, the particle is lifted away from the surface of the alloy. Diffusion of carbon around the surface of the particle forms a skin of carbon around the outside of the filament (c). Eventually the entire surface of the particle is covered with carbon and the filament ceases to grow (d) (after Baker *et al.* [18]).**

### 2.1.3 Carbon diffusion

The steady-state diffusion of interstitial atoms such as carbon and nitrogen in iron is governed by Fick's first law of diffusion. This states that the rate of flow of diffusing atoms is dependent on the difference in concentration of the diffusing element, the diffusivity in the matrix and the cross-sectional area through which the flow occurs [24].

Expressed in mathematical form:

$$\frac{\partial m}{\partial t} = -D \cdot A \cdot \frac{\partial c}{\partial x} \qquad (8)$$

where: $\frac{\partial m}{\partial t}$ is the rate of diffusion

D is the diffusivity in the matrix

$\frac{\partial c}{\partial x}$ is the concentration gradient through the material.

The diffusivity is dependent on a number of factors such as temperature, lattice structure, alloy composition and the concentration and size of the diffusing atoms [11][24]. An example of the effect of the structure of the crystal lattice on diffusion is the high rate of diffusion along grain boundaries and dislocations [24]. These are regions in which the atoms are less closely packed than the undisturbed crystal. This results in a lower activation enthalpy for the diffusion of solute atoms and thus a higher rate of mass flow of the diffusing element.

However, the higher diffusivity in these regions is often offset by the small volume available for diffusion. Where the average grain boundary width is small, most of the flow of atoms will still be through the grains themselves. Most of the flow of diffusing atoms will take place along grain boundaries only if:

D(b)/D(l) >> average grain diameter/average grain boundary width

where D(b) and D(l) are the grain boundary and lattice diffusivities [24].

Empirical work done by Grabke and Schnaas [25] on the carburisation of the iron-based superalloy Incoloy 800 shows that the progression of carburisation is almost completely dependent on the diffusion of carbon in the base metal. The rate of carburisation can be approximately described by the parabolic expression:

$$\xi = \sqrt{2k't} \qquad (9)$$

where $\xi$ = depth of the carburised zone

t = elapsed time

and $k'$ is given by

$$k' = \frac{\varepsilon \cdot D_c \cdot C_c}{\upsilon \cdot C_M} \qquad (10)$$

where $D_c$, $C_c$ = Carbon diffusivity and solubility of carbon in the iron/nickel matrix at the surface after carbide precipitation has taken place

$C_M$ = Concentration of the main carbide-forming elements i.e. mainly the concentration of chromium

$\upsilon$ = Average stoichiometric ratio C/M of the MC carbides

$\varepsilon$ = Factor accounting for the blockage of diffusion by carbide particles

There is therefore scope for the control of carbon diffusion through the careful selection of alloying elements, which affect the solubility and diffusivity of carbon in the matrix. Examples of these are nickel and silicon. This will be discussed in more depth in section 2.3 on resistance to carburisation and metal dusting.

### 2.1.4 Carbide formation

**Carbide formation in low-alloy steels**

In low alloy steels increased carbon levels from carburisation can result in the precipitation of iron carbides along grain boundaries. The most stable carbide is cementite ($Fe_3C$) [26]. Other, less stable carbides from the ξ-phase $Fe_4C$ to the ε-phase $Fe_2C$, can also form [5]. Precipitation of meta-stable cementite at the surface of iron foils in gaseous environments with carbon activities higher than one has been observed by Hochman [27] and Grabke [17] (Figure 2-3).

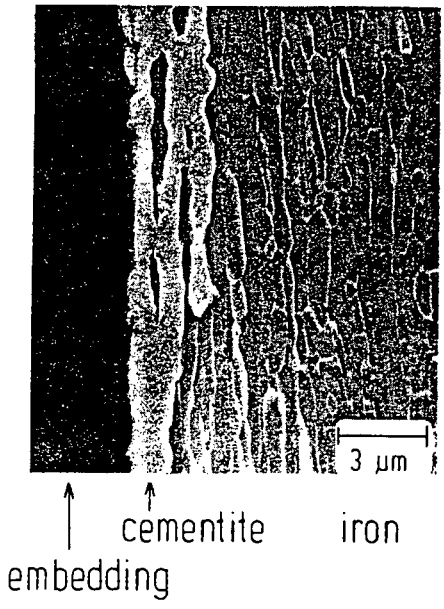


**Figure 2-3 SEM micrograph showing a cementite layer at the surface of an iron foil after exposure in a CO-$H_2$-$H_2O$ atmosphere at 475 °C (after Grabke [17]).**

**Carbide formation in high-temperature alloys**

Carburisation of alloys containing higher levels of chromium, such as austenitic stainless steels, can result in the formation of stable, predominantly chromium carbides of the form $M_{23}C_6$, $M_7C_3$ and $M_3C_2$ [5], which may also contain varying amounts of iron and nickel [25].

Stability diagrams of the Cr-C-O system, such as the one shown in Figure 2-4, are useful for determining the stable oxide and carbide phases for a given atmospheric oxygen partial pressure and alloy carbon activity [28]. The diagram predicts the precipitation of $Cr_3C_2$ at regions of the alloy, usually close to the surface, in which the carbon activity is near to unity. As the carbon activity decreases further into the alloy, precipitation of first $Cr_7C_3$ and then $Cr_{23}C_6$ carbides will be favoured.

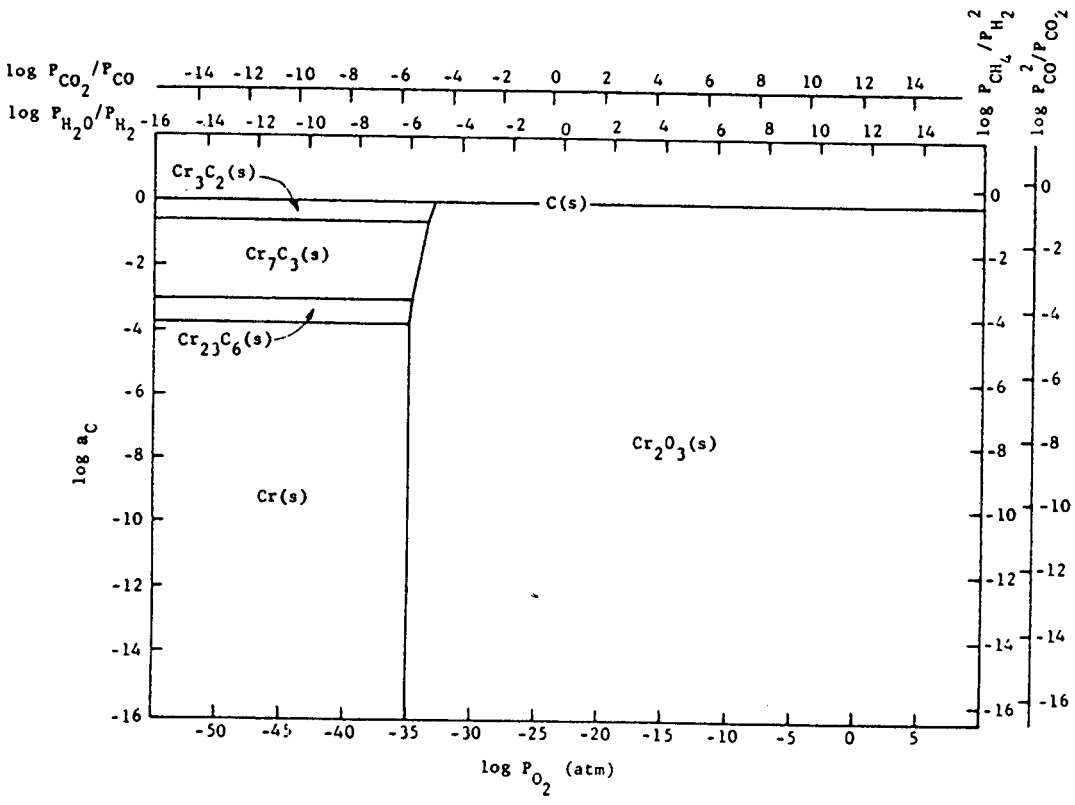


**Figure 2-4 Stability diagram of chromium carbides and oxides at 620 °C (after Hemmings *et al.* [28]).**

This progression was observed in part by Schnaas and Grabke, who studied the carburisation of various Fe-Cr-Ni alloys in $CH_4/H_2$ mixtures with a carbon activity of unity in the temperature range 800-1100 °C [25]. Their results revealed the presence of two zones of carbide precipitation. $M_7C_3$ (M = Cr, Fe and Ni) carbides were formed near the surface and $M_{23}C_6$ occurred further into the alloy (Figure 2-5). They did not report observing $Cr_3C_2$ carbides near the surface.


**Figure 2-5 Precipitation of $M_7C_3$ carbides near the surface and $M_{23}C_6$ carbides below in a Fe-20Cr-32Ni alloy after exposure to a $CH_4$-$H_2$ mixture at 800 °C (after Schnaas *et al.* [25]).**

Stable $M_7C_3$ and $M_{23}C_6$ carbides resulting from the carburisation of high alloy steels, such as a 13% Cr steel (Alloy 410) and a Fe-27Cr-32Ni alloy, were also observed by Grabke [17]. These carbides, which precipitated at relatively low temperatures of around 500 - 600 °C, were fine and were observed after etching as a dark fringe around pits caused by metal dusting attack (Figure 2-6).

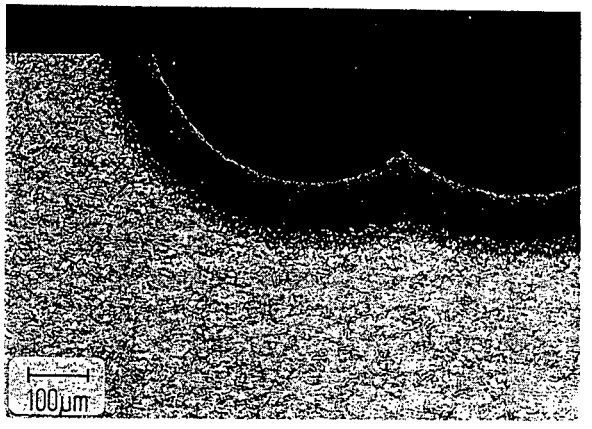


**Figure 2-6 Carburised region surrounding pits caused by metal dusting on alloy AISI 410 exposed for 6 days at 600 °C in a flowing CO-$H_2$-$H_2O$ atmosphere (after Grabke [17]).**

Harrison, Norton, Derricott and Marriot [29] observed $M_7C_3$-type carbides at the surface of a 25Cr-21Ni steel (alloy HK40) after carburisation at 1000 °C. These carbides contained about 56% (by weight) Cr and 42% Fe, giving a composition of approximately $Cr_4Fe_3C_3$.

Carburisation exposures of Fe-18Cr and Fe-18Cr-8Ni at 600 °C conducted by Nolan, Banks and Lister [13] again revealed the precipitation of mostly $M_7C_3$-type carbides with a Cr/Fe ratio of about 2. These carbides precipitated on either sides of some grain boundaries (Figure 2-7). Demel and Degisher [30] found that the Cr/Fe ratio of nucleated carbides depended on the size of the particles. Small particles less than 0.5 µm contained more than 99% chromium. Iron was added to these particles as they grew until about 10% iron was present in particles between 2 µm and 5 µm.

Superalloys such as Incoloy 800 contain carbide-forming elements such as Ti, Nb, Ta, Mo and W [5]. Titanium and niobium are particularly strong carbide formers and nucleate preferentially to chromium carbides [31].

**Precipitation of chromium carbo-nitrides**

The effect of nitrogen as a carbide former during the carburisation of Cr-Fe-Ni alloys was observed by Demel *et al.* [30]. Plate-like $Cr_2(CN)$ precipitates nucleated within the grains of a Fe-15Cr-50Ni alloy as carburisation progressed. These carbo-nitrides nucleated preferentially to the normal $M_{23}C_6$ grain boundary carbides. As the carburisation concentration in the alloy increased, the nitrogen in the carbides was replaced by carbon. Briant, Mulford and Hall [32] found that nitrogen retards the precipitation and growth of chromium carbides at the grain boundaries by nucleating preferentially as $Cr_2N$ nitrides. These were observed by Kikutchi, Masanori and Choi [33] and are shown in Figure 2-8. This effect is strengthened by manganese and molybdenum, which stabilise nitrogen at the grain boundaries.


**Figure 2-7 $M_7C_3$ precipitates on either side of a grain boundary. Alloy is Fe-18Cr carburised at 600 °C for 1500 hours in a $CO_2$-CO mixture (after Nolan *et al.* [13]).**

In gaseous environments with carbon activities exceeding unity, the unstable carbide $M_3C$ (M=Fe, Ni) has been observed to form once the chromium in the alloy has been

tied up in chromium carbides. This intermediate carbide then decomposes into a product of metal particles and carbon in the process of metal dusting [34].

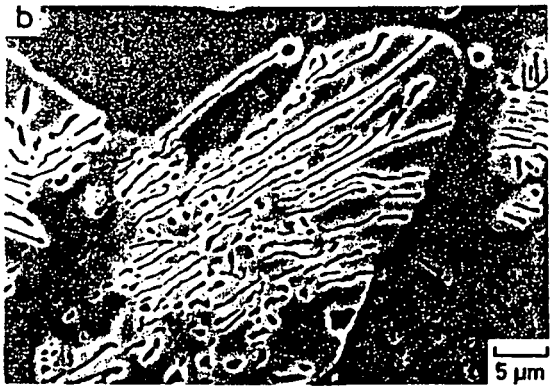


**Figure 2-8 $Cr_2N$ precipitates in a 25Cr-20Ni-0.59N steel aged at 800 °C for 48 hours (after Kikutchi *et al.* [33]).**

# 2.2 Metal dusting of low and high alloy steels

## 2.2.1 Introduction

Metal dusting is a unique form of carburisation-induced corrosion that differs from the ordinary degradation of alloys by carburisation. During carburisation the inward diffusion of carbon results in the precipitation of carbides such as $M_7C_3$ and $M_{23}C_6$ which leads to embrittlement of the matrix and loss of oxidation resistance [11]. Metal dusting corrosion, while usually accompanied by carburisation, requires an atmosphere with a carbon activity greater than one so that carbon deposition as graphite can occur. This results in the degradation of the alloy into a dust-like reaction product of metal particles, carbides, oxides and carbon [5][8][12][19].

## 2.2.2 Industrial experiences of metal dusting

Metal dusting has been experienced in many environments containing hydrocarbon gases over the last four decades. In particular, coal-conversion and methane reforming plants have reported corrosion of reactor components due to metal dusting. A few of these cases are discussed in this section. Attention is given to the nature of the gas environments and the affected alloys.

One of the earliest reported occurrences of metal dusting was investigated by Prange at the Phillips Petroleum Company in 1959 [1]. An "elusive" problem had manifested itself in catalyst tubes in which butane was dehydrogenated to butene over a chromia-alumina catalyst. Prange noticed that for some alloys used as the tube material, a "red oxide dust" covered the catalyst and caused plugging of the tube from carbon build-up.

Among the alloys that showed high susceptibility to this problem were pure iron and nickel, high-silicon cast iron (Duriron), 9Cr-1.4Mo steel and Cr/Ni steels with less than 20% Cr. Alloys that performed well generally had more than 24% Cr. A 18Cr-12Ni-2.5Si steel showed good resistance, as did a 30Cr-65Co-4W alloy. After further laboratory and plant exposures, it was decided to use the more expensive 310 stainless steel as the catalyst tube material due to its good resistance to "oxide dust" formation.

Other features of this corrosion problem were a black scale containing graphite, $Fe_3O_4$ and nickel, as well as grain boundary carburisation and highly localised regions of carburisation of the inside of AISI 302 tubes [1].

In 1958 an "unusual type of deterioration" that did not "appear to fit the generally accepted corrosion mechanism by chemical attack or erosion by particles" [3] was noticed on AISI 310 tubes after 3000 hours of service in a coal conversion plant. The affected tubes were situated in a secondary preheater downstream of a methane reformer. The feed gas passing through the tubes consisted mainly of $H_2$, CO, $CH_4$ and $H_2O$ at a temperature of 650 °C. Examinations of the tubes revealed that they had suffered from sporadic carburisation leading to "severe" pitting on the inside surfaces. Metallographic examinations showed that carburisation of the alloy had occurred underneath the regions of metal loss. Components made from AISI 304 in similar conditions showed no signs of attack. No clear reason was evident for this difference in susceptibility.

Eberle and Wylie [2] reported metal wastage of components in a waste heat boiler after three weeks of operation. The affected alloys were AISI 347 (Co-18Cr-8Ni) and 310 (Fe-25Cr-20Ni) which were exposed to a $CO/H_2$ mixture between 480 and 900°C.

Other reported instances of metal dusting include the perforation of alloy 800 tubes in a preheater for coal-gasifier gas in 1976 [35]. The gas consisted of $H_2$, CO and steam at temperatures between 540-870 °C. Metal dusting has also occurred in the downstream sections of coal gasifiers [36] and in a butane dehydrogenation system, where 12Cr and 18Cr-11Ni steels were attacked at 590 °C [1].

In 1994 metal dusting corrosion was experienced in waste heat boilers downstream of secondary methane reformers at the DSM ammonia plant in Geleen in The Netherlands [4]. During the period between June 1986 and September 1993 various components were attacked by metal dusting. These were a boiler liner (alloy 800H) as well as the high-nickel weld metal (alloy 82). A boiler cone made from alloy 800H, after experiencing metal wastage, was replaced by a cone made from Incoloy DS (Fe-37Ni-18Cr-2Si). After two years the entire cone wall thickness of 5 mm had been removed in some places. The outlet gas consisted mainly of $H_2$, $N_2$, CO, $CO_2$ and $H_2O$ at a temperature of 1013 °C and a pressure of 34.7 bar.

Metallographic examinations of a specimen of alloy 800H revealed the presence of well defined regions of carburisation in the alloy (Figure 2-9). At the surface a band of alloy super-saturation, covered by a metal dusting product of carbon and metal particles, was observed. Beneath this is a carburised zone in which carbide precipitation has occurred. This region extends into the base metal along the grain boundaries which have been carburised.

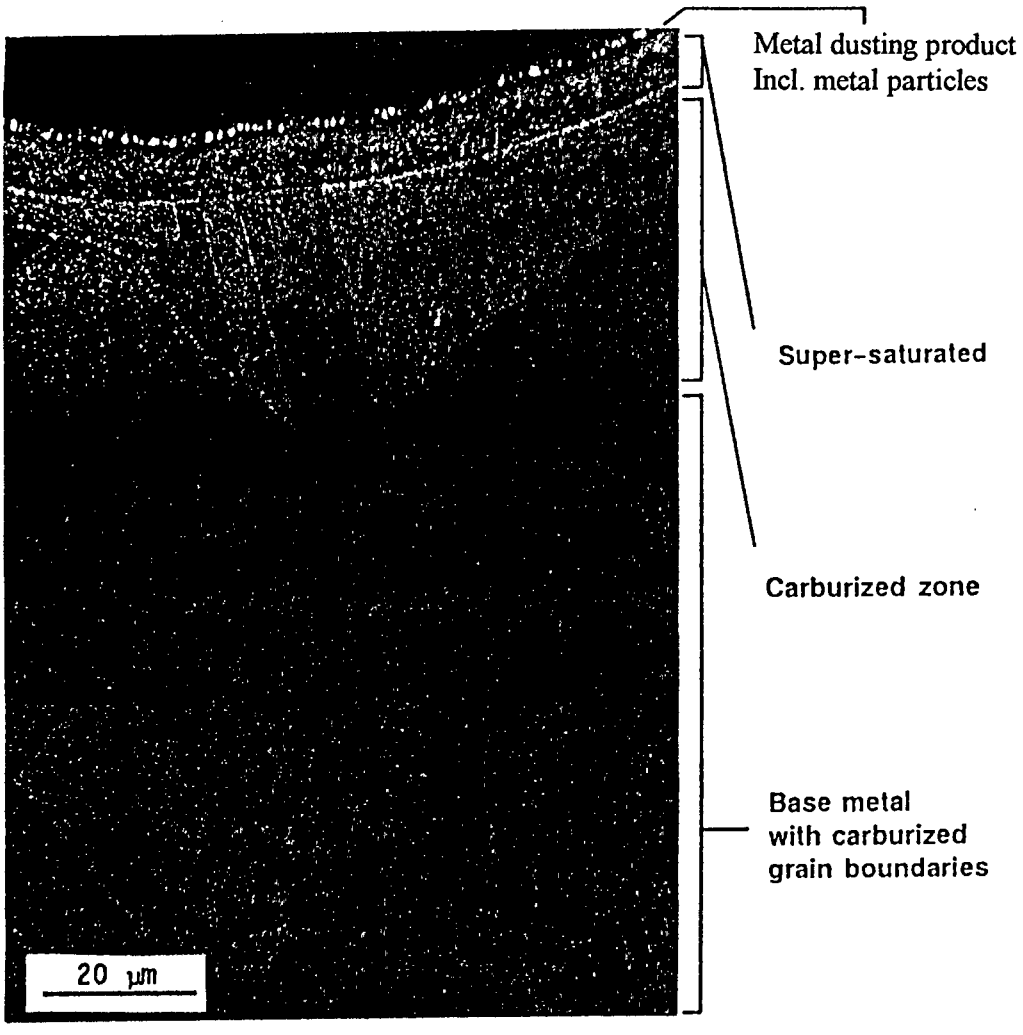


**Figure 2-9 Metal dusting attack of an alloy 800H specimen at 650 °C located at a boiler outlet downstream of a methane reformer. Etched with glyceregia (after Gommans *et al.* [4]).**

An exposure of nine alloys was conducted by inserting samples of the alloys in one of the waste heat boilers operating at approximately 900 °C and 35 bar pressure. The alloys tested were:

| | |
|---|---|
| AC66 | Fe-27Cr-32Ni-Nb + Cu |
| AISI 310 | Fe-25Cr-20Ni-2Si |
| 353MA | Fe-25Cr-35Ni-1.5Si + Cu/N |
| AISI 310S | Fe-25Cr-20Ni-.5Si |
| 253MA | Fe-21Cr-11Ni-1.5Si + Cu/N |
| Incoloy DS | Fe-18Cr-37Ni-2Si |
| SX | Fe-18Cr-20Ni-5Si + Cu/Mo |
| Saramet | Fe-18Cr-17Ni-5Si |
| 304 alonised steel | Fe-18Cr-8Ni (pack aluminised) |

After 16 000 hours most of the samples had either been carburised or attacked by metal dusting. Specifically, Incoloy 800H suffered heavy carburisation and carbide precipitation, and the 310 steels were attacked to a depth of 100 μm. The only material that performed well was the 304 stainless steel that had been aluminised. Interestingly, this alloy contains the lowest levels of chromium and nickel out of the alloys tested. The aluminising treatment had resulted in low carbon solubility and diffusivity in the aluminised layer, although carbides were observed at a depth of 200 μm. Metal dusting was not observed, and the aluminised layer had not been damaged.

Experiences of metal dusting in steam reforming plants have been reported by Richardson [8]. Components such as heat exchanger tubes, ferrules and reformer exit pipes have been corroded locally at a rate of more than 10 mm/year in some cases. An alloy that has performed well in some instances is the ferritic 446 stainless steel due to its good diffusivity for chromium. Components made from 304 stainless steel also showed good resistance in circumstances where alloy 800 had been heavily attacked.

An Inconel 600 burner liner in a secondary methane reformer at Mossgas in MosselBay disintegrated due to severe metal dusting damage in December 1993 [6]. Inspection of the failed part revealed "extreme metal thinning" at specific areas. Adjacent components made from Incoloy 800 showed relatively little damage. The difference in the performance of the two alloys was attributed to the difference in chromium content.

The results of an alloy exposure programme conducted in the secondary reformer environment showed that the most susceptible alloys were those of the highest nickel content: Inconel 600 (15Cr-72Ni-0.5Si) and Haynes 214 (16Cr-75Ni-4.5Al). AISI 310 stainless steel showed the least visible damage after the 6 month exposure.

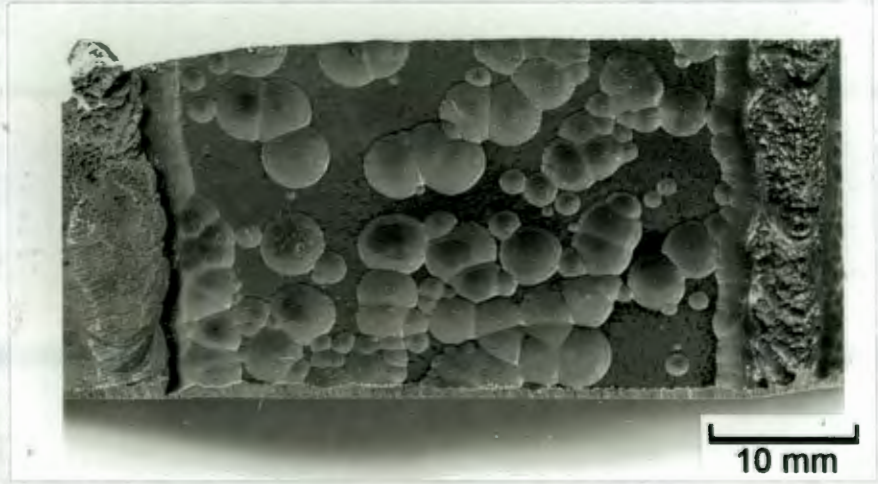


**Figure 2-10 Surface pitting on sections of a Mossgas methane reformer burner liner made from Inconel 600.**

Metal dusting has also occurred in a variety of other industries. An example is the heat treating industry [37]. Components of carburising furnaces such as fan housing assemblies and refractory anchors have been attacked. Alloys that have suffered metal dusting damage in these environments include stainless steels such as 310, as well as various nickel and iron-based alloys. The temperature at which metal dusting occurred was usually between 540 and 820 °C. Corrosion of these alloys was particularly active where the gas environment was stagnant. These conditions occurred, for example, in the small spaces found at the interface of refractory liners [5].

Investigations of these histories of metal dusting have led to few clear predictions regarding the exact conditions in which metal dusting will occur [5]. The occurrence of metal dusting is generally unpredictable [8], inconsistent and highly sensitive to changes in the temperature and process conditions [4]. The above summary also shows that alloys, which perform well in some environments, fail dramatically in others.

### 2.2.3 Research into metal dusting

Research into the new phenomenon of metal dusting began in the late nineteen-fifties in an attempt to explain the metal loss and carbon deposition that had been observed and with a view to designing or choosing an optimum alloy for metal dusting resistance. Over the past forty years this research has led to the development of a mechanism of metal dusting that is widely accepted today. This process is described briefly in this section.

Among the first researchers to investigate metal dusting was Prange [1] who was unable to define clearly the mechanism behind the metal deterioration, but suggested an unstable metal-containing vapour phase may be responsible for the removal of metal. However, later studies by Hochman [7], who used infra-red and mass spectrometry techniques to analyse the gas composition downstream of the reaction site, disproved this theory.

A possible mechanism for the corrosion was considered by Hoyt and Caughey [3] in which iron, nickel, cobalt and some metallic oxides catalyse the reaction

$$2CO \Leftrightarrow CO_2 + C.$$

This process results in carburisation of the alloy and carbide precipitation. Carbon from this reaction is also deposited as "threadlike filaments" which lift metallic particles and carbide nuclei away from the surface as they grow [38].

Further experiences of this type of corrosion led to the formation of a special NACE task group on metal dusting. A series of metallurgical investigations led to the proposal of a mechanism [26] in which carbon enters the steel matrix through the reactions

$$2CO \Leftrightarrow CO_2 + C$$

and

$$H_2 + CO \Leftrightarrow C + H_2O.$$

Carbon transferred to the alloy results in the precipitation of $Cr_{23}C_6$ carbides, first at grain boundaries, and then further into the grain. A large change in density and volume is caused by the growth of these carbides, with the result that the grains are either disintegrated or lifted from the steel, resulting in metal loss. This was observed more recently by Nolan *et al.* [13] whose exposures on 9Cr-1Mo steels at 480 °C showed that extensive carburisation of grain boundaries can lead to disintegration or removal of entire grains.

Hochman [12][27] and Ratliff [39] conducted studies of the mechanism of CO and $CH_4$ attack on iron, nickel and cobalt alloys. Specimens of these alloys suffered either general deterioration, or extensive pitting, or both. The extent of the deterioration depended largely on the type of alloy, the temperature and the dissociation characteristics of the gas.

On the basis of this work Hochman proposed a mechanism of metal dusting in pure iron in which the following processes occur:

- carbon monoxide is absorbed into the surface of the metal via the Boudouard reaction

$$2CO \Leftrightarrow CO_2 + C$$

- this carbon diffuses into the metal, which is the rate controlling process. The increase of the carbon concentration in solid solution is evidenced by the decoration of grain boundaries and dislocations.

- when saturation of the surface is reached cementite ($Fe_3C$), which is initially meta-stable, precipitates and grows until it becomes thermodynamically unstable. At this point the cementite breaks down into a mixture of iron and carbon.

- this stage is followed by the rapid breakdown of the supersaturated iron surface and deposition of filamentous carbon, which contains particles of iron, $Fe_3C$ and other iron carbides.

Recent research into metal dusting of low and high-alloy steels as well as nickel-based alloys has been done by Grabke, Krajak, Muller-Lorenz and Strauss [40]. The results from tests on low alloy steels such as 2 1/4Cr-1Mo and 1Cr-1/2Mo steels show that these materials are rapidly attacked by metal dusting. The specimens suffered general and uniform wastage, and a constant rate of metal loss was measured [41]. This metal loss rate was independent of the gas composition and varied only with temperature

and alloy composition. The steel with higher amounts of alloying elements did show a slightly lower wastage rate. The samples were covered by powdery carbon deposits [19] containing about 1-2% Fe [41]. This deposition was not affected by surface treatments such as abrading or polishing. The high susceptibility of these metals to metal dusting was attributed to the low chromium levels in the alloys which failed to form a protective oxide scale which was impervious to carbon penetration [19].

A nearly continuous cementite layer was observed at the surface of the specimens (Figure 2-11). This layer decomposed into metal particles and carbon at its outer face. At the same time, it grew inward as the carbon-saturated matrix precipitated into cementite. The thickness of the carbide layer remained constant at about 0.5 μm as it progressed into the alloy [17].

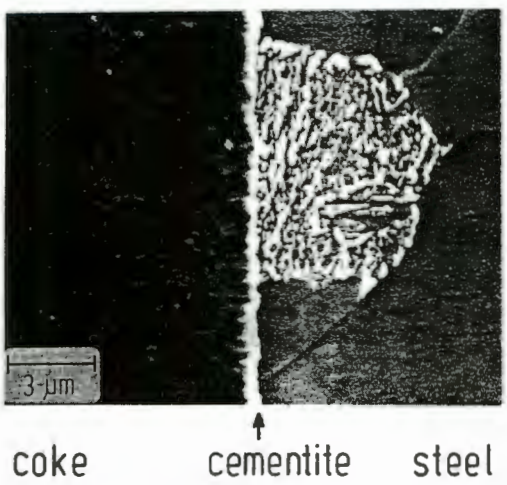


**Figure 2-11 Cementite layer at the surface of a 1Cr-Mo steel exposed to a flowing CO-H2-H2O mixture at 650 °C for 150 hours (after Grabke [17]).**

The results of TEM analysis of iron foils at various stages of the metal dusting process conducted by Pippel, Woltersdorf, Grabke and Strauss [42] allowed a more comprehensive description of the metal dusting mechanism for iron. These results confirmed the presence of an intermediate carbide $M_3C$. The processes of carbide breakdown, graphite nucleation and growth and coke formation were also observed. This model is now generally accepted and is summarised below. Figure 2-12 is an illustration of the process.

**Mechanism of metal dusting [42]**

1. Carburisation of the iron is initiated by carbon transfer from the gas atmosphere to the iron surface. Carbon is deposited either as graphite according to

$$CO + H_2 \Leftrightarrow C\ (graphite) + H_2O$$

or is dissolved into the metal by

$$CO + H_2 \Leftrightarrow C\ (dissolved\ in\ Fe) + H_2O.$$

This carbon diffuses into the metal which eventually becomes supersaturated (Figure 2-12 a).

2. The supersaturation of the matrix at the surface results in the formation of an inhomogeneous cementite layer according to the reaction

$$3Fe + C\ (dissolved) \Leftrightarrow Fe_3C.$$

At 650 °C this occurs at a carbon activity ($a_c$) of 1.3 [43]. The outer surface of the layer is in equilibrium with the high $a_c$ of the gas atmosphere. At its inner surface the layer grows into the metal as the supersaturated iron/carbon solution precipitates as cementite. At this stage the carbon can move through the cementite layer along grain boundaries, free spaces and, more slowly, through interstitial diffusion (Figure 2-12 b).

3. As the cementite layer increases in thickness the rate of carbon transfer through the layer slows until carbon is deposited on the surface as graphite. At the interface of the graphite and cementite the $a_c$ drops to a value of unity (Figure 2-12 c). This is below the value of 1.3 necessary for cementite stability, and so the cementite decomposes into metal particles and carbon according to:

$$Fe_3C \Leftrightarrow 3\,Fe + C.$$

4. The free carbon atoms resulting from this reaction attach themselves to the ends of the graphite planes already on the surface. The iron atoms diffuse through the graphite layer to the outer surface, where they agglomerate into particles of about 10 nanometers in diameter. These particles then act as catalysts for further carbon deposition (Figure 2-12 d).

The end result of this process is a mixture of metal particles and graphite on the surface of the metal. The deposition process slows as the particles are eventually covered with graphite, thereby reducing their catalytic effect. However, in the fast gas flows of industrial reactors, the deposit is continually swept away thus exposing fresh metal to further carburisation.

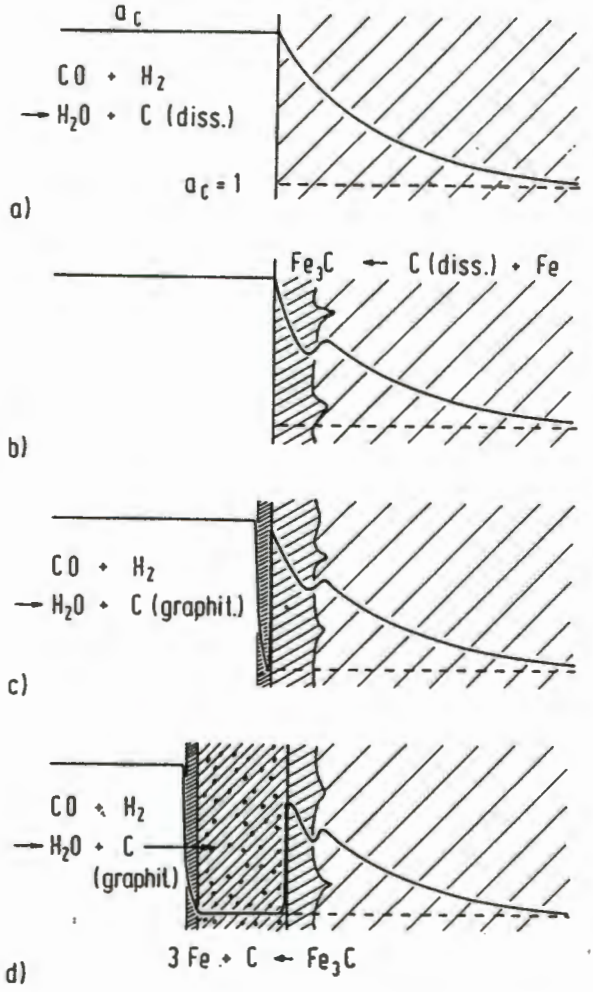


**Figure 2-12 Mechanism of metal dusting of iron. The process starts with carburisation of the alloy (a) leading to cementite formation (b). Graphite is deposited on the cementite layer (c), which causes the breakdown of the cementite into a mixture of metal particles and carbon (d) (after Grabke [17]).**

**Metal dusting of high alloy steels**

The appearance of metal dusting in highly alloyed chromium steels differs from the uniform thinning and deposition on iron and low-alloy steels [17]. Exposures on high alloy austenitic stainless steels have shown that the presence of a surface chromia layer, which is usually formed on these alloys, retards carburisation and, therefore, metal dusting [19]. Carbon penetration of the alloy is consequently limited to regions in which the oxide layer has failed. In these regions the matrix is carburised and stable chromium carbides are formed [43]. It is only when the chromium in the alloy is tied up in these carbides that the meta-stable $Fe_3C$ carbide forms, and metal loss begins [34].

The localised nature of metal dusting attack leads to the formation of small pits, which gradually widen to form large the large hemispherical pits shown in Figure 2-13 [17].


**Figure 2-13 Surface pitting of a Fe-25Cr-20Ni steel attacked by metal dusting in a CO-$H_2$ atmosphere at 500 °C (after Grabke [17]).**

## 2.3 Variables affecting resistance to metal dusting

This section describes some approaches to the control of metal dusting of uncoated alloys. These approaches involve the use of alloying elements and additions of inhibitors to the environment. Alloying elements can play an important role in reducing the concentration of carbon at the surface - the most effective means of preventing carburisation and hence metal dusting [11]. Alloying elements also affect metal dusting resistance by changing the solubility and diffusivity of carbon in the alloy. Increasing the concentration of carbide forming elements such as Cr, Ti and Nb is also beneficial [5][34]. Gaseous inhibitors such as steam and $H_2S$ have also proven effective in decreasing the severity of metal dusting attack [11][7]. The role of the main alloying elements used in austenitic stainless steels in retarding metal dusting is summarised in Table 2-1.

### 2.3.1 Control of metal dusting by reducing the surface carbon concentration

This approach to carburisation control is the most effective, since lowering the surface carbon concentration reduces the driving force for inward carbon diffusion [11]. This reduction is best achieved through the presence of a stable oxide layer, free from defects, on the surface of the metal [7][25][30]. Poisoning carbon deposition sites on the metal can also reduce the concentration of carbon at the surface
surface [11].

**Role of oxide layers in reducing surface carbon concentration**

The majority of the alloys used in carburisation environments are austenitic stainless steels with high levels of chromium [34]. Thus, the most influential oxide for the protection of these steels is chromia ($Cr_2O_3$). The effectiveness of this oxide was demonstrated by Grabke *et al.* [19], whose metal dusting exposures on high-alloy

austenitic stainless steels showed that the presence of a stable chromia layer greatly retarded the attack by metal dusting. Where metal dusting did occur, it was limited to localised regions where the oxide had broken down. Specimens of a Fe-20Cr-12Ni alloy that had their oxide layers removed by electropolishing suffered attack by metal dusting immediately, and large deposits of carbon were observed after one week of exposure. It was thus the ability of an alloy to form a protective chromia scale that was found to be the governing factor in the alloy's resistance to metal dusting.

The oxides of aluminium ($Al_2O_3$) and silicon ($SiO_2$) have also been found to be effective in reducing the surface concentration of carbon [44][45][46][47]. Hochman [12] demonstrated the effectiveness of $Al_2O_3$ by preoxidising specimens to which various amounts of aluminium had been added. The specimens showed good resistance to metal dusting attack, which was attributed to the formation of good thermodynamic surface barriers.

However, Richardson [8] argues that the rates of diffusion of oxide-forming elements is too low in the temperature range of 450-750 °C for the sufficiently rapid restoration of damage to the oxide layers. He concludes that none of the high-temperature alloys currently in use offers any obvious long-term solution to the problem of metal dusting.

**Formation and stability of oxide layers**

To be an effective barrier to the penetration of carbon, an oxide layer must resist breakdown during long exposures, which may involve creep of the material and cyclic environmental conditions [11]. Oxide stability is promoted by high levels of oxide-forming elements, fast diffusion paths that allow the transport of these elements to the surface, and a sufficiently high oxygen partial pressure in the gas atmosphere [47].

Concentration of alloying elements for oxide stability

In general the minimum concentration of oxide-forming elements such as chromium and aluminium for the establishment of a protective oxide is guided by four criteria [47]. The first is that the activity of the oxide-forming element at the metal/oxide interface must be of a level such that the oxide species formed is the most stable. Secondly, the oxide-forming element must be able to diffuse out of the alloy fast enough to maintain the growth of the oxide. This must occur without the concentration falling below the level required by the first criterion. The third criterion involves the progression from internal oxides, which are not protective, to the formation of a protective external oxide scale. The internal oxide blocks the inward diffusion of oxygen into the alloy and thus facilitates the formation of the external protective scale. For this to happen there must be a critical volume fraction of internally formed oxide present at the metal/oxide interface. A fourth criterion is that the rate of spreading of the protective oxide scale must be fast enough to prevent the formation of more rapidly growing, non-protective oxides on exposed surfaces of the alloy.

Experimentally, Grabke [19] found that ferritic steels with a chromium content of 18-28% showed good resistance to metal dusting due to protective oxide layers. Steels with a lower Cr content (12-13%) were resistant for a few weeks but their long-term resistance was dependent on the temperature of the environment.

According to Hochman [12], resistance to metal dusting of iron alloys is increased if the chromium and silicon contents follow the relation

$$\%Cr + 2\times\%Si > 24\ \%.$$

These levels serve as a guide to maintaining stable oxide layers where some steam is present in the gas flow.

Steinkusch [48] found that the silicon levels of about 2 to 2.5% had the greatest effect in providing resistance to carburisation. This content is found in AISI 314 stainless steel, and has been credited with this alloy's good performance in some carburising conditions.

Lai [46] found that alloy 214 with 4.5 % aluminium performed consistently better than other alloys in carburisation tests where the oxygen potentials were kept below the value needed for $Cr_2O_3$ formation. The presence of an aluminium oxide layer $Al_2O_3$ was the reason given for the high resistance of this alloy.

Grabke *et al.*[43] conducted exposures of Fe-Mn alloys that showed that alloys containing more than about 5% Mn form a green protective MnO layer. This layer suppressed metal dusting for about 4 days in the test atmospheres.

Fast diffusion paths for oxide stability

It is essential that the overall diffusivity of oxide-forming elements is high enough to facilitate the repair of damage to the oxide layer. Defects in the oxide layer can arise during thermal cycling or mechanical straining of the base alloy [47]. The temperature range in which metal dusting occurs is generally unfavourable for diffusion of these elements [8]. A high density of "fast diffusion" paths along which elements such as chromium, silicon and aluminium can reach the surface is therefore necessary. Such paths are found mainly along grain boundaries and dislocations [24]. Ferritic lattices are also beneficial since the diffusivity is an order of magnitude higher than in austenitic lattices [34].

The effects of grain size and near-surface deformation are therefore important factors in an alloy's resistance to metal dusting. Grabke demonstrated this by annealing test specimens at 1000 °C to achieve large grain size and then electropolishing to remove any surface deformation. This treatment effectively reduces the density of fast diffusion paths to the surface. The specimens show a high susceptibility to metal dusting with carbon deposition occurring after only one week of exposure [19].

Specimens that are ground to 80-grit SiC paper show a higher resistance to carburisation due to the increased amount of near-surface deformation.

Small grains are also beneficial for $Cr_2O_3$ formation since this oxide nucleates preferentially at grain boundaries. Small grains therefore present a smaller area over which the oxide must then spread [47].

Richardson [8] mentions that nickel reduces the diffusion rate of chromium in the alloy and thus retards the rate at which a damaged area on the chromia scale can be regenerated. This would have the effect of increasing a high nickel alloy's susceptibility to metal dusting. High nickel alloys such as alloy 800 will therefore be the most susceptible to metal dusting.

Oxygen partial pressure of the gas environment

An important contributing factor to oxide formation and stability is a sufficiently high oxygen potential in the gas environment. A common source of oxygen in carburising environments is the dissociation of steam [5] according to

$$2H_2O \Leftrightarrow 2H_2 + O_2.$$

Consequently, steam content is important for oxide formation and carburisation resistance, and $H_2O/H_2$ ratios can be adjusted within limits to increase the partial pressure of oxygen [25].

This effect was demonstrated by Schnaas and Grabke [25]. In their work on alloy 800 in CO-$H_2O$-$H_2$ environments the $H_2O/H_2$ ratio was adjusted so that a chrome oxide layer could form on the surface of the alloy. The surface concentration of carbon was found to be negligible and no internal carburisation had occurred.

**Reducing surface carbon concentration by poisoning carbon deposition sites**

Prevention of carbon adsorption can be achieved by poisoning adsorption sites on the alloy surface [12]. Sulphur is an effective poisoning agent and acts by saturating carbon adsorption sites and carbide precipitation sites on the alloy surface [27]. Sulphur also replaces carbon in the $Fe_3C$ lattice, thereby making this carbide more stable. Addition of sulphur is usually done by introducing a small amount of $H_2S$ to the gas stream. The major disadvantage of this approach in some industrial situations is the negative effect of the $H_2S$ on downstream catalysts [8]. Sulphur may also be incorporated into the alloy [12].

## 2.3.2 Increasing metal dusting resistance by retarding the rate of carbon diffusion in the alloy

**Role of alloying elements on carbon diffusion and solubility**

Alloy compositions and structures can be adjusted to minimise the diffusion of carbon through the matrix in the event of oxide breakdown [11]. Silicon is thought to reduce the solubility and diffusivity of carbon in austenite [49][50]. Goldstein and Moren [51] found that, for low-alloy steels, solid solutions of chromium and silicon in low concentrations and nickel in high concentrations reduce carbon diffusivity, thereby slowing the rate of carburisation. Investigations by Schnaas and Grabke [25] on the diffusion of carbon in Fe-Ni alloys indicate that carbon diffusion is lowest in alloys with 80% Ni and that the slowest rates of carburisation occur at a Ni:Fe ratio of 4:1.

Demel *et al.* [30] observed a dependence of the nature and rate of carburisation on alloy composition in their experiments on Fe-Cr-Ni alloys. Low nickel alloys carburised mainly along grain boundaries and showed the highest effective carburisation rate.

Steel and Engel [52] also found nickel to be beneficial in reducing carburisation of Fe-Ni-Cr alloys. The role of chromium is dependent on the nickel contents. For alloys with 26 to 45 % Ni, an increased chromium content reduced carbon absorption slightly. When the nickel content was increased to between 46 and 70 %, carbon absorption increased with increasing chromium content.

### 2.3.3 Increasing resistance to metal dusting by increasing the concentration of carbide forming elements

By combining equations (9) and (10) in section 2.1.3 (p. 13), it can be seen that the rate of carburisation of alloy 800 can be described by the equation

$$\xi = \sqrt{2 \cdot \frac{\varepsilon D_c C_c}{\upsilon C_M} \cdot t} \qquad (11)$$

Hence the rate of progression of carburisation in the alloy is inversely proportional to the square root of the concentration of the carbide-forming elements ($C_M$). As already mentioned, the main carbide-forming element in austenitic stainless steels is chromium. Thus a high chromium content would help to slow the rate of carburisation. Alloys containing other carbide-formers such as Ti, Ta, Nb, Mo and W [5] should therefore show an improved resistance to carburisation and metal dusting. This would be due to a decreased rate of chromium depletion, leaving more Cr free to form a protective oxide layer.

The effect of nitrogen would seem to be beneficial, since this favours the precipitation of $Cr_2(CN)$ carbo-nitrides [30]. The activity of nitrogen is generally high enough to tie up the inward diffusing carbon in finely dispersed carbides, thus preventing grain boundary carburisation. This results in good carburisation resistance of the alloy. An additional benefit of $Cr_2(CN)$ formation is a reduced rate of chromium depletion since the precipitation of the more chromium-intensive $Cr_{23}C_6$ carbides is retarded. This increases metal dusting resistance, since metal dusting can only start once the

chromium is tied up by carburisation [34]. Briant *et al.* [32] demonstrated this effect by showing that nitrogen increases resistance to sensitisation in austenitic stainless steels.

### 2.3.4 Retarding metal loss by preventing carbide breakdown

It is possible that the alloying elements Cr and Mn will act to stabilise the intermediate $M_3C$ carbide. However, these elements tend to first form stable carbides such as $M_7C_3$ and $M_{23}C_6$. The alloy is thus depleted of these elements as carburisation proceeds. This effect will therefore have no long-term effect on an alloy's resistance to metal dusting [43].

| Alloying element | Effect on metal dusting resistance |
|---|---|
| **Iron** | • Forms metastable $Fe_3C$ carbide [42]<br>• substitutes for Cr in $M_7C_3$ and $M_{23}C_6$ carbides [30] |
| **Chromium** | • Forms protective $Cr_2O_3$ layer<br>• stabilises intermediate $M_3C$ carbide [43]<br>• reduces carbon diffusivity [51] |
| **Nickel** | • Reduces solubility and diffusivity of carbon and chromium in matrix [8]<br>• reduces carburisation in Fe-Cr-Ni alloys [52] |
| **Silicon** | • Forms oxide layer [47]<br>• reduces carbon diffusivity [51] |
| **Aluminium** | • Forms strong oxide layer [47] |
| **Sulphur** | • Poisons sites for carbon deposition. Effective as alloying element or as $H_2S$ addition to environment [27]<br>• stabilises $Fe_3C$ [27]. |
| **Nitrogen** | • Forms $Cr_2(CN)$ carbo-nitrides [30]<br>• prevents grain boundary carburisation and retards chromium depletion [32] |
| **Manganese** | • Stabilises intermediate $M_3C$ carbide [34]<br>• forms protective Mn0 layer [43] |
| **Ti, Nb, Mo, W** | • Strong carbide formers-retards chromium depletion [5]<br>• good oxide formers [47] |

**Table 2-1 Summary of the role of alloying elements in resistance to metal dusting.**

# 3. The design of the metal dusting simulation furnace

## 3.1 Design criteria and constraints

The simulation of metal dusting in a laboratory environment requires the use of a furnace in which the flowing test gases can be safely heated to the required temperature. At the beginning of this project, none of the furnaces in the Department of Materials Engineering was capable of meeting these requirements. It was therefore necessary to design and construct a suitable rig for the simulation of metal dusting. The following section describes the design process.

The criteria that guided the successful design of the metal dusting simulation rig are:

- the furnace must heat the flowing gases to a minimum temperature of 700 °C
- the furnace should operate at atmospheric pressure
- the test section must be large enough to accommodate at least 20 specimens
- the temperature in the test section must be continuously monitored
- the temperatures in the test section must be within 5 °C of the setpoint temperature
- the furnace must be able to run continuously for at least two weeks
- the test gas must have the composition 25% CO, 73% $H_2$, 2% $H_2O$.

Some of the constraints on the design of the rig are:

- the furnace must fit into the limited space of the room allocated to the project
- the room containing the rig must be equipped with an air-extraction system to prevent the build-up of dangerous gases
- the test gases must be safely transported through the furnace and then disposed of without danger of explosion or contamination of the surrounding environment

- the materials used for the furnace tube and specimen holder should be easily obtained and reasonable in cost
- the total period of construction of the furnace should not exceed one year.

The following aspects of the design, although not essential, are considered desirable for the ease of manufacture and operation of the furnace:

- the power supply to the heating element should be a 220 volt source from the mains supply
- where possible, components already available in the department should be used
- components of the rig that are not available should be made in the department's workshop.

## 3.2 The design philosophy

At an early stage of the design process three major challenges in the construction of the metal dusting simulation rig were identified. The first was the safe heating to 650 °C of the flammable and toxic gases - hydrogen and carbon monoxide. The second was to configure the heating element in such a way that a constant temperature test zone was established. The third challenge involved the design of a specimen holder capable of supporting a large number of specimens in the small space available.

These challenges were overcome in part by incorporating features of existing laboratory furnaces in the department, as well as those described in the literature pertaining to metal dusting simulation into the design of the rig. Other components that were necessary to solve these problems were developed and modified during the construction of the rig.

## 3.3 Description of the metal dusting simulation furnace

In this section the apparatus is described and the main performance characteristics listed. In addition, the thermodynamic characteristics of the test gas mixture at the test temperature are described. This is followed by a detailed description of the various systems that comprise the furnace.

In the final design pre-mixed simulation gas is passed through a ceramic tube in which it is heated to the test temperature of 650 °C. In the test section the gas passes over test specimens suspended in the furnace tube. The gas is then cooled, and exits through a ventilation system to the atmosphere.

Figure 3-1 shows a graphic representation of the furnace layout. A photographic description is shown in Figure 3-2. The main performance characteristics of the furnace are presented in Table 3-1. A comparison with the design criteria listed in section 3.1 shows that the final design meets or exceeds all of the requirements.

| | |
|---|---|
| Voltage source | 220 V |
| Maximum recorded temperature in test zone | 750 °C |
| Temperature gradient in test zone | 0.8 °C/10 mm |
| Operating pressure | 1 bar |
| Operating gas flow rate | 8.2 litres/hour |
| Maximum uninterrupted operating period | 3 weeks |
| Maximum number of specimens in test zone | 30 |

**Table 3-1 Specifications of the metal dusting furnace**

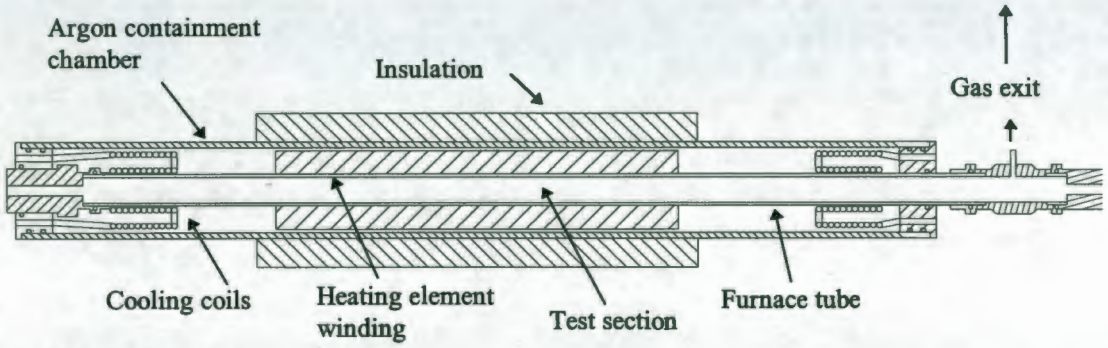


**Figure 3-1 Schematic diagram of the metal dusting simulation rig.**

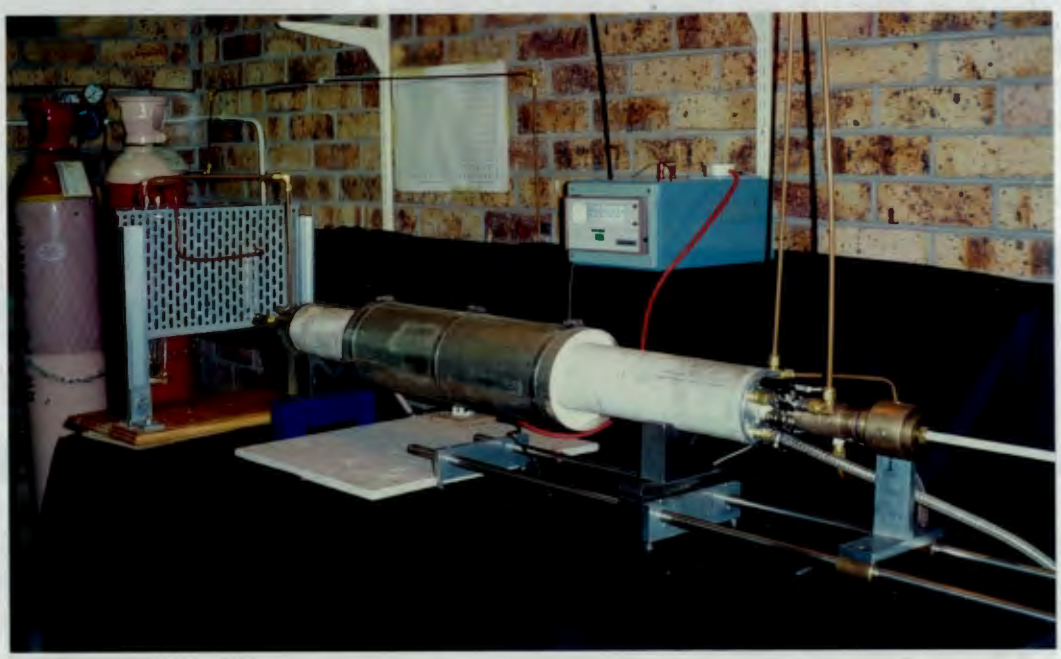

**Figure 3-2 The metal dusting simulation furnace.**

### 3.3.1 Detailed rig description: Analysis of main components

The following section describes the individual components of the simulation rig. Systems that form part of the design are:

- gas storage, transport and disposal
- flow control and humidification of the gas stream
- power supply and heating element
- temperature measurement and power control
- specimen support
- leak prevention and containment.

**System of gas storage, transport and disposal**

A flow diagram showing the path of gas flow through the furnace is shown in Figure 3-3.

A mixture of 76% $H_2$, 24% CO is supplied from a local gas company in 50-litre containers. A second gas cylinder contains argon, which is used for purging the furnace tube of oxygen. The gas is routed through a 1/4 inch cleaned, medical-grade copper pipe to the flow meter and humidifier. It then passes through the furnace tube. A vapour trap at the exit side of the furnace collects any excess water vapour before the gas is routed into an extraction tunnel that leads to the atmosphere.

Two gate valves allow the flow of gas to be shut off at any time. A three-way valve allows the gas to bypass the flow meter and humidifier and flow directly into the furnace tube. This is used when the furnace is being purged with argon and the humidifier is not required.

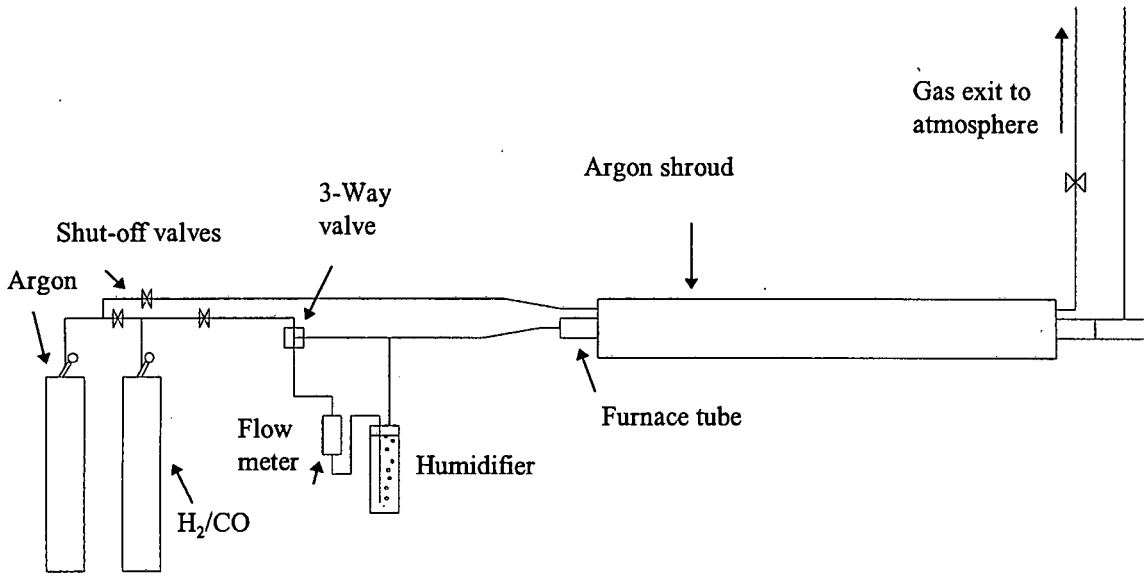


**Figure 3-3 Flow diagram of the test gas mixture.**

**Flow control and humidification of the gas stream**

The rate of gas flow through the furnace is controlled by a flow meter equipped with a fine metering valve. A flow rate of 8.2 l/hr is used for the tests. After passing through the flow meter the dry $H_2$/CO mixture is saturated with water vapour in a humidifier. The flow meter and humidifier are shown in Figure 3-4.

The humidifier consists of a perspex tube, 50 mm in diameter and 300 mm in height and filled with distilled water. The gas enters the water through a diffuser, which breaks the gas into small bubbles for faster transfer of water vapour to the gas. These design features ensure that the gas is saturated with water vapour. The water in the humidifier is held at a temperature of 20 °C ± 2 °C by a circulating water supply that surrounds the perspex tube. This water is routed from the cooling coils of the furnace into a container that surrounds the humidifier. Figure 3-5 shows a graph of saturation water vapour content vs. humidifier water temperature. It can be seen from this graph that a room temperature of 20 °C yields the required water vapour content of about 2%.

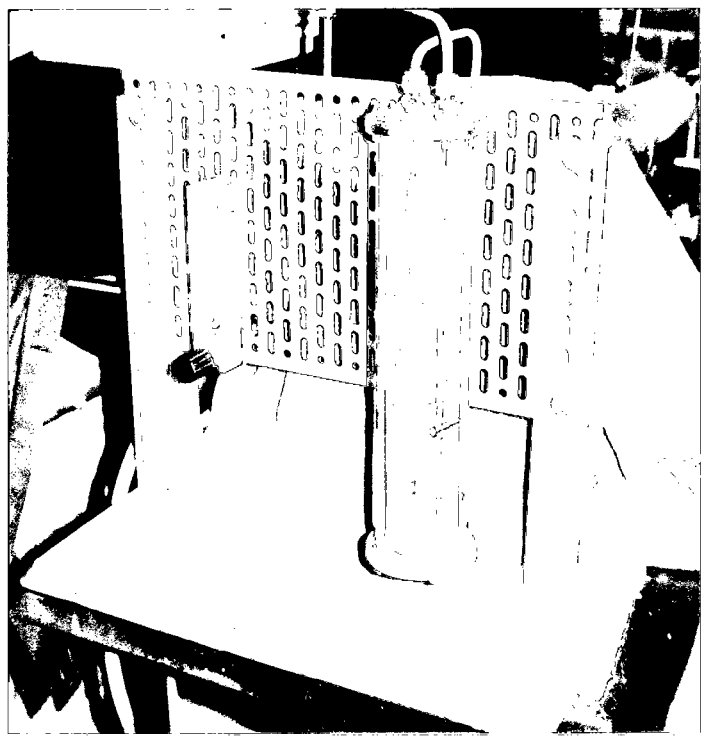

**Figure 3-4 Photograph of the flow meter and humidifier used in the metal dusting rig.**

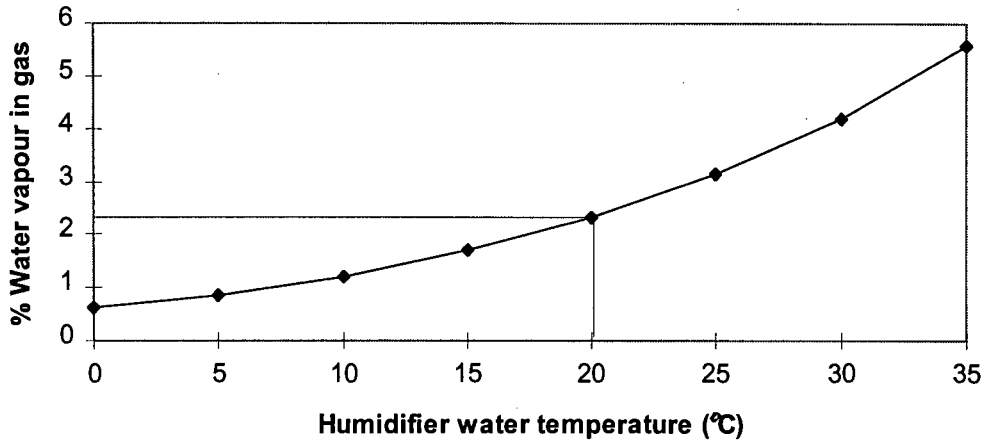


**Figure 3-5 Water vapour content of the saturated test gas mixture as a function of the humidifier water temperature.**

### Power supply and heating element

The furnace tube is heated by means of a resistive wire wound around the exterior of the tube. The spacing between the wire coils has a significant effect on the temperature profile along the tube. It was decided at an early stage of the design process to achieve the requirement of constant temperature in the test zone by varying the spacing of the element coils. This entailed experimenting with a number of different winding patterns and recording the resulting temperature profiles. A successful winding pattern would be one that resulted in a temperature gradient of not more than 1.3 °C/10 mm over a length of at least 80 mm, corresponding to a maximum temperature difference of 10 °C.

The element wire was wound by rotating the tube on a lathe and feeding the wire onto it under tension via a geared tool support. The spacing of the wire coils was changed by varying the gearing of the tool holder. Once the wire was wound onto the tube, it was clamped into position at either end. The winding was then lightly covered by a furnace cement which, when set, holds the coils in place.

Uniformly wound tube

The first pattern tested consisted of a uniform spacing of 3 mm between the coils. This arrangement produces a roughly parabolic temperature profile (Figure 3-6). Heat transport by the hot, flowing gas causes the curve to lean in the direction of the gas flow. The lowest average temperature gradient is about 5.5 °C /10 mm occurring between 310 and 160 mm from the start of the winding. This may be low enough to accommodate two or three sets of specimens spaced 10 mm apart. The temperature difference would then be 6 to 10 degrees, or 1 % of the test temperature. While this meets the maximum temperature difference requirement, the number of specimens that could fit into this region is too low.

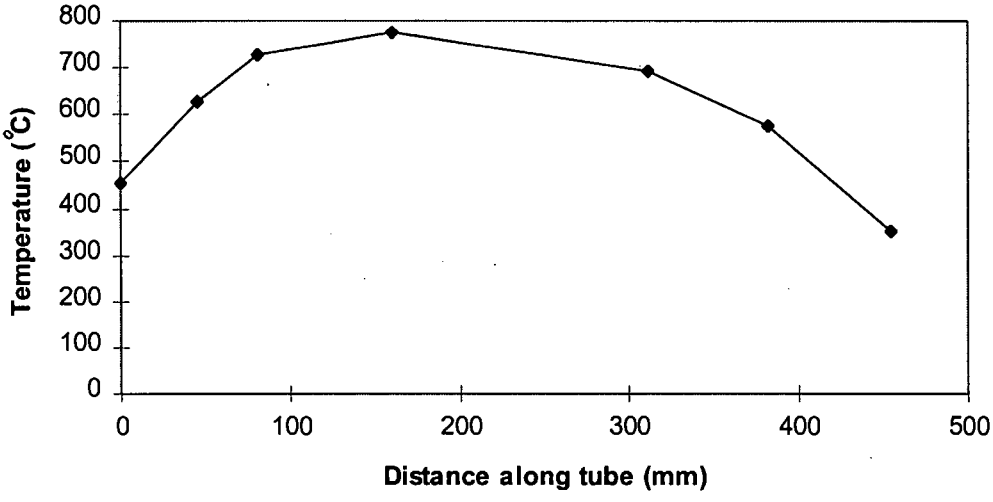


**Figure 3-6 Temperature profile for a uniformly wound tube.**

These results were used to modify the spacing of the wire coils at various points along the tube. A number of different winding configurations were tested until the configuration shown in Figure 3-7 was found to satisfy the design requirements. The final temperature gradient of 0.8 °C/10 mm in the test section is well below the design criterion of 1.3 °C/10 mm.

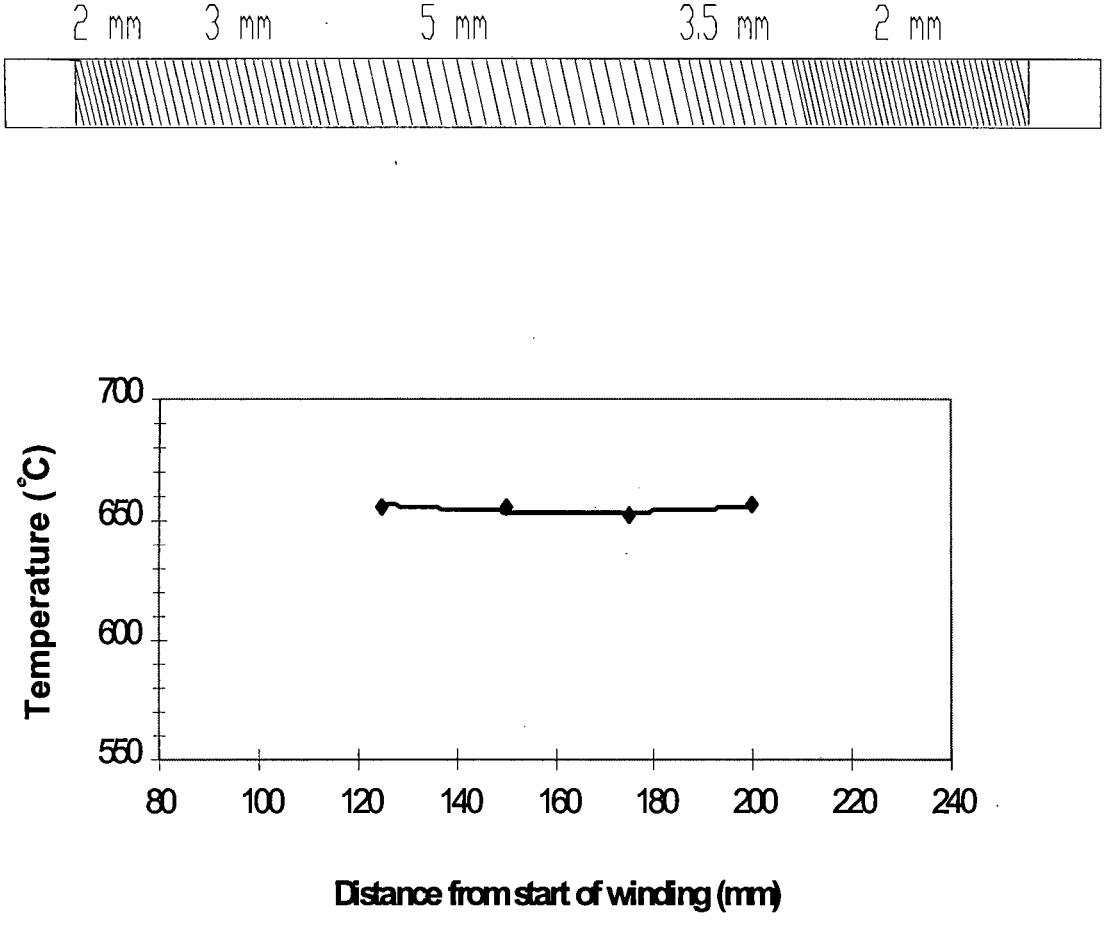


**Figure 3-7 Winding configuration of the heating element and resulting temperature profile in the test section of the tube.**

**Temperature measurement and power control**

Two K-type thermocouples are used to monitor temperatures of the furnace. The first is positioned under the element windings and measures the tube wall temperature. The second thermocouple is inserted into the tube and monitors the temperature of the specimens in the test zone. This thermocouple is protected from the carburising atmosphere by a ceramic sheath, 10 mm in diameter.

A Eurotherm temperature controller is used to control the supply of power to the heating element. During heating of the furnace the reading from thermocouple 1 is fed into the controller. This is done to control the heating rate of the tube wall and thus prevent cracking of the tube due to thermal shock. Once the furnace has reached the test temperature, thermocouple 2 is connected to the controller. This ensures a constant temperature in the test zone. These components are shown schematically in Figure 3-8.

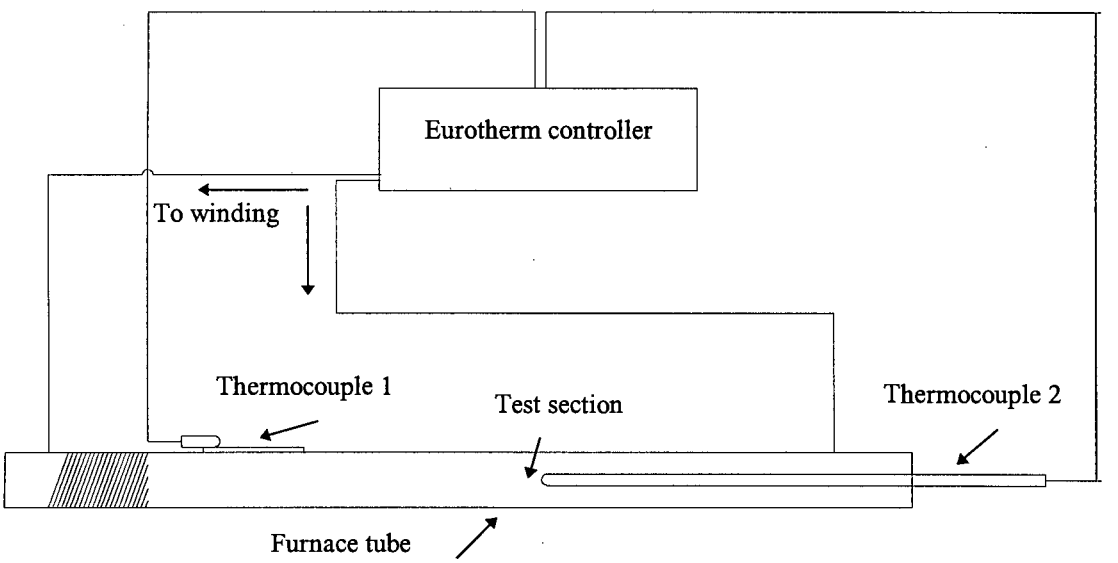


**Figure 3-8 Set-up of the two thermocouples and temperature controller used to maintain a constant temperature in the test section.**

**Test specimens and specimen holder**

The test specimens are rectangular blocks with dimensions of 6 x 4 mm and 1-2 mm in thickness. A hole, 2 mm in diameter, is drilled through the specimens near the top edge. This hole allows the specimen to be suspended from a ceramic support rod in the specimen holder.

The specimen holder is attached to the end of the ceramic thermocouple sheath inserted into the test section. The holder consists of three alumina rods, 1.8 mm in diameter and 80 mm in length, supported at either end by a hollow bead that is bonded to the sheath (Figure 3-9). The test specimens are suspended on these rods. This arrangement places the specimens as close to the centre of the tube as possible and allows them to surround the tip of the thermocouple.

The specimens are moved in and out of the test zone by sliding the thermocouple sheath along the length of the tube.

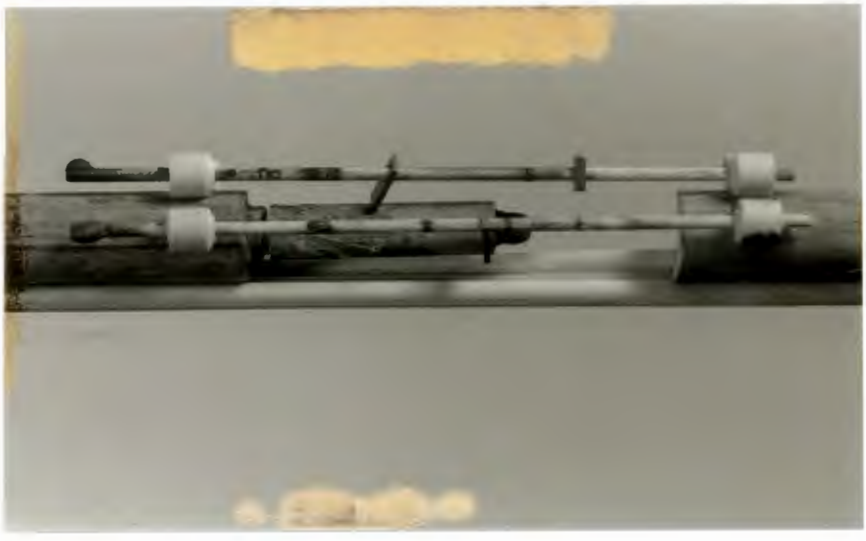

**Figure 3-9 The specimen holder used to support the test specimens in the furnace tube.**

**Leak prevention and containment**

At temperatures above 600 °C both hydrogen and carbon monoxide are above their auto-ignition temperatures. It is therefore important that the furnace is sealed to prevent leakage of oxygen into the furnace or leakage of the gases out of the furnace. A gas-tight seal is achieved by the use of end caps that incorporate O-rings at each end of the furnace tube. A gas-tight seal for the thermocouple is provided by a collar that slides over the thermocouple sheath and threads into the exit-side end cap (Figure 3-10). The collar presses against two O-rings, which seal the gap between the sheath and the end cap. This arrangement allows the sheath to slide in and out of the tube while maintaining a gas-tight seal.

The effectiveness of the seals was tested by pressurising the tube with air at 300 KPa and measuring the rate of pressure loss. A high rate of pressure loss would indicate the leakage of air through one or more of the seals. This test, repeated a number of times, showed that the pressure drop was negligible and that the seals worked well.

A second ceramic tube surrounds the main furnace tube and acts as a containment vessel in the case of a gas leak. This outer tube is filled with argon and reduces the risk of explosion should any leaks occur. This tube is also sealed by a system of end caps and O-rings. The caps are designed to support the inner tube and allow access of electrical wires, thermocouple wires, cooling water pipes and gas lines to the inner tube while maintaining a gas-tight seal (Figure 3-11). Copper cooling coils are placed inside the tube at either end and prevent the temperature from rising beyond the safe range of the O-rings (Figure 3-10).

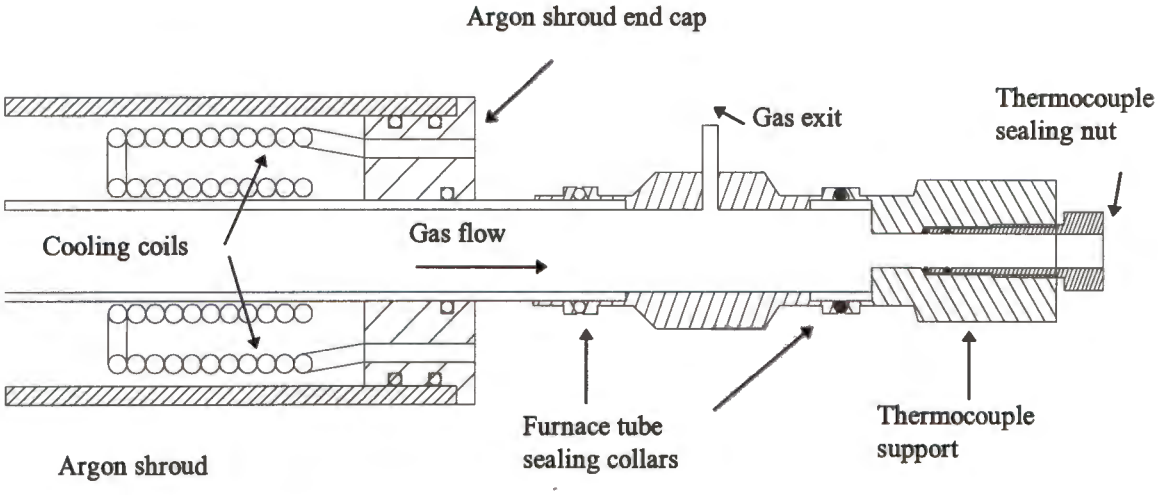


**Figure 3-10 Arrangement for sealing the ceramic tube against leakage of the test gases.**

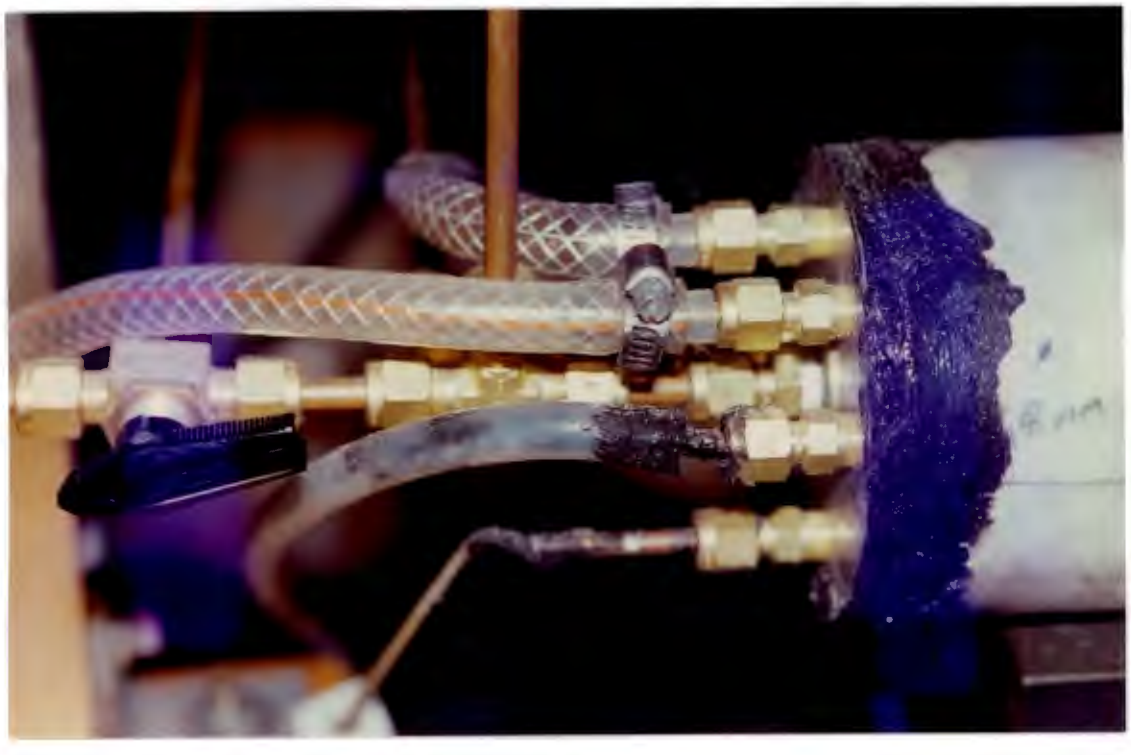

**Figure 3-11 End cap of the secondary containment tube.**

### 3.3.2 Rig evaluation and future modifications

Extensive testing of the rig in which temperature measurements along the length of the tube were taken showed that the desired temperature profiles could be achieved. It was decided at this stage to commence the metal dusting exposures. The results of these exposures provided confirmation that the furnace set-up was adequate for controlled metal dusting simulation.

Two future modifications to the rig could be carried out. These are:

1. Modifying the element winding pattern in order to extend the length of the constant temperature test section. This could be done by experimenting with various winding patterns, or by incorporating multiple controllers along the length of the test section.

2. Modifying the humidifier in order to provide a facility for varying the water-vapour content of the simulation gas.

# 4. Experimental Methods

## 4.1 Materials tested

Following a review of the literature concerning experiences with metal dusting in industry, it was decided to include four alloys in the metal dusting simulation tests. These were:

- 1 1/4 Cr, 1/2 Mo 'low alloy' steel
- AISI 310 stainless steel
- Incoloy 800H
- Fe-18Cr-9Mn-0.5N (Chromanite/HNSS)

The first three alloys have all suffered from metal dusting corrosion in various industrial environments. The high nitrogen stainless steel, Chromanite, containing 0.5% nitrogen, was tested in order to study the influence of nitrogen on the alloy's resistance to metal dusting. Table 4-1 shows the composition and as received condition of each of these alloys.

| Alloy | Composition | Microstructural condition | As received condition | Designation |
|---|---|---|---|---|
| CrMo | Fe-1.25Cr-0.5Mo-0.2 C | dual phase ferrite and pearlite | Extruded pipe | CrMo |
| AISI 310 | Fe-25Cr-20Ni-2Mn-1.5Si-0.03S-0.25C | austenitic | Cold rolled plate | 310 |
| Incoloy 800H | Fe-20Cr-32Ni-1.5Mn-0.38Ti-0.38Al-0.5 Si-0.05C | austenitic | Cold rolled plate | 800H |
| Chromanite | Fe-18Cr-9Mn-0.5N | austenitic | Cold rolled plate | HNSS |

**Table 4-1 Composition and as received condition of each of the four alloys tested [53].**

## 4.2 Characterisation of the gas atmosphere

The composition of the gas mixture was selected on the basis of recommendations made by Grabke [54] for standardised simulation of metal dusting. Figure 4-1 shows carbon activities for this mixture at temperatures between 450°C and 750°C. Carbon activities well in excess of unity are achieved in this temperature range.

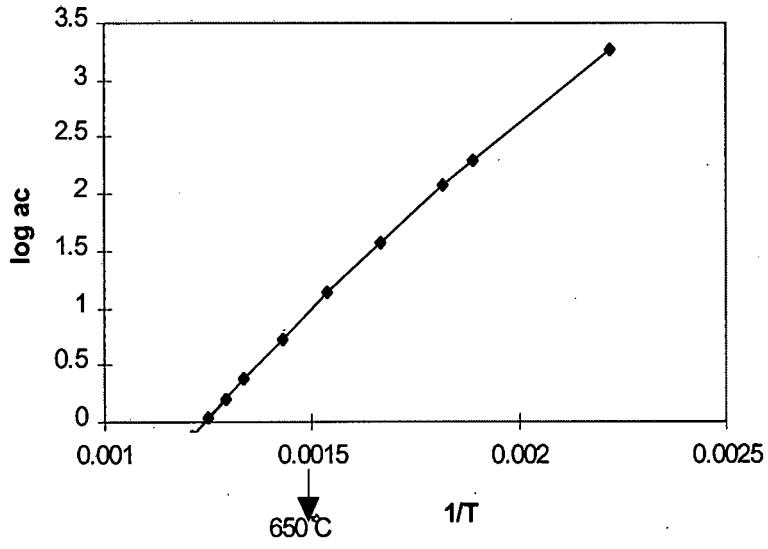


**Figure 4-1 Carbon activity of the gas mixture as a function of temperature.**

Selected thermodynamic characteristics of the gas mixture at the test temperature of 650 °C are presented in Table 4-2.

| | |
|---|---|
| Nominal composition | 75% $H_2$ , 23% CO, 2% $H_2O$ |
| Carbon activity (based on entrance composition) | ≈ 16 |
| Absolute Pressure | 1 bar |
| Oxygen partial pressure | ≈ 2.4 KPa |

**Table 4-2 Thermodynamic characteristics of the test gas mixture at 650 °C.**

## 4.3 Metal dusting corrosion testing

### 4.3.1 Specimen preparation

Specimens for testing were prepared from the alloy samples by first machining the samples into blocks 6 mm by 4 mm by 70 mm long. Individual specimens having a thickness of about 2 mm were then cut from these blocks.

**Heat treatments**

Specimens were tested in both the as received and annealed conditions. Selected specimens were annealed at 1200 °C for five hours before grinding and polishing.

The main effect of the annealing treatment was to increase the effective mean diameter of the grains from 76 μm to 253 μm. Annealing the alloys also reduces the dislocation density and vacancy density within the specimens. The effect of annealing can be seen in
Table 4-3 which presents the bulk Vickers hardness values of annealed and as received specimens of alloy 800H, 310 and HNSS. In all three alloys the significantly lower hardness of the annealed specimens indicates the effect of annealing on reducing the amount of cold work in the matrices.

The increased grain diameter and decreased dislocation density increases the specimens' susceptibility to metal dusting by reducing the diffusivity of the matrix. This decreased diffusivity retards the rate at which chromium and other oxide-forming elements can diffuse to the surface. This reduces the ability of the alloy to repair damage to the protective chromia layer, which can occur due to thermal stresses on the specimen. Once the oxide layer is permanently damaged, metal dusting can proceed freely at the site where the damage has occurred. The decreased diffusivity

will also retard the diffusion of carbon into the alloy, thus reducing the alloy's susceptibility to metal dusting. However, since carbon is a smaller atom than chromium, this effect will not be as significant as the reduced diffusivity for chromium and the overall effect will be an increased susceptibility to metal dusting.

The decreased vacancy density as a result of annealing is beneficial to the alloy's resistance to metal dusting. The lower amount of vacancies reduces the number of nucleation sites for chromium and iron carbides and thus retards the formation of these carbides. This has the effect of leaving more chromium in solution where it can be used to maintain the oxide layer. Since the precipitation of iron carbides is the first stage of metal dusting, retarding iron carbide formation delays the onset of metal deterioration.

However, both the as received and annealed specimens were ground and polished after the heat treatment stage, thus introducing new cold work into the surface regions of the specimens. This reduces the effect of annealing on dislocation and vacancy density in the samples. The main difference between the annealed and as received specimens is therefore the effective mean diameter of the grains.

| Alloy | As received | Annealed |
|---|---|---|
| 800H | 125 | 81 |
| 310 | 141 | 100 |
| HNSS | 220 | 128 |

**Table 4-3 Bulk Vickers hardness values of as received and annealed specimens of alloys 800H, 310 and HNSS.**

**Surface finishes**

Two surface conditions were used in the tests - abraded and polished. Abraded specimens were prepared by grinding with 80-grit silicon-carbide paper. Polished specimens were ground with 80 then 120, 360, 600, 1200 and finally 4000-grit silicon-carbide paper. They were then polished to a scratch-free finish on a polishing pad using colloidal silica suspension. Figure 4-2 shows optical micrographs of as received, abraded (Figure 4-2 a) and annealed, polished (Figure 4-2 b) specimens of alloy 800H.

**Passivation and depassivation of sample surfaces**

Specimens of alloy 800H were given either a passivation or depassivation treatment in preparation for the third test series. The specimens were suspended in a 1 N sulphuric acid solution connected to an Amel system 5000 potentiostat. The specimens were then passivated at a potential of +0.5 mV and depassivated at -0.6 mV for five minutes.

a)

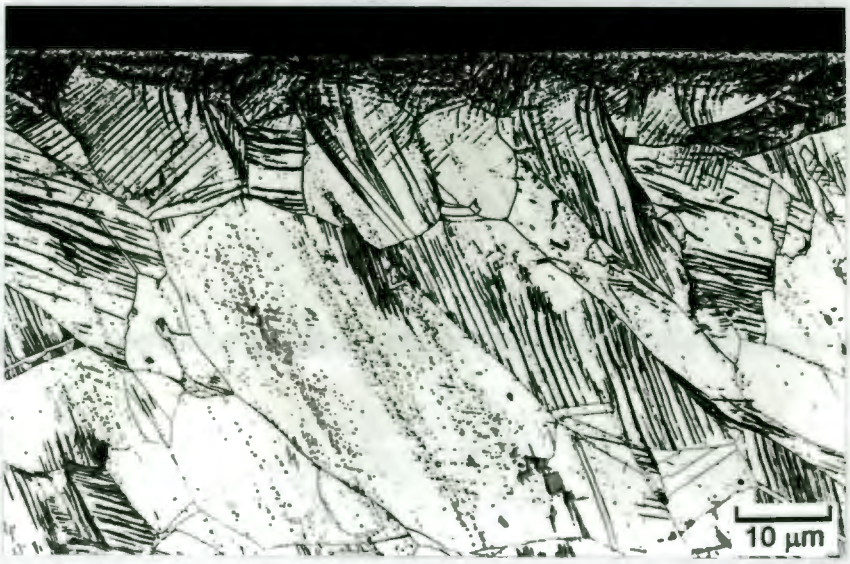


b)

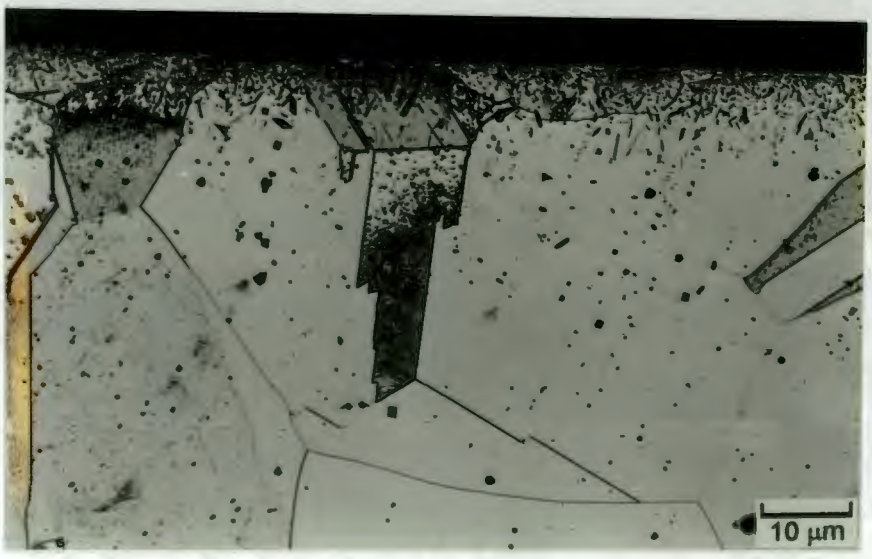


**Figure 4-2 Optical micrographs of as received, abraded a) and annealed, polished b) specimens of alloy 800H.**

### 4.3.2 Standard procedure followed in conducting metal dusting corrosion tests

Before the start of each test the specimens were ultrasonically cleaned in ethanol for five minutes. They were then dried and weighed on a *Sartorius* digital balance scale to an accuracy of 0.03mg. Following this, the specimens were positioned on the specimen test rack and inserted into the furnace tube. A high level of cleanliness of the samples was maintained throughout this procedure.

The furnace was then heated to the test temperature while the tube was purged of oxygen by flowing argon. When the temperature in the test zone reached 650 °C testing commenced by replacing argon with the test gas mixture. The specimens were exposed to the carburising environment for 24 hours in the case of the CrMo specimens and periods ranging between 120 and 320 hours for the other three alloys. At the end of the test period the flowing $H_2/CO/H_2O$ mixture was replaced by argon and the furnace allowed to cool. The specimens remained in the test zone during cooling.

The test rack was then carefully removed from the furnace and the carbon deposition on each sample was noted. The samples were then placed under a stereo light microscope, where the deposit was observed at a magnification of two to three times. Specimens showing interesting surface features were removed at this stage for observation in the SEM. The surface deposit on the remaining specimens was then scraped off with a plastic blade and stored in marked capsules for further analysis. This was followed by ultrasonic cleaning of the samples in ethanol and weighing. Selected specimens of each alloy were then removed for metallographic analysis. The remaining specimens were then re-exposed in the furnace for a further week.

## 4.4 Plan of testing

Three series of exposures were carried out during the course of the project. The aim of the first test series was to establish the corrosion of a low alloy CrMo steel by metal dusting. The exposure period was 24 hours long. A high alloy steel (AISI 310) was also tested to compare the different resistance's of the two alloys. The results of these exposures was then used to formulate a testing plan for three high alloy steels.

The second series was conducted over periods ranging between 120 and 320 hours. Eight specimens of each of the three alloys 310, 800H and HNSS were initially exposed. One sample of each alloy was removed at the end of each exposure in order to observe the metallographic changes over time. Mass change measurements and observations of the carbon deposition were made to assess the different resistance's to metal dusting of the alloys.

In the third series of exposures eight pairs of alloy 800H specimens were exposed for periods of 160 hours. The aim of this test series was to determine the effect of surface roughness, heat treatment and passivation/depassivation of the samples. Each pair was prepared in such a way as to give unique combinations of these three variables. The experimental matrix is shown in Figure 4-3.

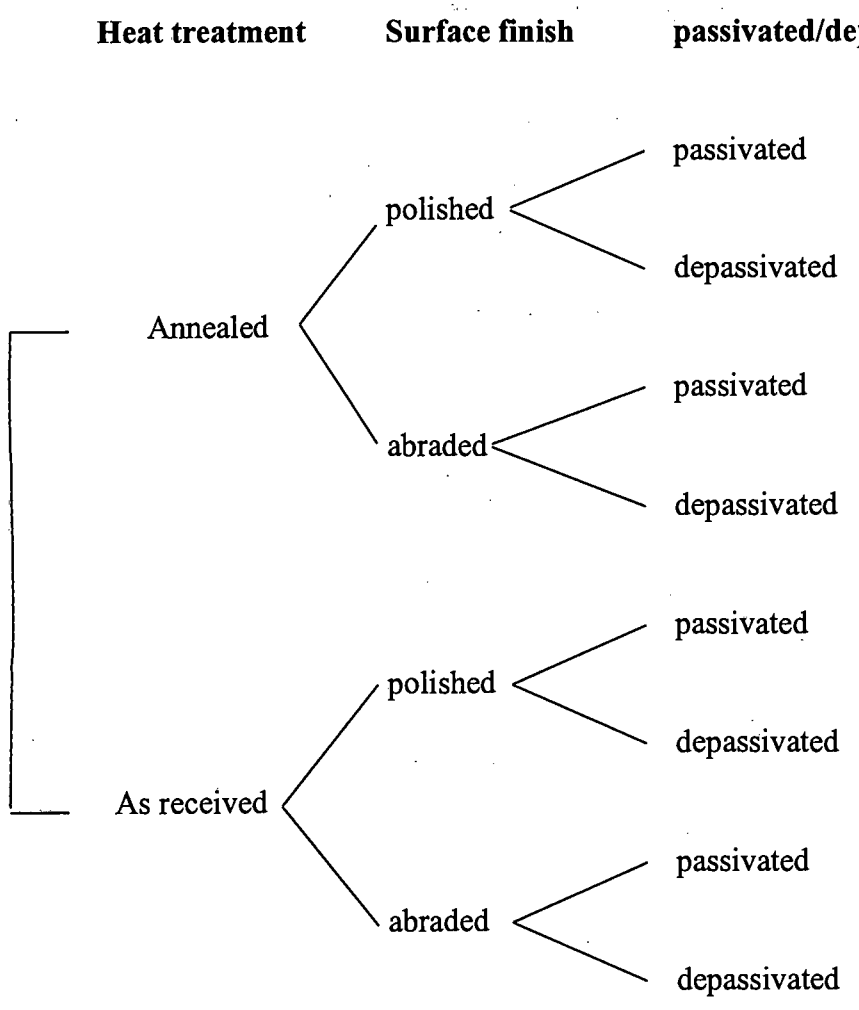


**Figure 4-3 Experimental matrix for third test series of alloy 800H specimens.**

# 4.5 Microscopy

## 4.5.1 Specimen preparation for metallurgical examination

Exposed samples were mounted in thermosetting plastic to give a fifteen-degree taper section through the specimen. The samples were then ground and polished to a scratch-free finish on a *Struers RotoPol* automatic polisher.

Specimens of the CrMo alloy were etched in a 2.5% Nital solution to reveal their microstructure. Specimens of the other three alloys were electrolytically etched in a solution of 8 g. oxalic acid in 100 ml distilled water at 10 volts for 5 seconds to reveal the carburised matrix.

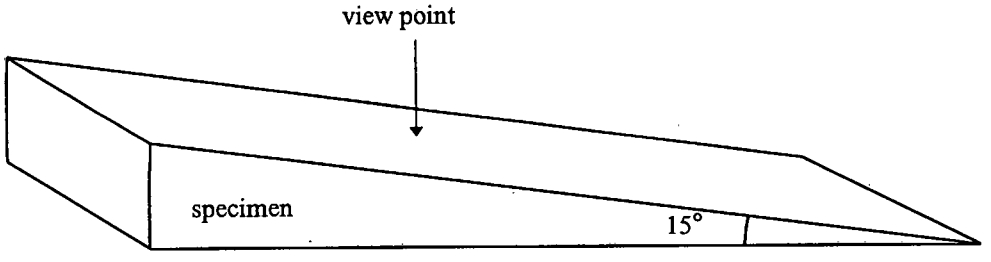


**Figure 4-4 Diagram of the taper section through a specimen used for microscopy.**

### 4.5.2 Microscopy of specimen taper sections

The mounted specimen taper sections were prepared for examination by optical microscopy by cleaning ultrasonically in alcohol. They were then viewed and photographed in a *Reichert MeF3A* light microscope.

Preparation for scanning electron microscopy was again initiated by ultrasonic cleaning in alcohol. The plastic specimen mounts were then fixed to aluminium stubs with a conductive carbon paste and coated with a gold/palladium or carbon conductive film. Secondary and backscattered electron detectors of Cambridge S200 and S440 scanning electron microscopes were used to analyse and photograph the taper sections.

### 4.5.3 Microscopy of topographical features

A stereo light microscope was used to give low magnification, three dimensional views of the surface features of corroded specimens. The samples were observed in an unprepared state directly after being removed form the furnace.

Specimens showing topographical features such as carbon deposits and pitting were prepared for scanning electron microscopy by mounting on aluminium stubs and coating with either a gold/palladium or carbon conductive film.

# 5. Results

## 5.1 Results of metal dusting exposures of CrMo and AISI 310

The results of five exposures of CrMo and 310 specimens to a metal dusting atmosphere at 650 °C for 24 hour periods are presented in this section.

### 5.1.1 Features on exposed CrMo specimens

The specimens of alloy CrMo showed extensive carbon deposition, a constant rate of mass loss and significant carbide precipitation within the matrix.

**Carbon deposits**

From the first exposure period onwards all of the CrMo specimens were covered by large carbon deposits. After the second exposure of 45 hours a deposit of carbon weighing 0.1162g was removed from one of the specimens. This value corresponds to about 97% of the remaining specimen mass.

In most cases the carbon deposit had, macroscopically, a layered, blocky structure (Figure 5-1). Higher magnification observations in a scanning electron microscope revealed the presence of carbon filaments within the structure. Also visible in the deposit were metallic particles, about 20 μm in diameter (Figure 5-2). The largest of these particles could also be observed as bright flecks under a stereo light microscope. An EDS analysis showed that the particles had a similar composition to the parent material, i.e., predominantly iron.

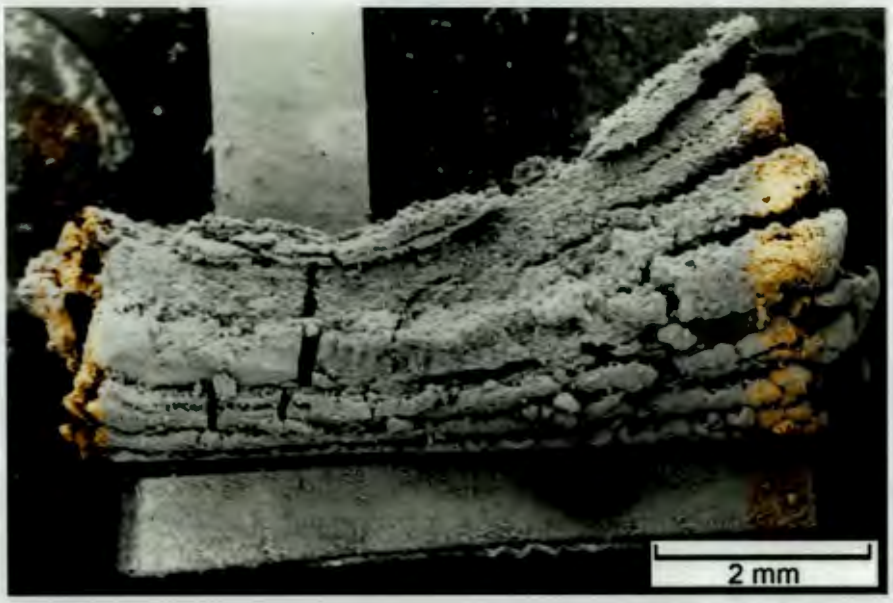


**Figure 5-1 Morphology of the carbon deposit on one side of a CrMo specimen. The deposit, growing outwards from the specimen, has expanded around a ceramic spacer (now removed).**

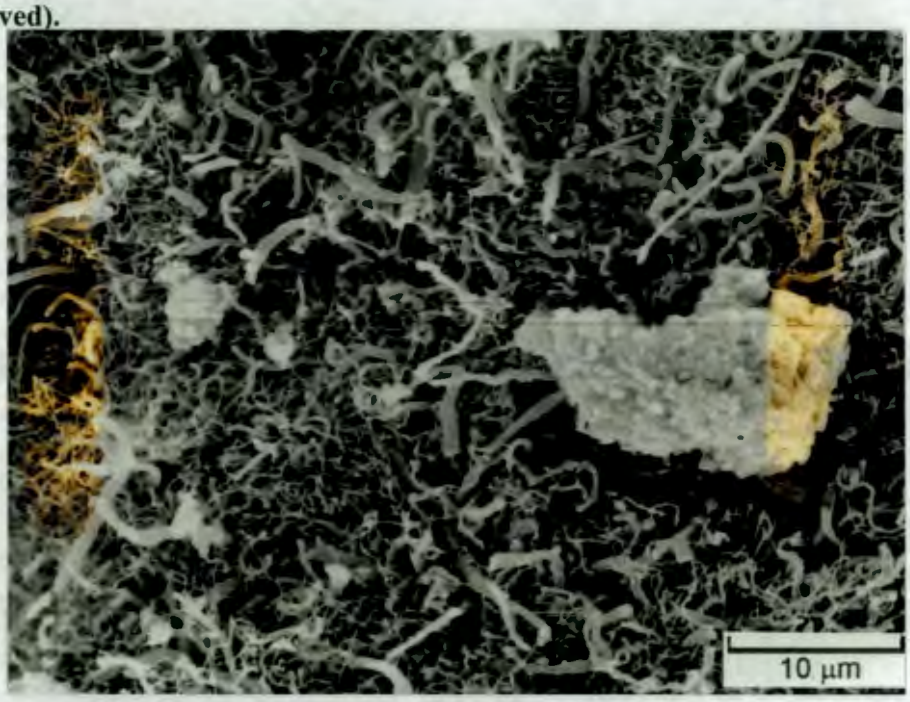


**Figure 5-2 Scanning electron micrograph of the filamentous carbon deposit on a CrMo specimen. An iron particle is visible on the right.**

**Specimen mass changes**

Mass measurements of the specimens after removal of the carbon deposition revealed significant mass loss of the CrMo specimens. These measured mass losses concurred with visual observations, which indicated a substantial thinning of the specimens. Figure 5-3 shows a plot of the average cumulative mass loss of the specimens against exposure time. A short incubation period is evident during the first exposure period. After this the rate of mass loss is constant at about 0.79 mg/cm$^2$.hr.

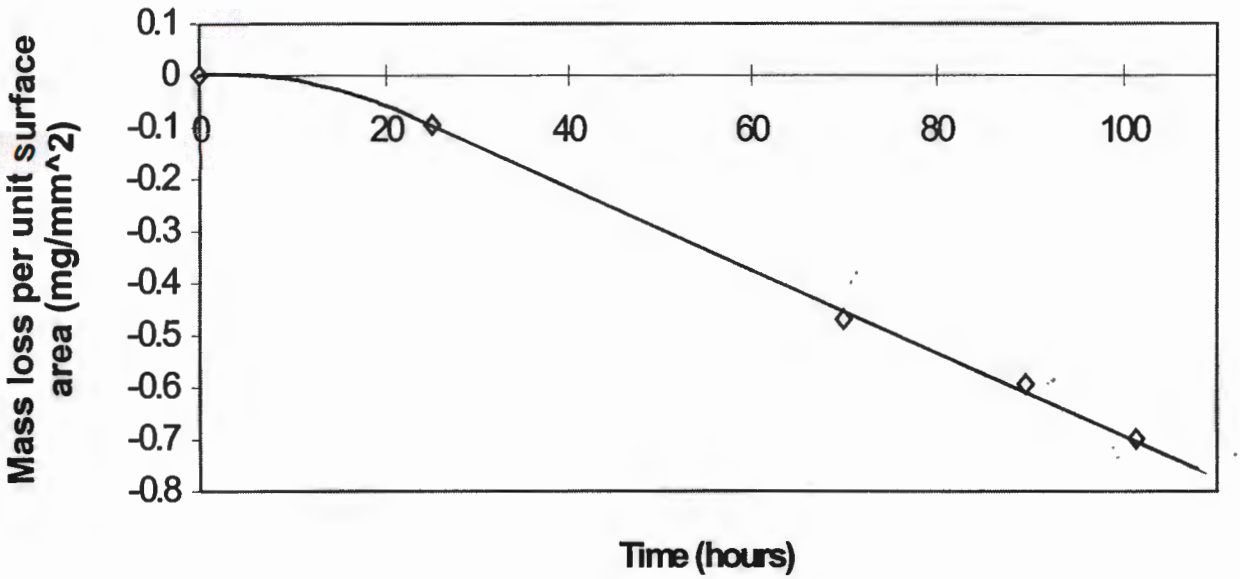


**Figure 5-3 Mass loss per unit area against time for the CrMo specimens. An incubation period of about 20 hours is evident before the start of mass loss at a constant rate.**

**Microstructural examination**

Figure 5-4 shows a two-degree taper section of a CrMo specimen exposed in the furnace for 100 hours. A carburised region consisting of fine precipitated carbides is visible near the surface of the specimen. A network of carbides along the grain boundaries, within the grains and along the surface of the specimen is also evident (Figure 5-5a and b). These carbides are again visible in the SEM micrographs of Figure 5-6. The depth of the surface carbide layer shown in Figure 5-6b is about 0.5 microns. Micro-hardness measurements of the carburised region show that the hardness of the specimen increases towards the surface .

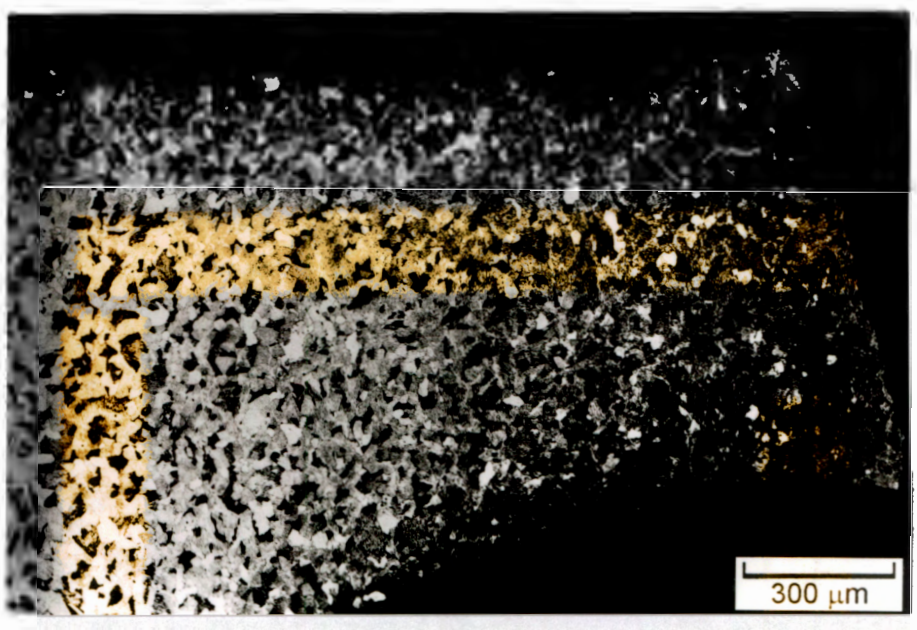


**Figure 5-4 Two-degree taper section of a CrMo specimen exposed for 100 hours. Carburisation of the matrix can be seen in near-surface areas on the right.**

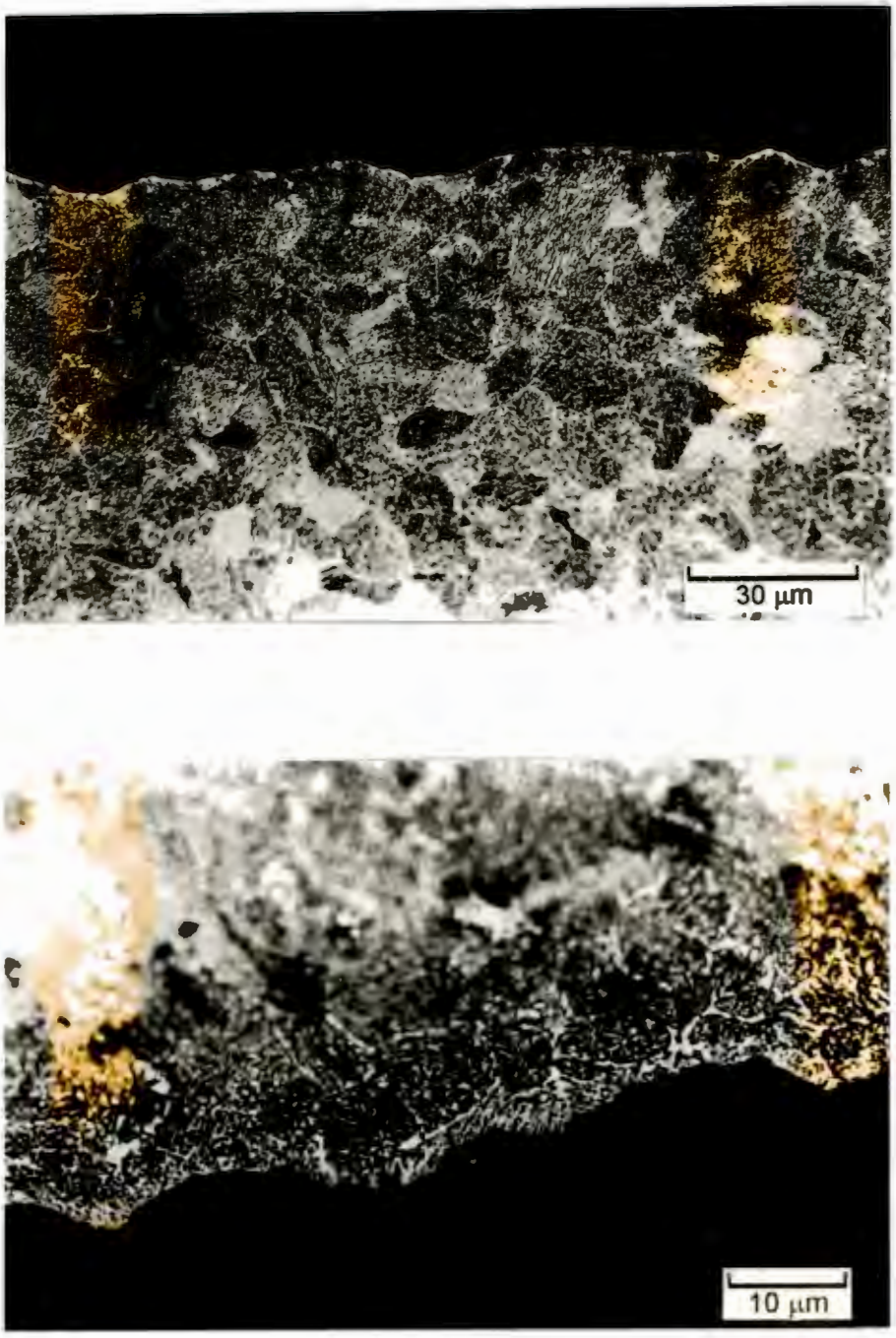


**Figure 5-5 Surface and grain boundary carbides near the surface of a CrMo specimen after 100 hours' exposure.**

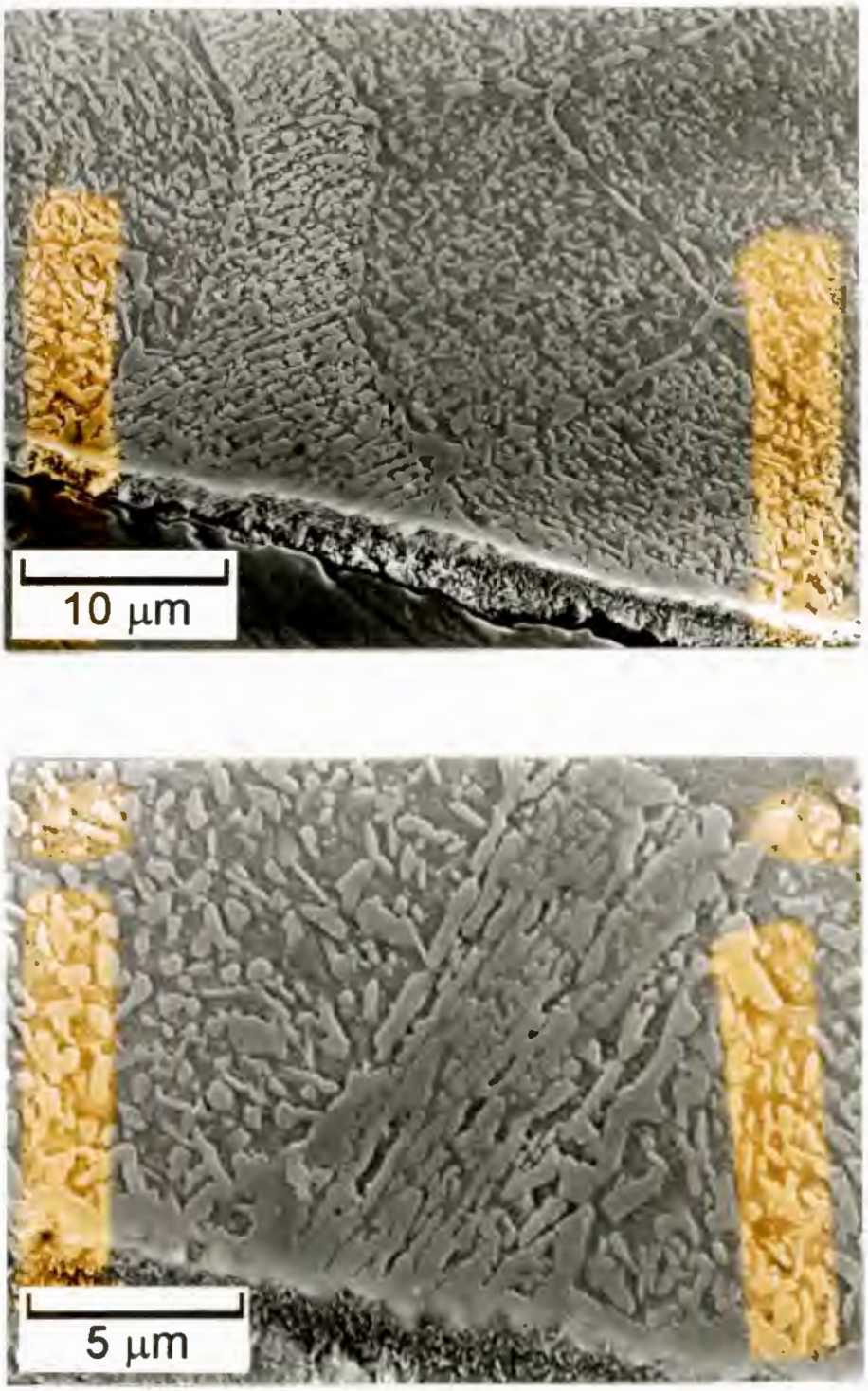


**Figure 5-6 SEM micrographs of a CrMo specimen cross-section showing carbides along grain boundaries and at the surface. The specimen has been exposed for 100 hours. The depth of the surface carbide layer is about 0.5 μm.**

### 5.1.2 Features on exposed AISI 310 specimens

**Carbon deposits and mass changes**

Throughout the series of exposures the alloy 310 specimens were free of carbon deposition. The contrast in the extent of surface deposits between the two alloys is shown in Figure 5-7. There was no significant change in mass throughout the exposures.

**Figure 5-7 Carbon deposits covering two CrMo specimens on either side of a deposit-free 310 specimen. The exposure time is 24 hours.**

**Microstructural examination**

The specimens generally showed little evidence of carburisation or carbide precipitation. Where this did occur, it was limited to small hemispherical regions of about 50 to 200 μm in diameter (Figure 5-8). Micro-hardness tests showed that the hardness increased from about 140 HV at the inner grains to about 510 HV in the carburised region.

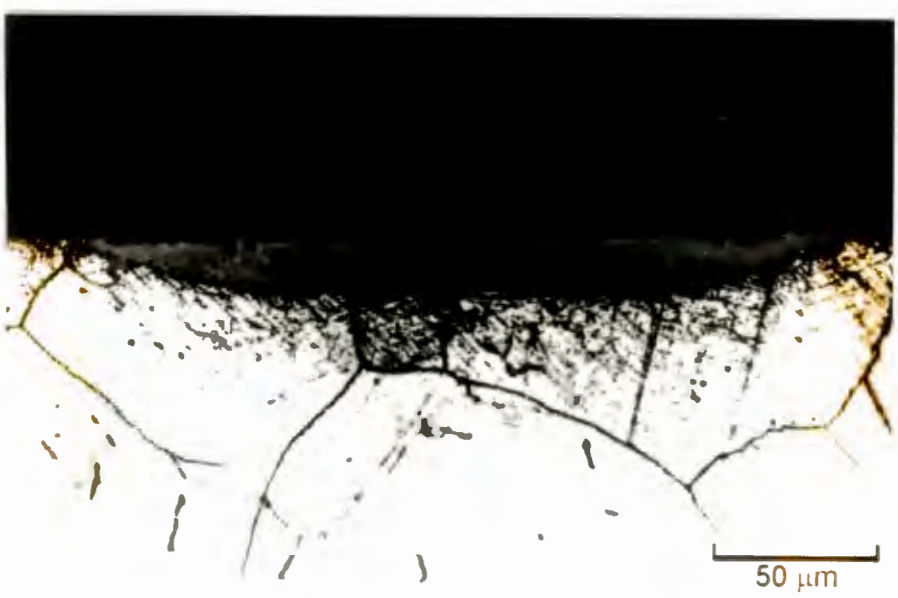


**Figure 5-8 Carburised region at the surface of an as received, polished 310 specimen after 100 hours.**

## 5.2 Results of exposures of alloy 800H, AISI 310 and HNSS to the metal dusting environment

Analysis of the test specimens to characterise the features of metal dusting focused on four areas. These were:

1. the deposition of carbon on the surface of the specimen
2. the formation of pits on the surface of the specimen
3. the changes in the specimens' mass
4. the changes in the microstructure of the specimen

### 5.2.1 Carbon deposition on sample surfaces

The nature and extent of carbon deposition on the three alloys during the series of exposures is shown graphically in Figure 5-9. Carbon was deposited on the surface of the alloy 800H and 310 specimens from the first week of exposure and continued throughout the test series, increasing in density and amount. This deposition occurred in the form of large protrusions (Figure 5-10) and as an even film of carbon filaments (Figure 5-11).

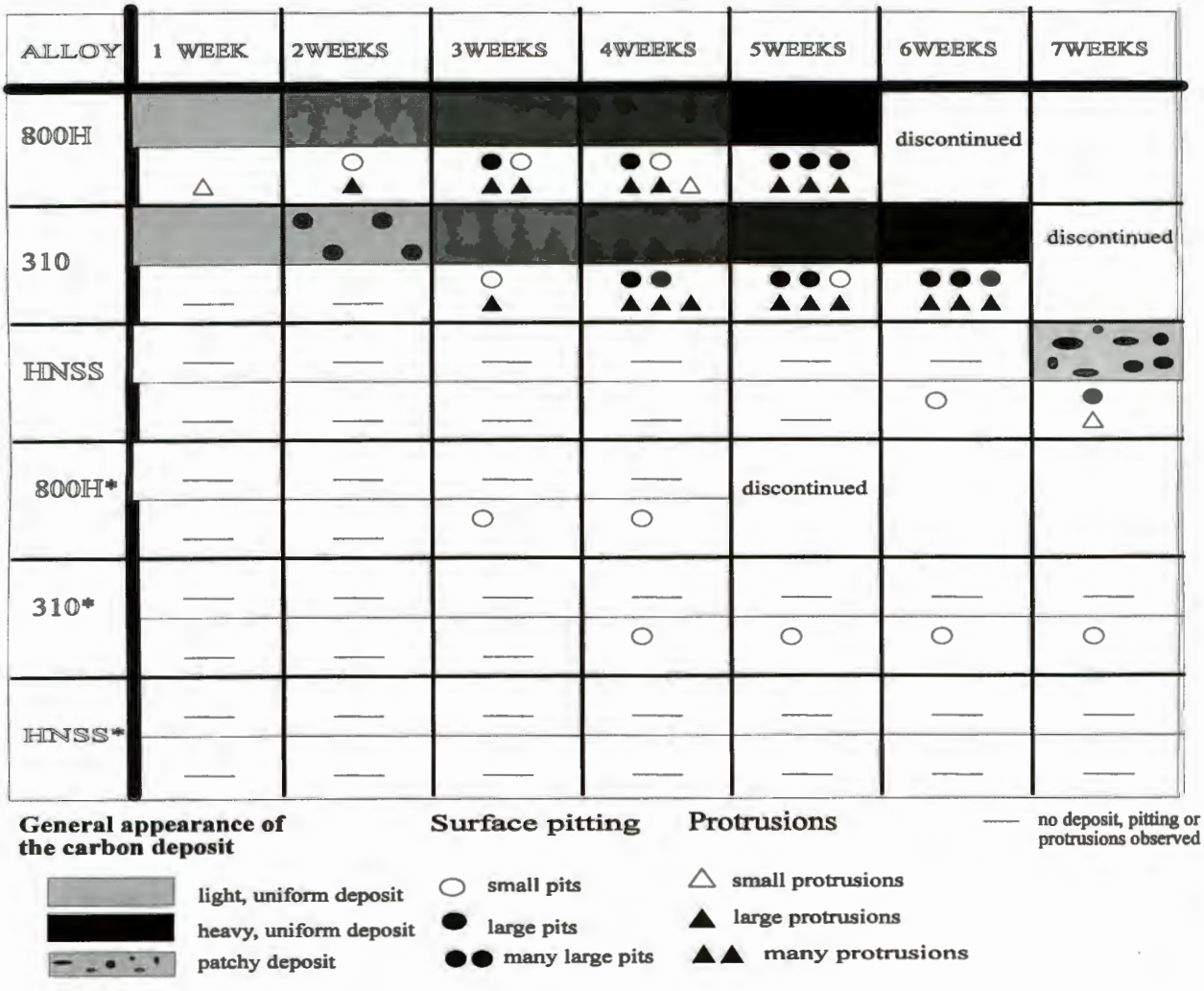


* As received, abraded specimens

**Figure 5-9 Carbon deposition and pitting on the alloy 800H, 310 and HNSS specimens.**

a)

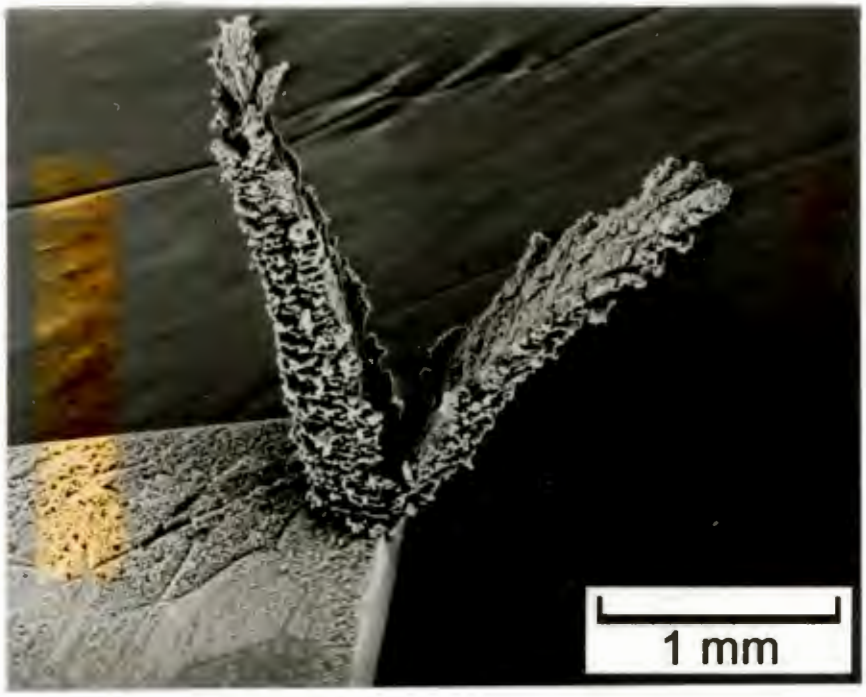


b)

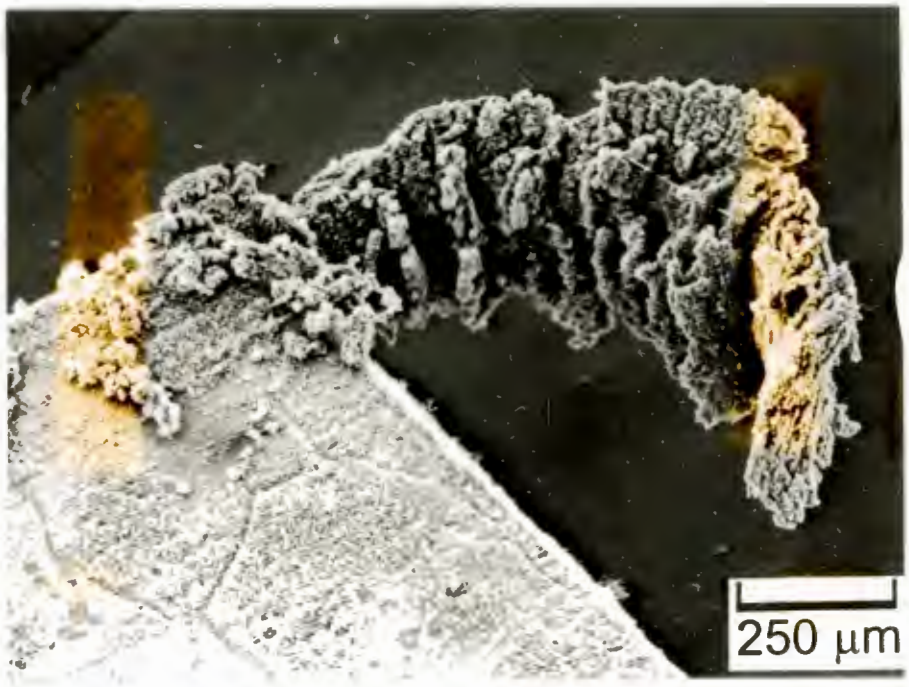


**Figure 5-10 Carbon protrusions grown from the surface of exposed specimens. Figures a and b show two annealed and polished specimens of alloy 800H after the first 160 hours of exposure in the furnace.**

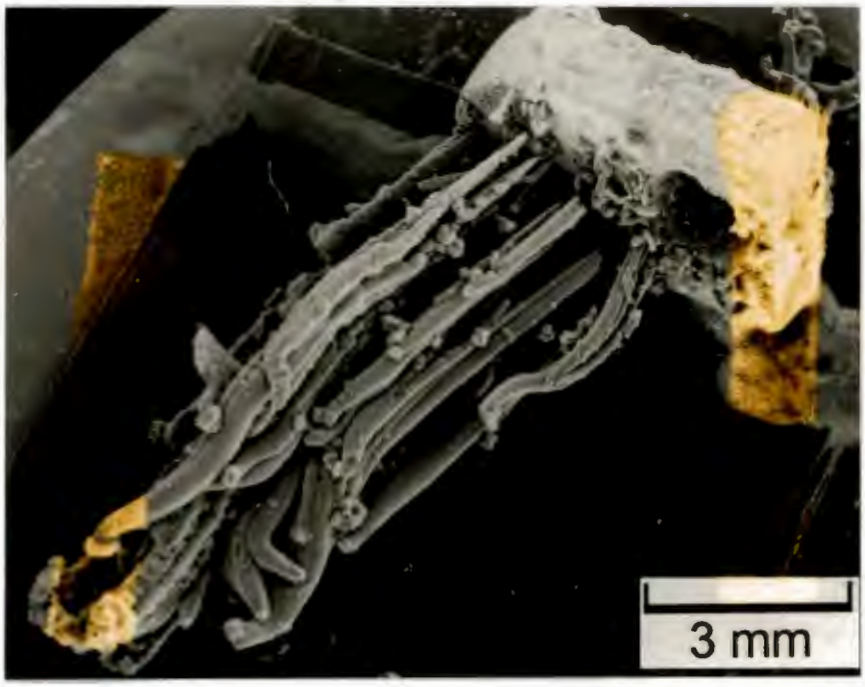


**Figure 5.10 c) Carbon protrusions on an annealed, polished 310 specimen after the fourth exposure of 300 hours.**

The protrusions were similar to those observed in Grabke's experiments and consisted of blocky, amorphous carbon, as well as carbon filaments (Figure 5-12). Removal of the protrusions revealed the presence of a pit at the base of each growth (Figure 5-13). An image of the filaments in the protrusions was obtained by using a backscattered detector in a scanning electron microscope (Figure 5-14). EDS analysis of the bright regions in the pictures revealed the presence of pure iron particles about 300 nm in diameter.

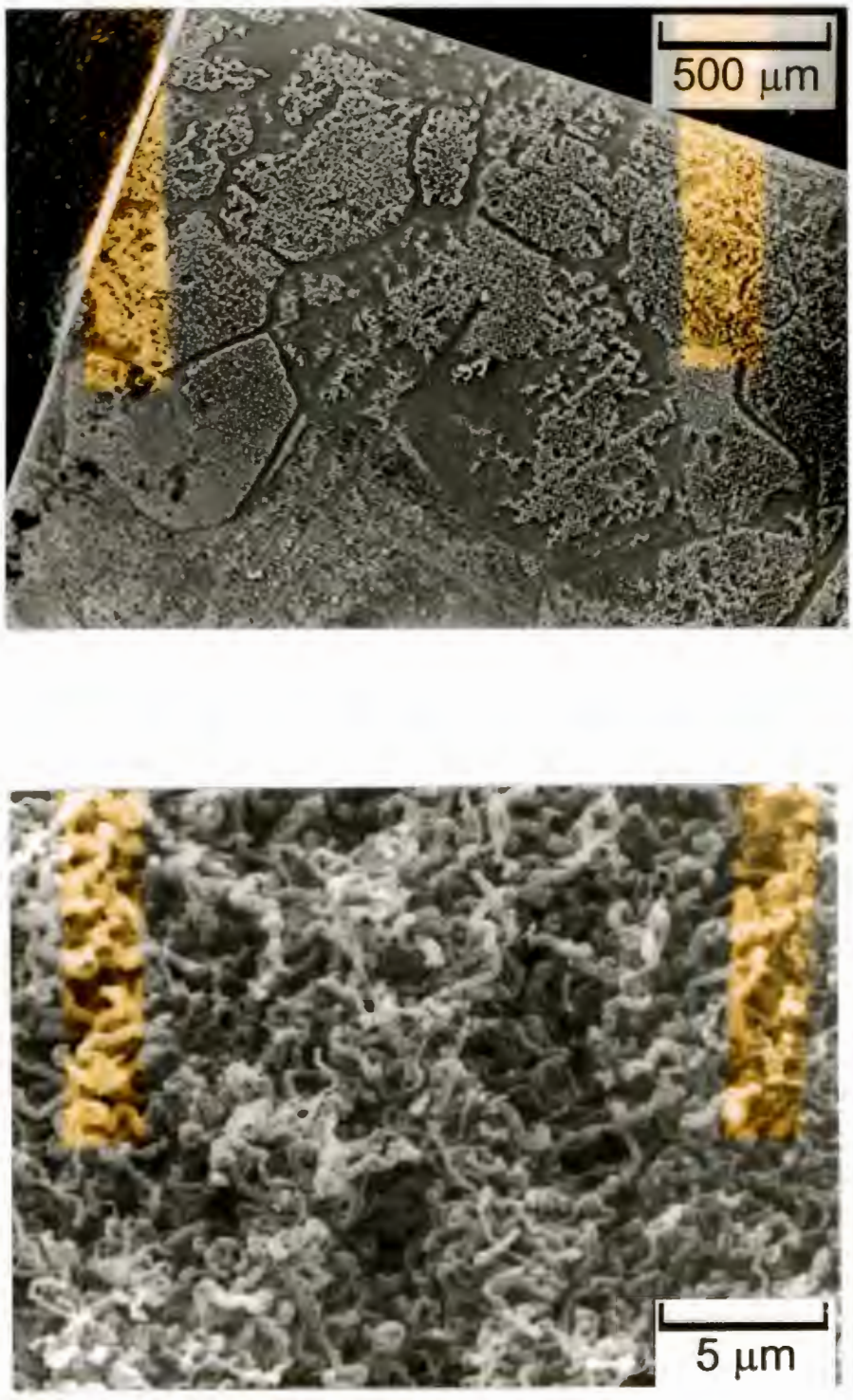


**Figure 5-11 Filamentous carbon on the surface of an annealed and polished 800H specimen after 161 hours.**

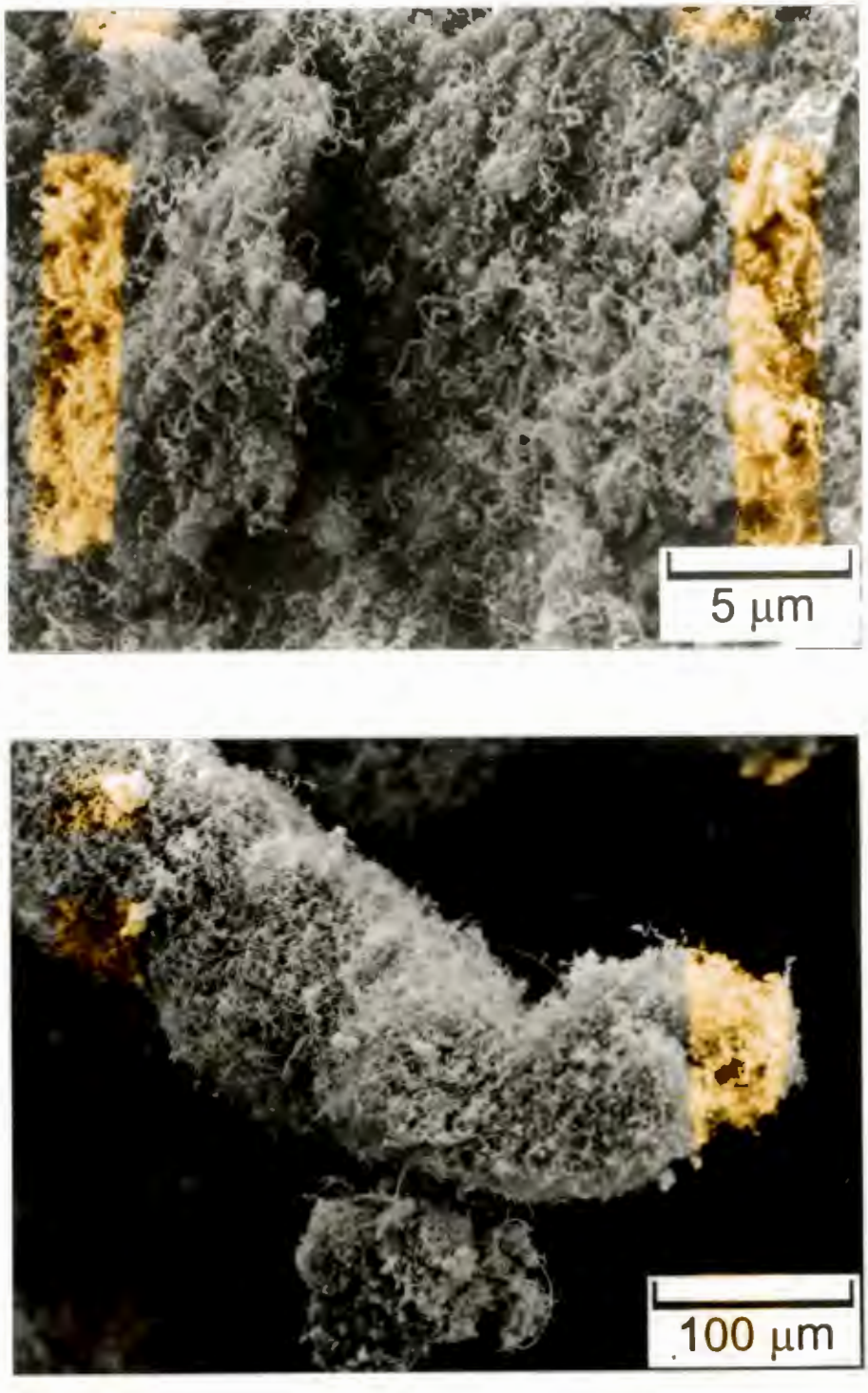


**Figure 5-12 Magnified views of carbon protrusions growing from annealed, polished specimens of alloys 800H and 310 after 1 week. The deposit consists of blocky and filamentous carbon.**

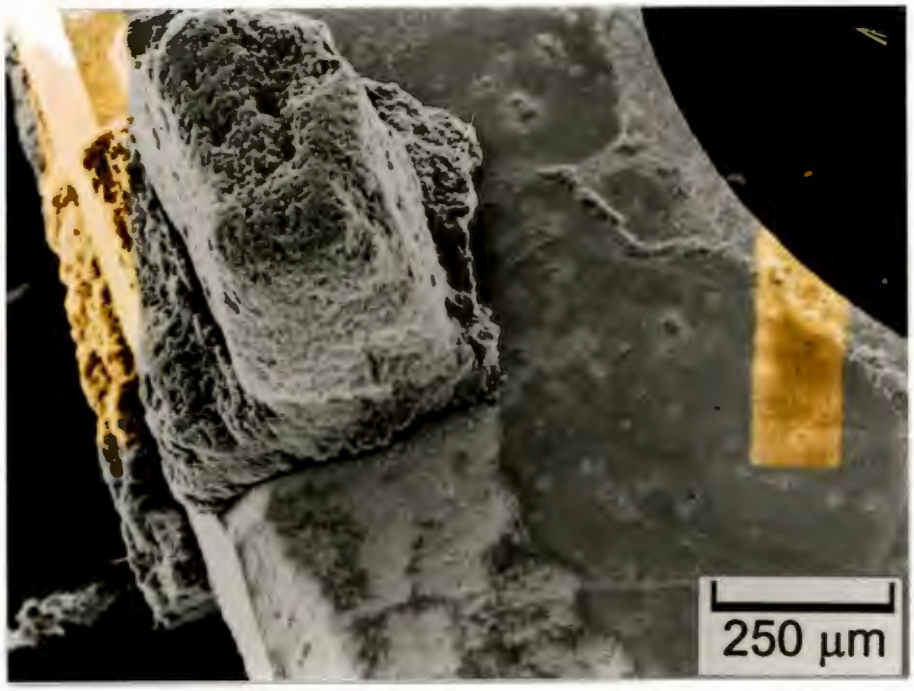


**Figure 5-13 Pitting at the base of a protrusion which has been partially removed. The specimen is an annealed and polished alloy 800H specimen exposed for 3 weeks.**

a)

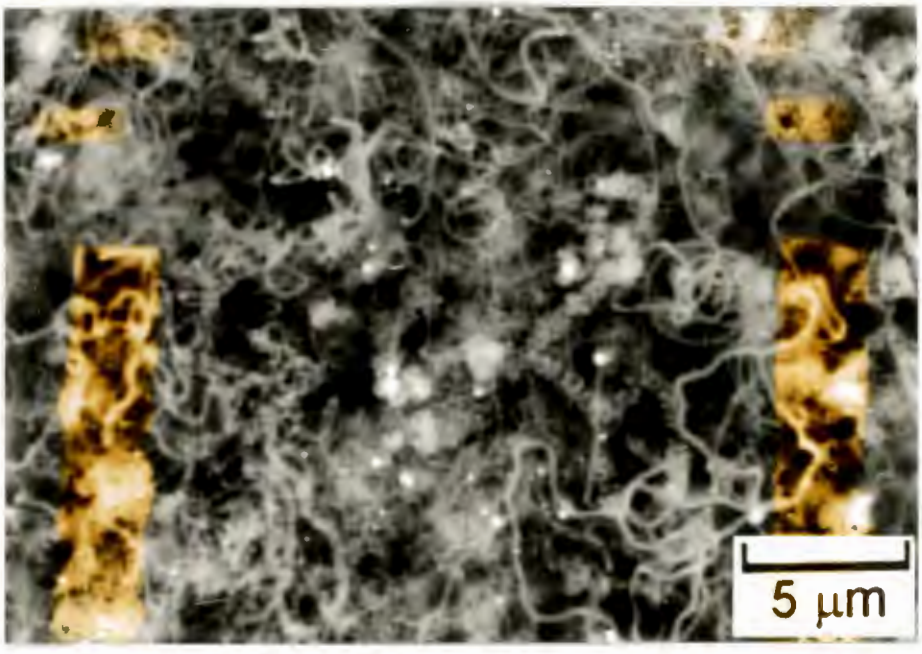


b)

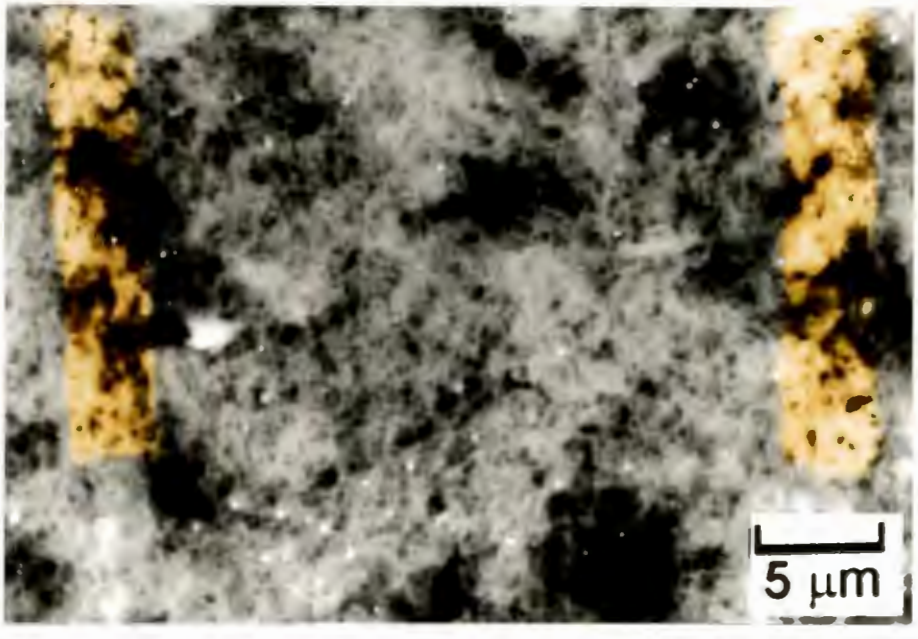


**Figure 5-14 Backscattered electron image of carbon filaments removed from the surface of annealed and polished specimens of alloys 800H (a) and 310 (b). The bright spots are iron particles. The specimens have been exposed for 160 hours.**

The carbon filaments found on the surface were characteristically between 2 and 10 microns in length and supported a metal particle at the tip (Figure 5-15). The filamentous carbon growth usually occurred over specific grains and was often absent along grain boundaries and the rougher surfaces of the specimen edges (Figure 5-16).

**Annealed and polished 800H specimens**

The 800H specimens were the first to exhibit protrusion growth, with two specimens having small, single growths after the first week. Protrusions had grown from most of the specimens by the end of the third week. At the end of the fifth week the carbon deposition and protrusion growth was so large that the specimens were removed from the test.

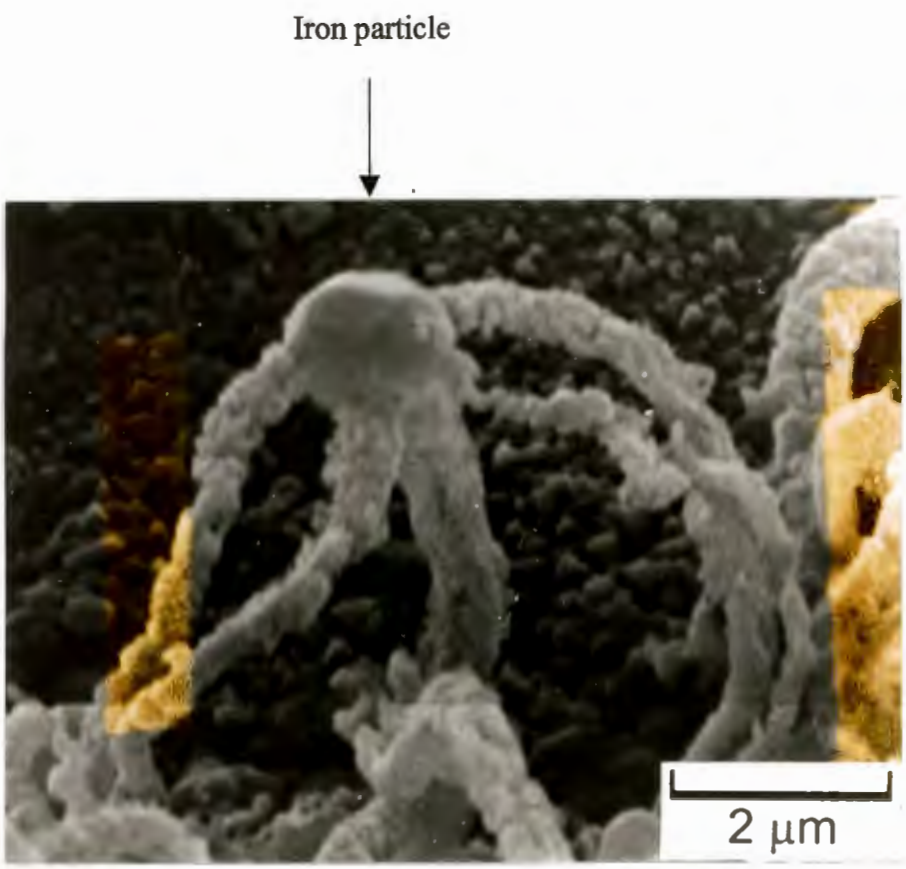


**Figure 5-15 Carbon filaments on the surface of an annealed and polished alloy 800H specimen after 1 week.**

a)

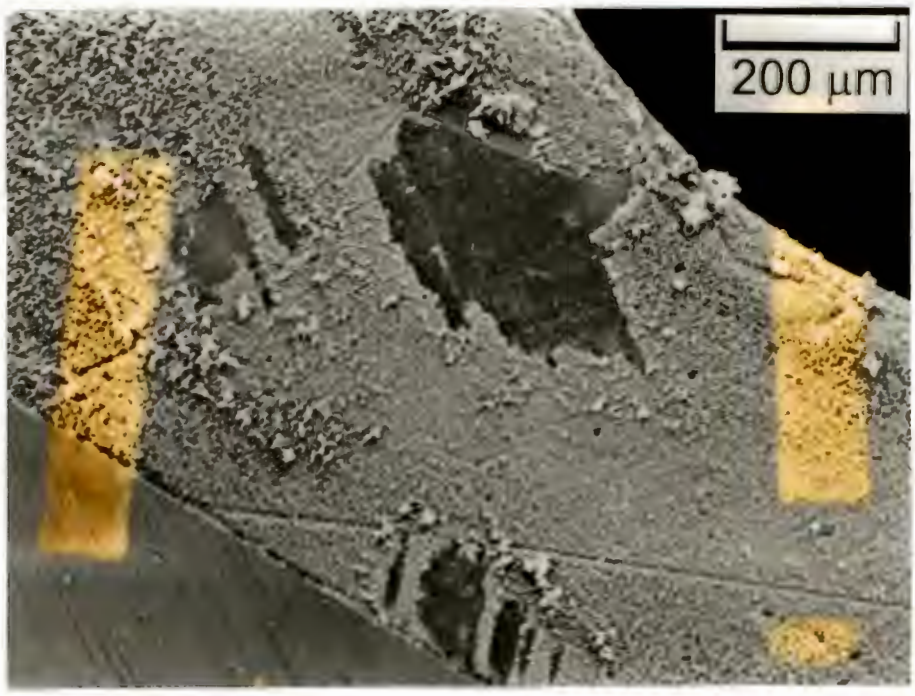


b)

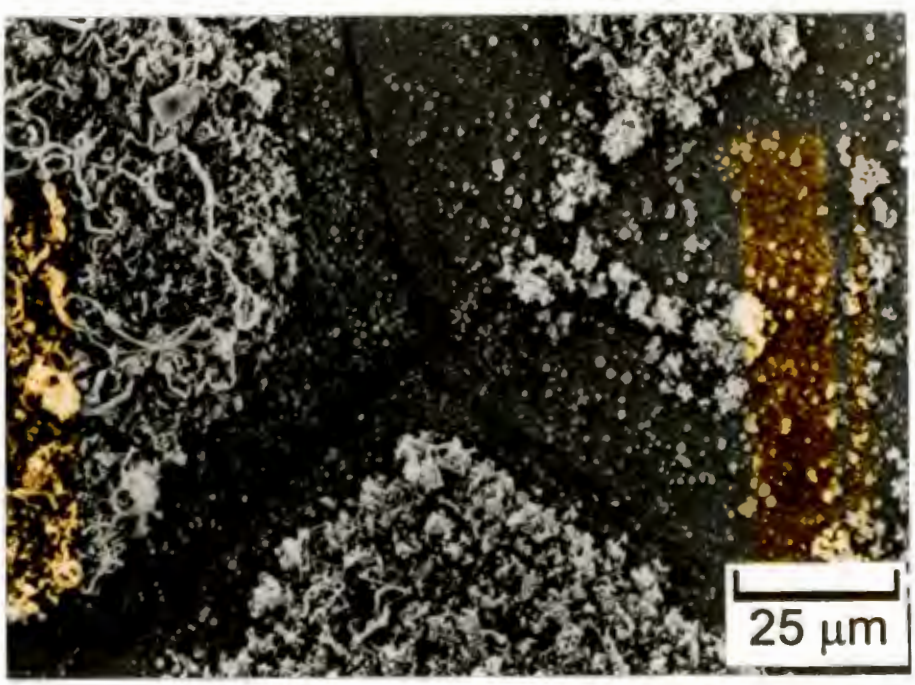


**Figure 5-16 Carbon deposits on the surface of an annealed, polished alloy 800H specimen after the first week. Figure a) shows the absence of carbon deposition on certain grains, grain boundaries and the rougher surface along the side of the specimen (left foreground). Figure b) shows the absence of deposition along grain boundaries.**

**Annealed and polished 310 specimens**

The amount of carbon deposition was initially less on the 310 specimens than on the 800H specimens. After the first week most of the specimens displayed a light covering of filamentous carbon. However, the occurrence of protrusion growth only occurred after the fourth exposure (Figure 5-10b). After the fifth week of testing, however, the amount of deposition on the samples was much the same as on the 800H specimens.

**Annealed and polished HNSS specimens**

In contrast to alloys 800H and 310, the amount of carbon deposition on the HNSS specimens was negligible for the first five weeks. When deposition was observed, it was limited to a very fine, even layer on the surface (Figure 5-17). After six weeks one specimen showed a fine, localised deposit of filamentous carbon on the surface. EDS analysis of this deposit failed to show the presence of metallic particles. A green tinge, possibly a layer of manganese oxide (MnO), and decoration of the grain boundaries was observed on the surface of the specimens from the first week until the end of the tests. After the ninth exposure the two remaining specimens showed a light covering of carbon that covered about 40 % of the two main faces.

**As received, abraded specimens**

The samples of all three alloys that were tested in an as received and abraded condition experienced very little carbon deposition (Figure 5-18). After four weeks one of the 800H specimens showed two small protrusions, each about three millimetres in length.

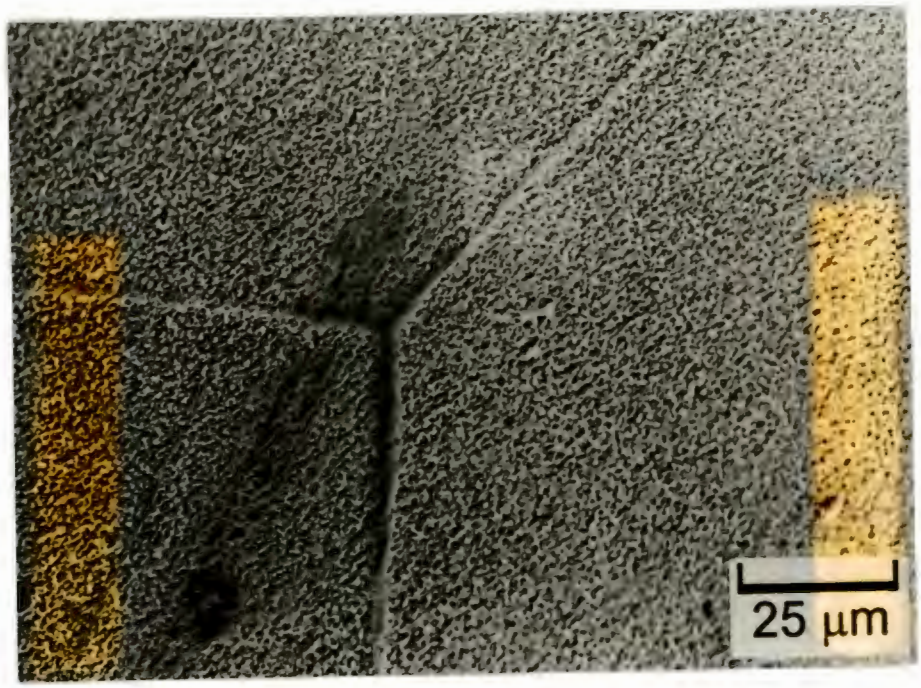


**Figure 5-17 Carbon deposition on the surface of an annealed, polished HNSS specimen after the fifth week of exposure.**

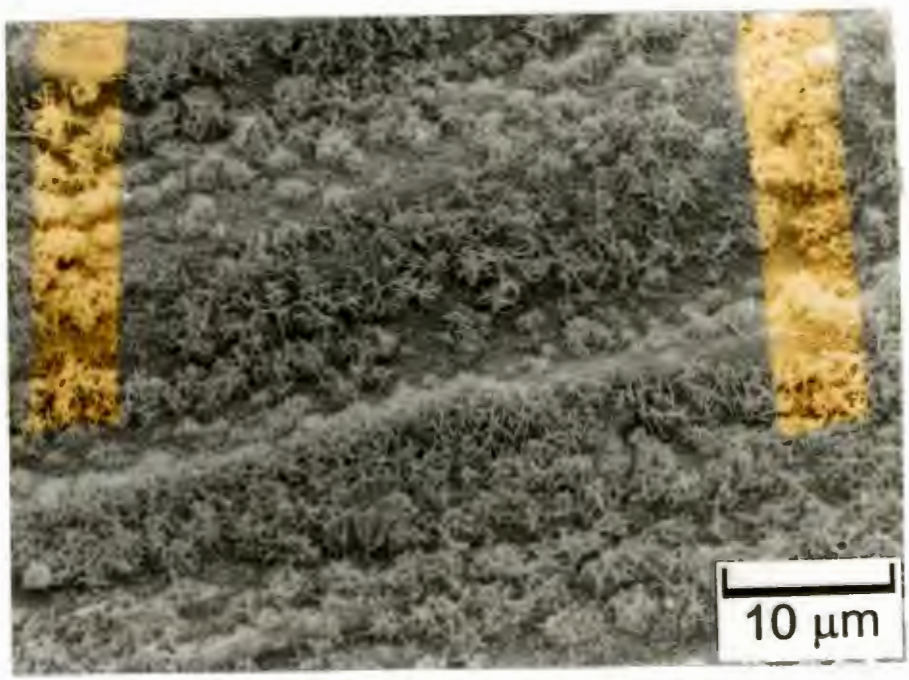


**Figure 5-18 Light carbon deposit on the surface of an as received, abraded 310 specimen after the fourth week of exposure.**

### 5.2.2 Surface pitting on the exposed 800H, 310 and HNSS specimens

The extent of pitting of the three alloys tested in the annealed, polished and the as received, abraded conditions is represented graphically in Figure 5-9. It can be seen in this diagram that alloys 800H and 310 suffered the most damage from pit formation and growth. Significant pit formation on the HNSS specimens only occurred after the ninth week of exposure, while the as received, abraded specimens of all three alloys showed negligible pitting damage.

Pitting of the two side surfaces of the 800H and 310 specimens was observed after 2 weeks of exposure to the metal dusting atmosphere. These pits were initially about 10 microns in diameter and occurred over a wide range of the surface (Figure 5-19 and Figure 5-20). On one 800H specimen a few larger pits of about 50 microns were present at the edge of the support hole (Figure 5-21). Figure 5-22 shows large regions of surface damage and pitting of a 310 specimen after 3 weeks. These areas of metal wastage were the only regions on the specimen surface that were covered by a carbon deposit. The side faces of the 800H and 310 specimens did not show any signs of pitting.

After the fifth week many large pits had formed on the surface of most of the 800H specimens (Figure 5-23). These were revealed when the large carbon protrusions growing from the pits were removed. Pits of a similar size were also present on some of the 310 samples after 5 weeks. However, the number of pits was much lower, occurring singly on these specimens (Figure 5-24).

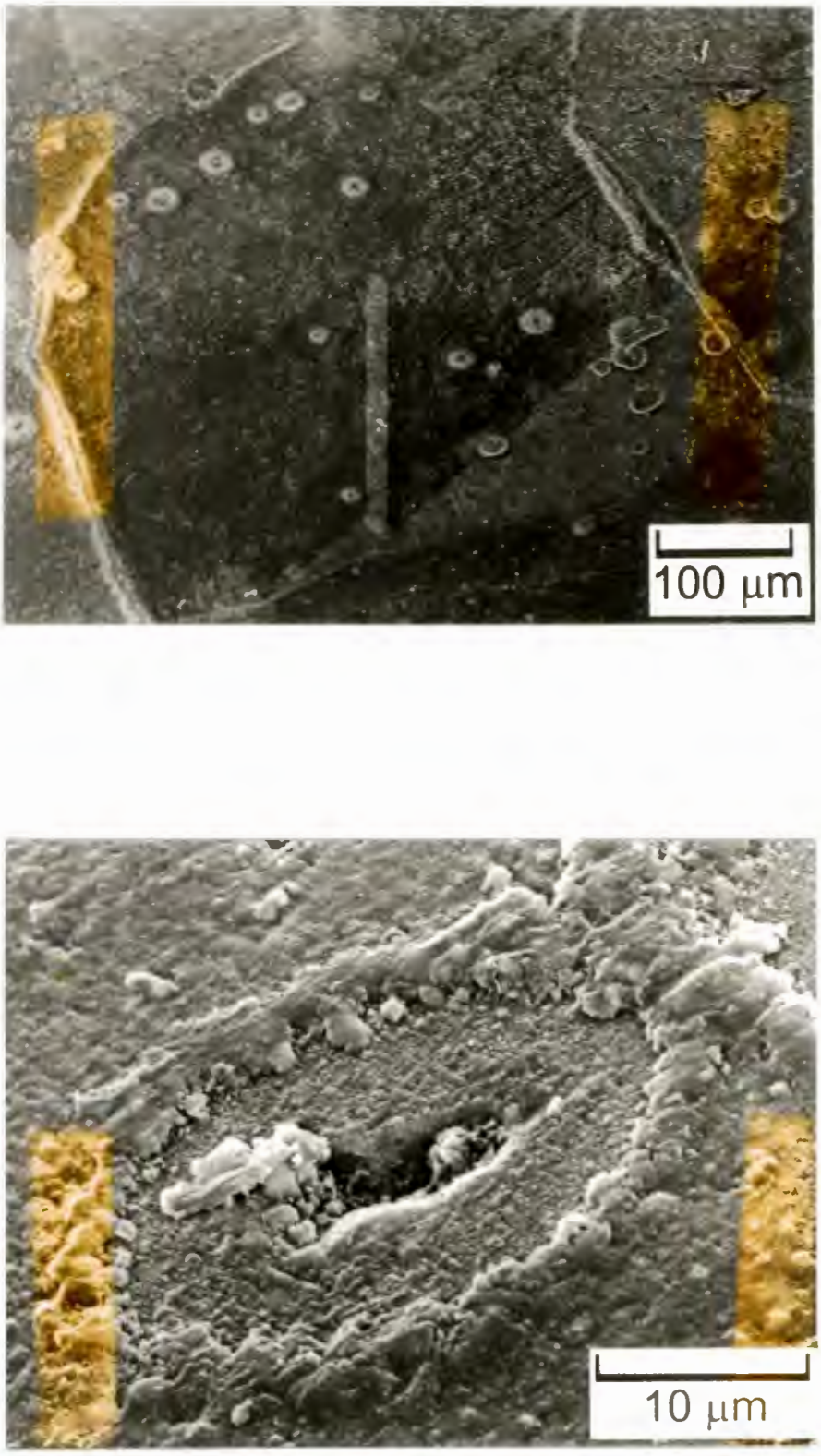


**Figure 5-19 Pitting on the surfaces of an annealed and polished 800H specimen after two weeks' exposure.**

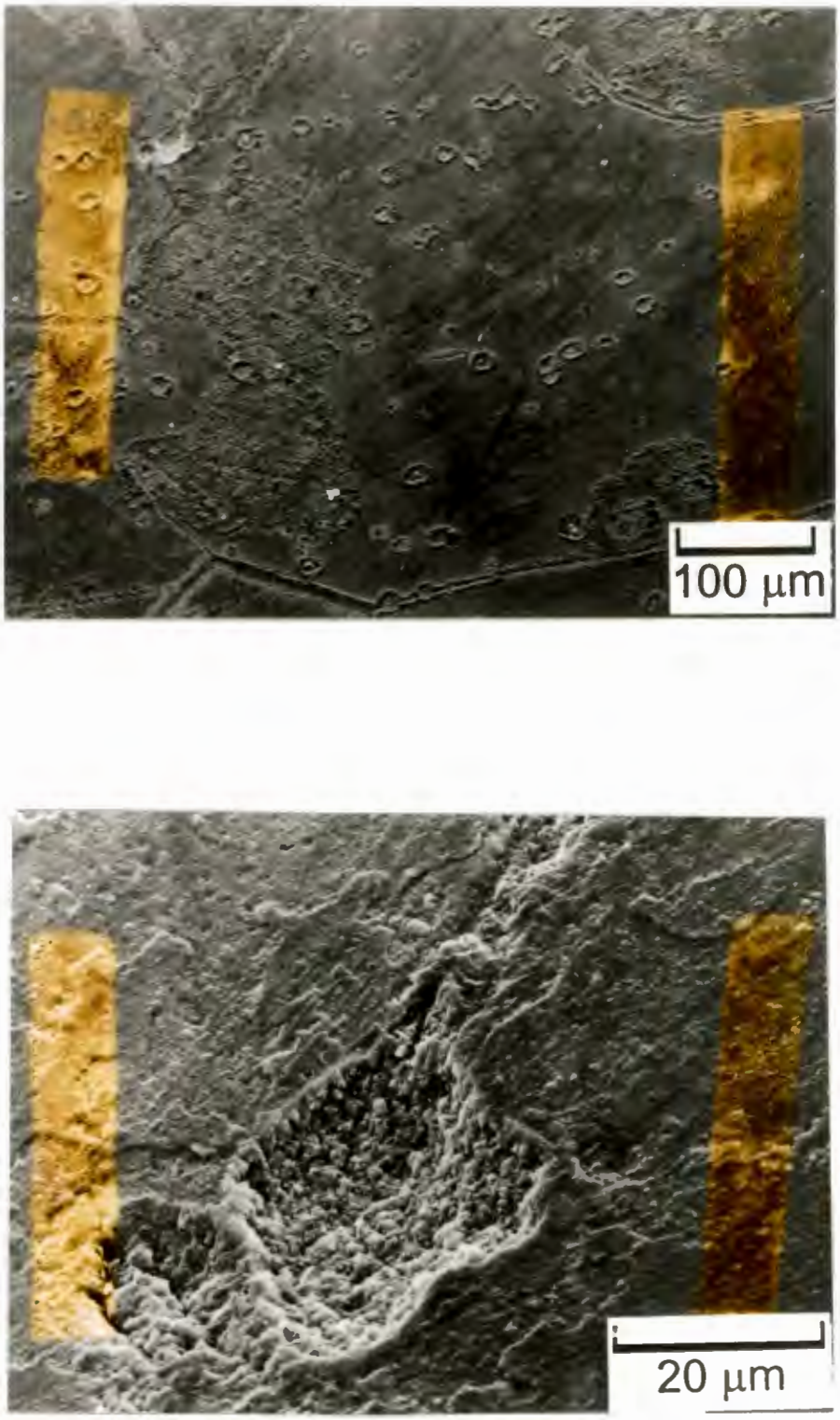


**Figure 5-20 Pitting on the surfaces of an annealed, polished 310 specimen after two weeks' exposure.**

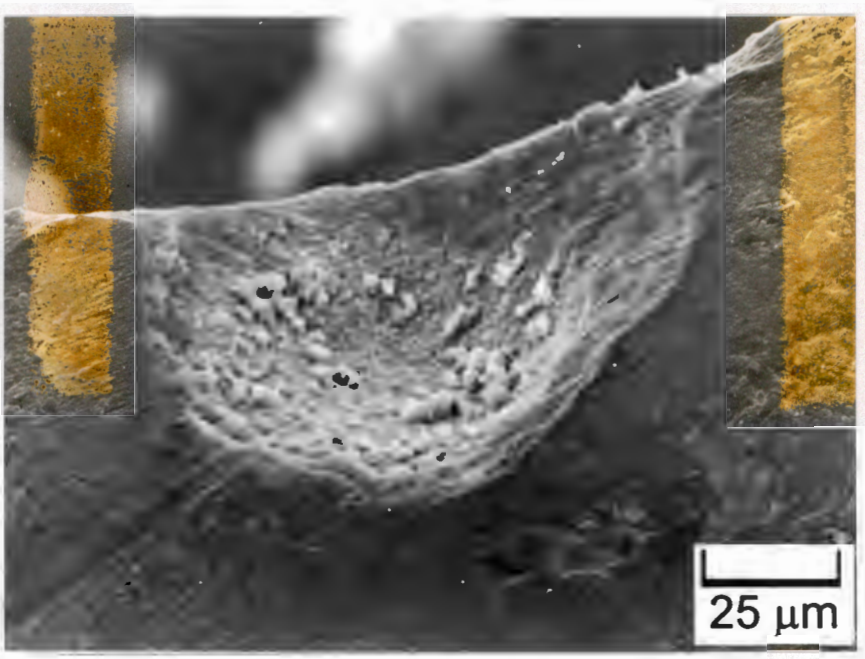


**Figure 5-21 Single, larger pit at the edge of the support hole of an annealed, polished 800H specimen after 2 weeks' exposure.**

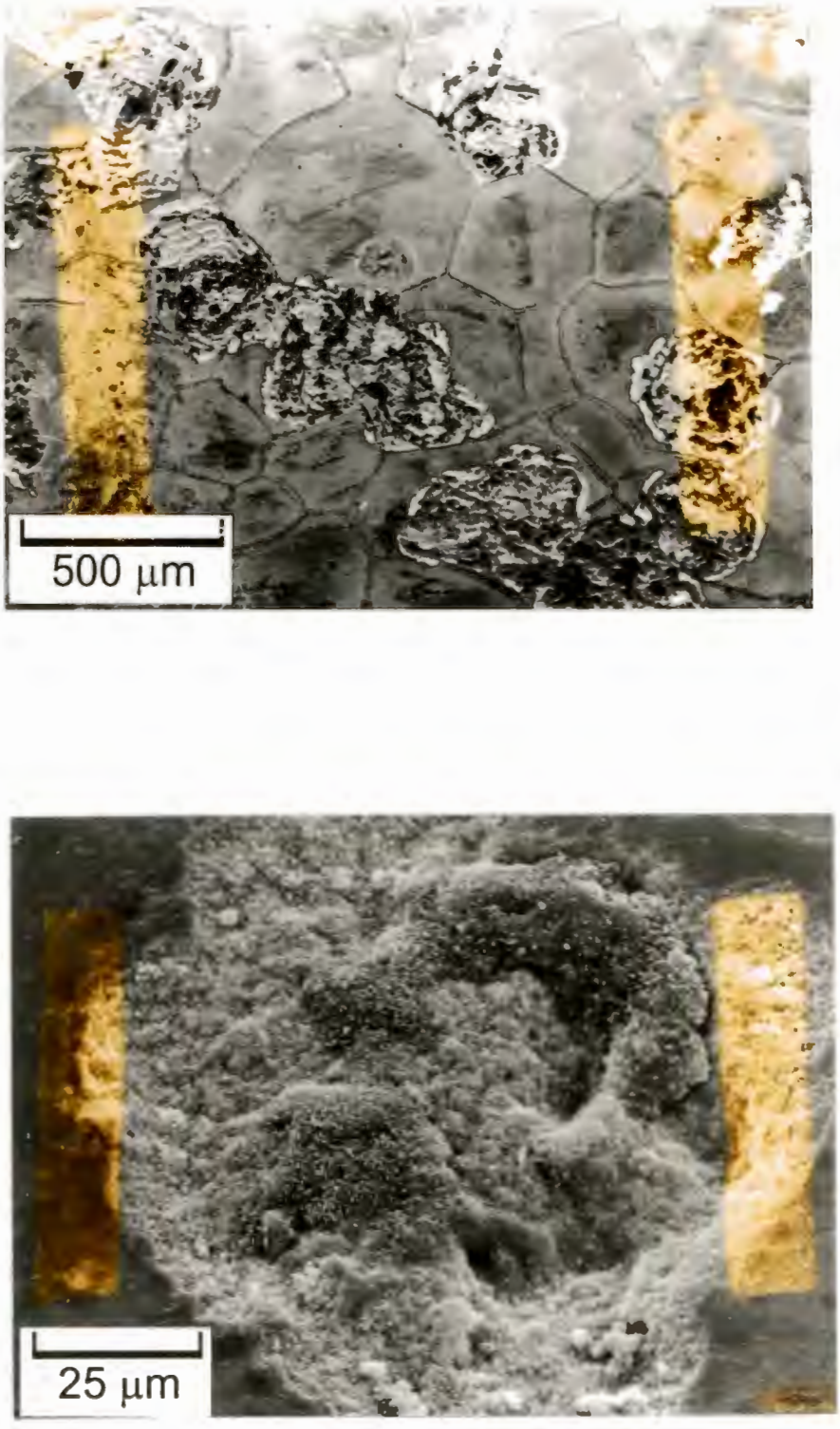


**Figure 5-22 Surface pitting of an annealed, polished 310 specimen after the third week of exposure.**

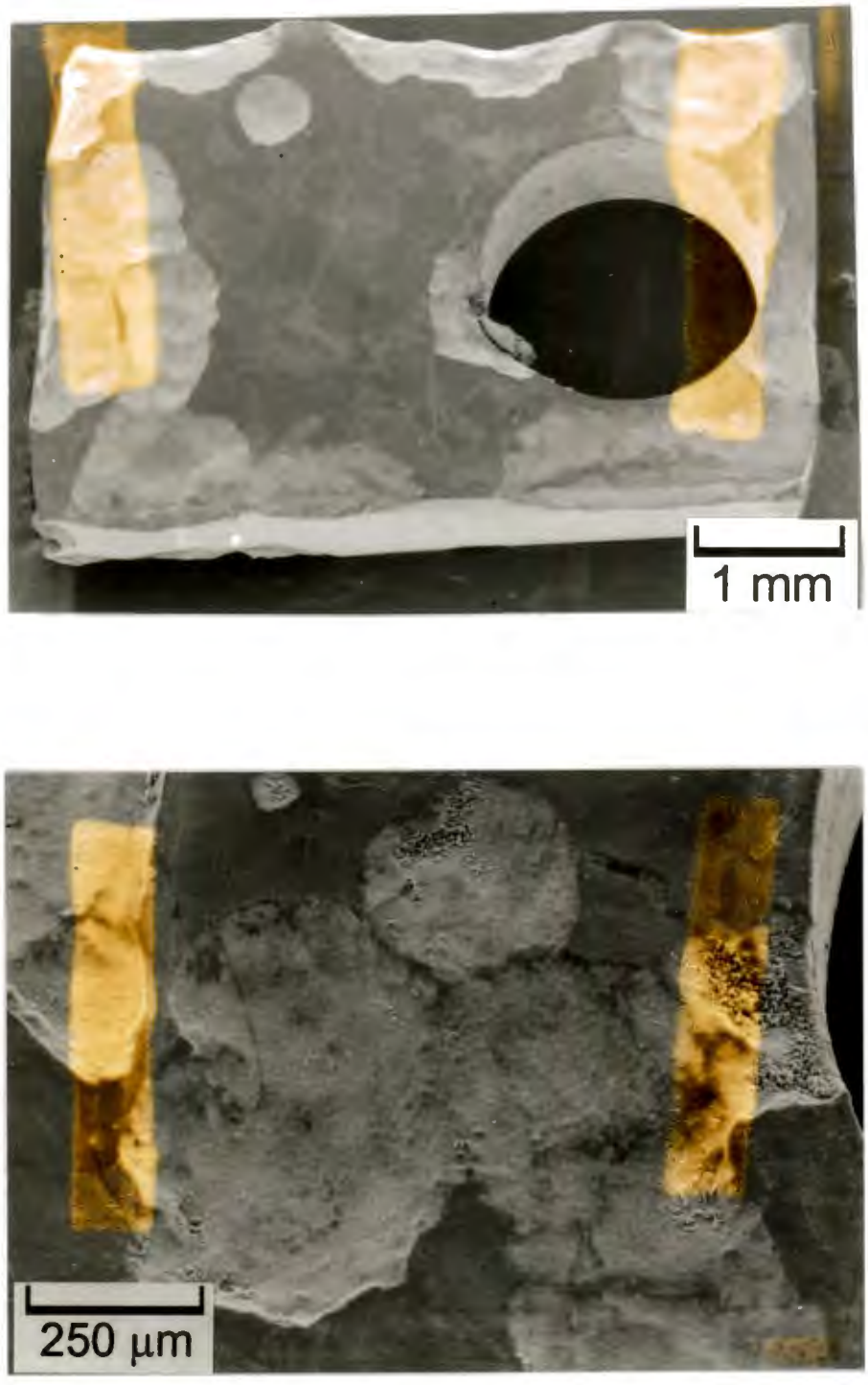


**Figure 5-23 Pitting of the surface of an annealed and polished alloy 800H specimen after 5 weeks.**

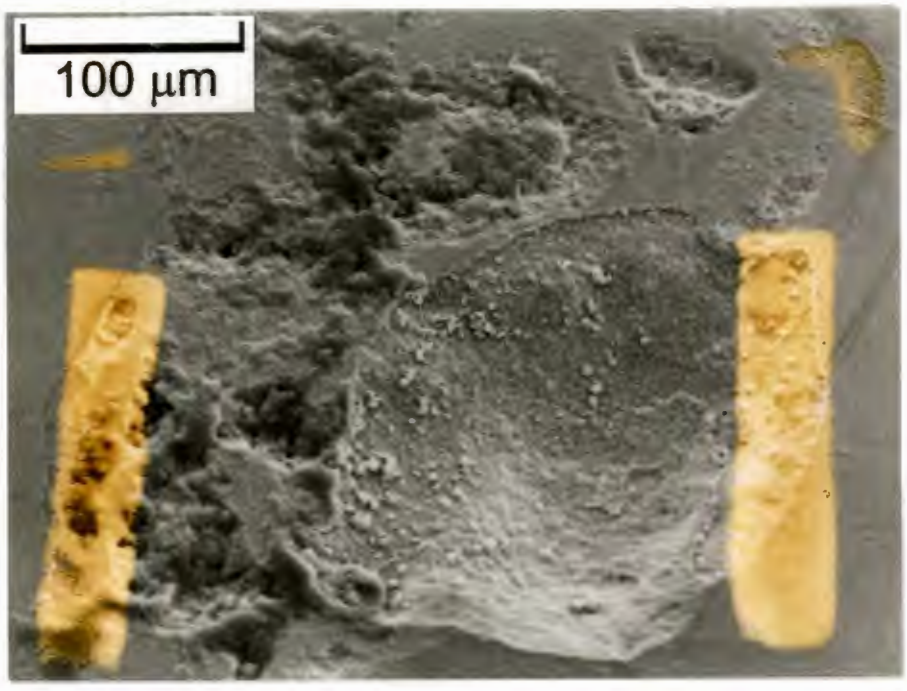


**Figure 5-24 Single pit on an annealed and polished 310 specimen after 5 weeks.**

The HNSS specimens showed a marked difference in the location of pitting compared to the 800H and 310 specimens. Pitting was observed only on the side faces of the specimens and not the main surfaces (Figure 5-25). The pits were about 10 microns in diameter, relatively deep and were found among small protruded regions, some of which had partially collapsed (Figure 5-26). A cross section of these pits is shown in Figure 5-27. Pitting of the main surfaces only occurred after 9 weeks of exposure and coincided with the onset of light carbon deposition. The size of the pits varied from about 10 microns to larger regions of metal loss of about 100 microns in diameter (Figure 5-28).

a)


b)

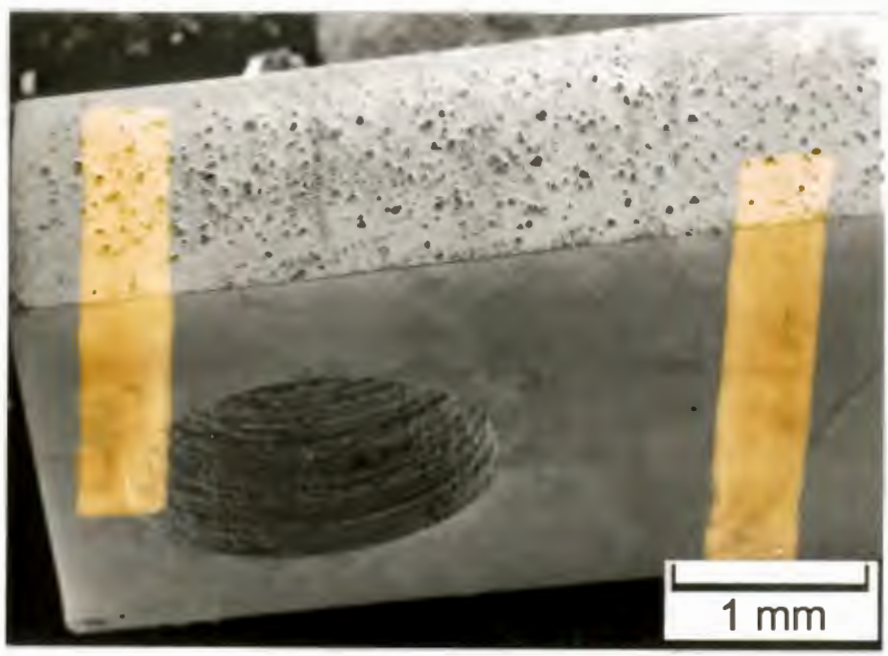


**Figure 5-25 Pitting on the side face of two annealed and polished HNSS specimens after 2 weeks (a) and 4 weeks (b).**

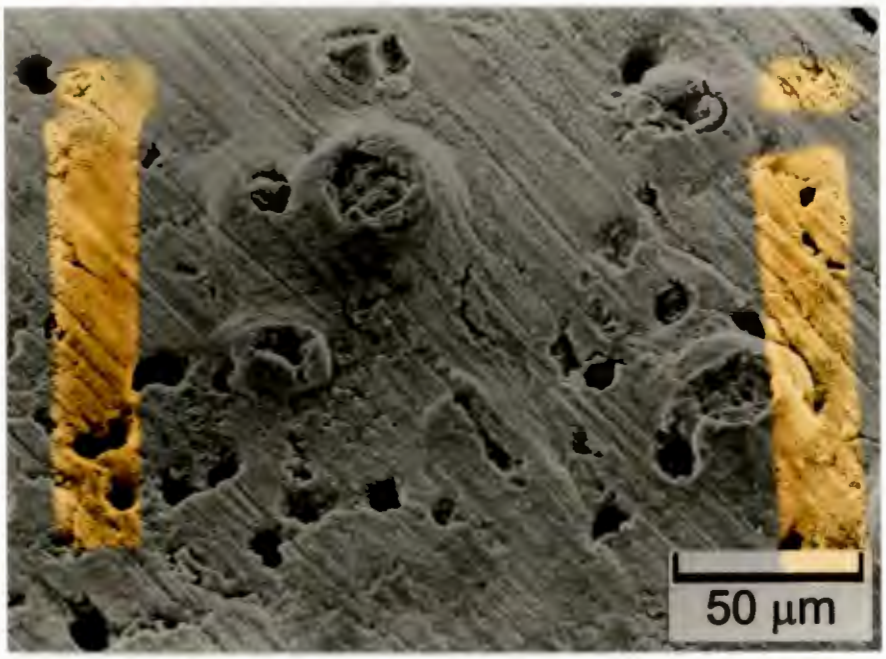


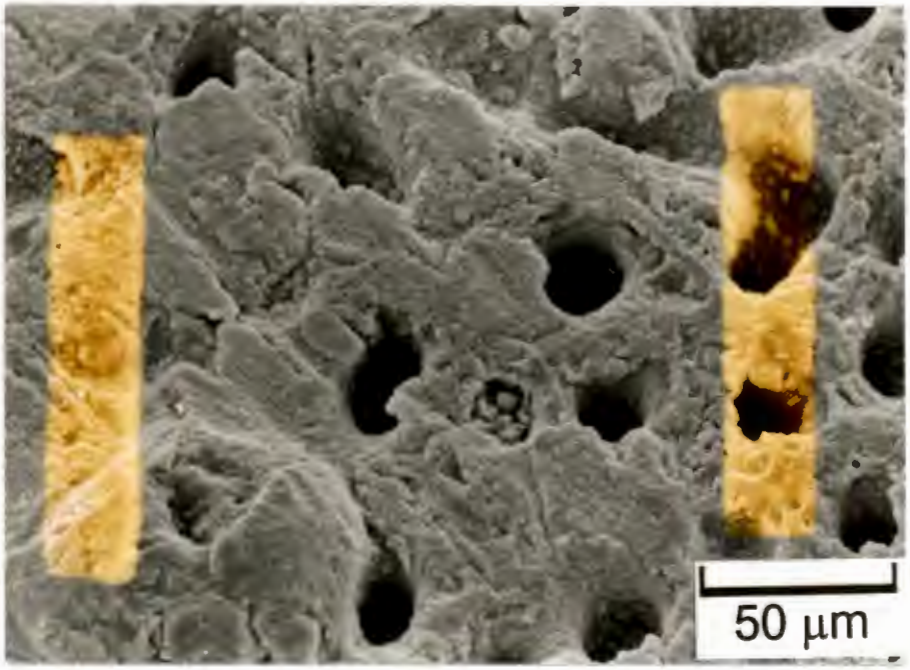


**Figure 5-26 Surface features on the side face of an HNSS specimen after 4 weeks' exposure.**

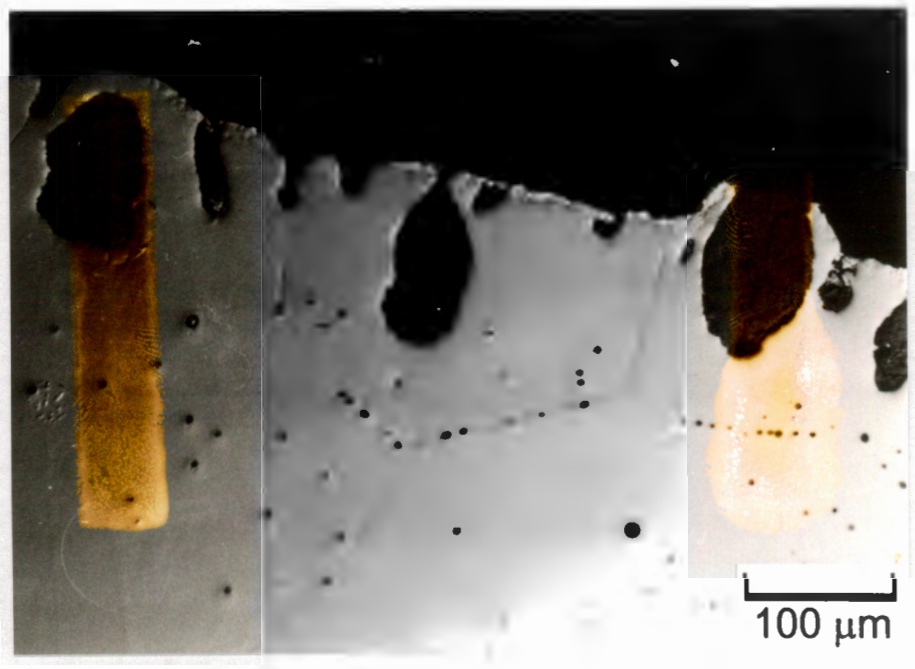


**Figure 5-27 Unetched cross section on an annealed, polished HNSS specimen. The pits in the micrograph have formed on the rougher edges of the specimen after 4 weeks of exposure.**

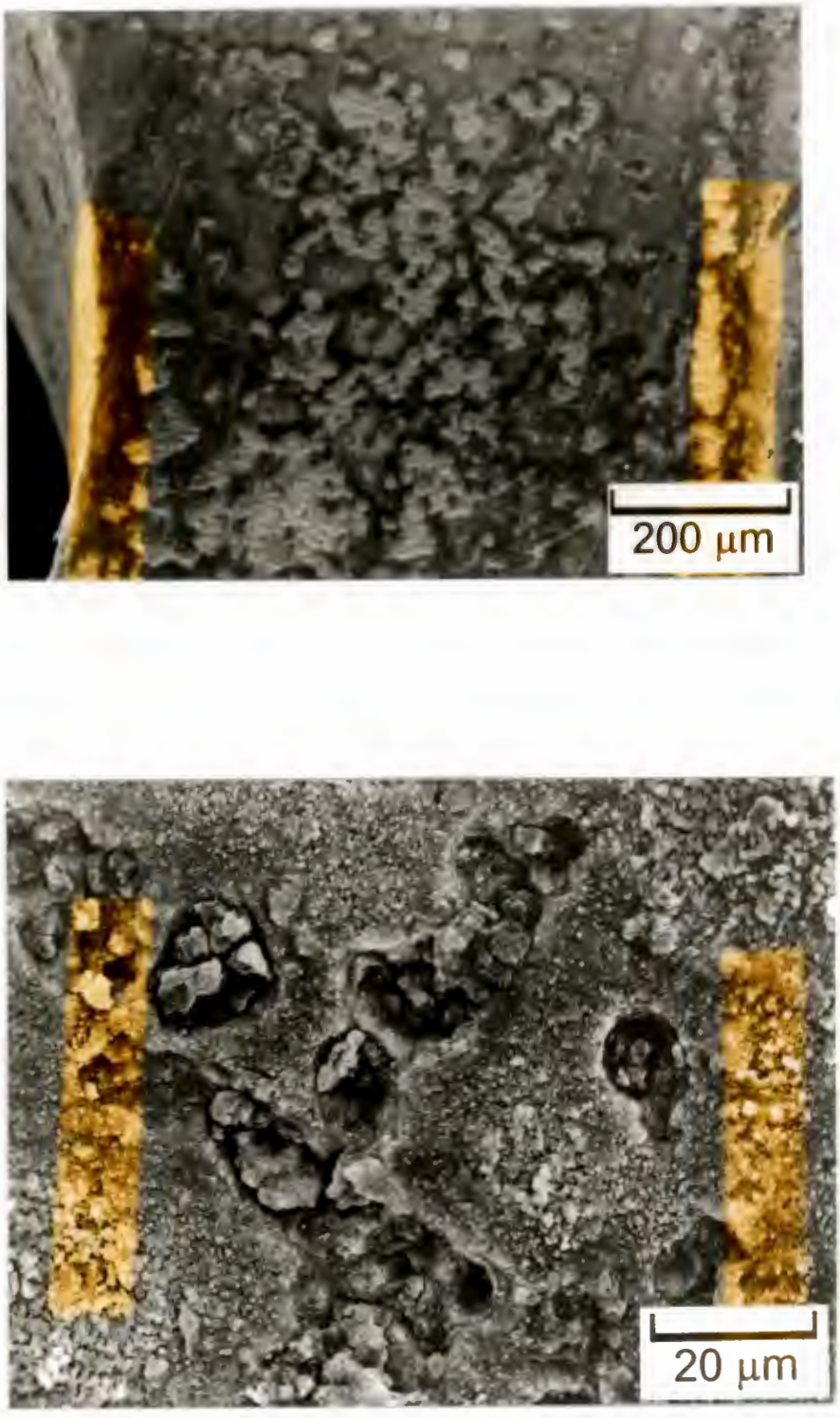


**Figure 5-28 Pitting of the main face of an annealed, polished HNSS specimen after 9 weeks.**

The extent of pitting of the as received and abraded specimens of alloy 800H was small. After 3 weeks only isolated pits of about 200 microns in diameter had formed (Figure 5-29). Pitting of the 310 and HNSS alloys was negligible (Figure 5-30).

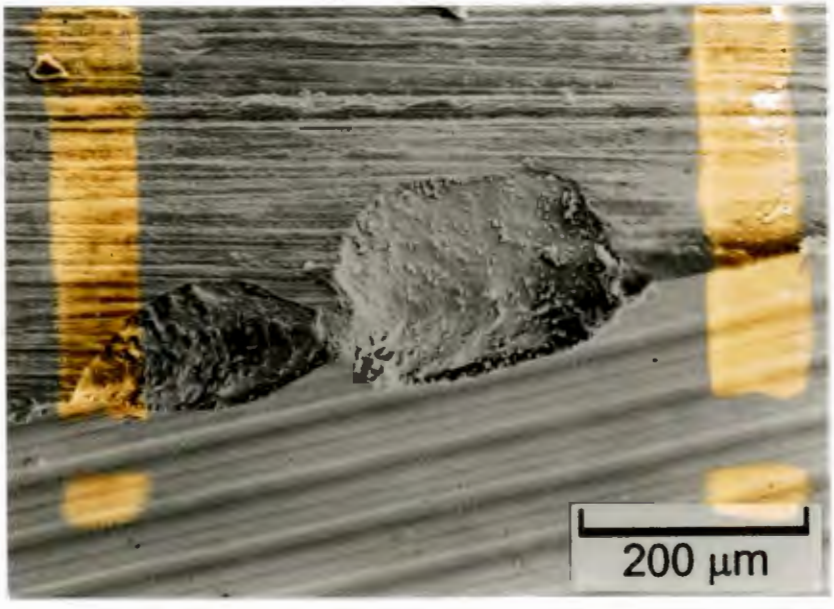


**Figure 5-29 Pitting at the edge of an as received, abraded specimen of alloy 800H after 3 weeks.**

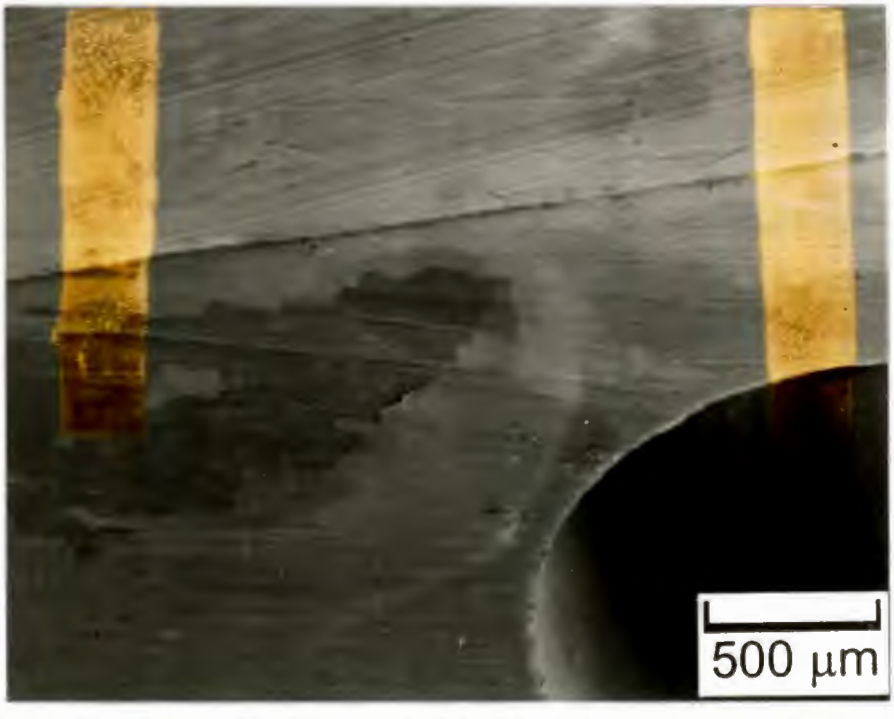


**Figure 5-30 Micrograph of an as received, abraded HNSS specimen after five weeks. No pitting has occurred at the surface.**

### 5.2.3 Results of specimen mass change measurements

The average specimen mass changes for the three alloys are presented in Figure 5-31. From this graph the following observations are made:

1. Specimens of Alloy 800H and AISI 310 in the annealed and polished condition show a gain in mass during the first 500 hours. The rate and amount of mass gain for alloy 800H is approximately four times higher than that for alloy 310. Specimens of HNSS do not show an appreciable increase in mass during the exposure.

2. For alloys 310 and 800H the initial period of mass increase is followed by mass loss. This begins after about 200 and 220 hours respectively. While the 800H specimens suffered heavy mass loss after about 550 hours, the other two alloys showed comparatively little loss in mass. The 310 specimens reach a stage of zero net mass change at the same time as the 800H specimens - after about 500 hours. However, for 310, subsequent mass loss is more constant and gradual, reaching a value of 3.4 $\mu g/mm^2$ after 1125 hours - an order of magnitude less than the 800H specimens. The mass loss of HNSS is negligible after 1300 hours.

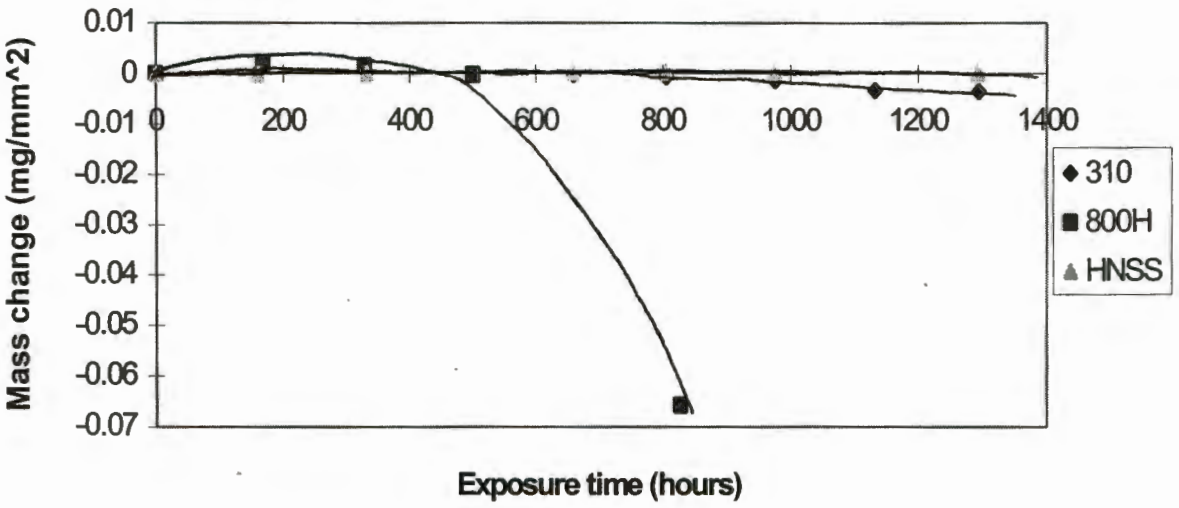


**Figure 5-31 Cumulative mass change per unit surface area vs. exposure time for annealed and polished specimens of alloy 800H, 310 and HNSS.**

The large amount of mass loss of the 800H specimens after the fifth week of exposure coincided with the removal of the heavy carbon deposit that exposed large pits on the specimen surface. Removal of the carbon deposit on the 310 specimens also resulted in some metal loss as smaller pits were exposed. Carbon deposition and pitting was absent from the HNSS and all as received, abraded specimens and no mass loss was recorded.

Figure 5-32 shows comparative plots between the annealed and polished specimens and the as received and ground specimens for the three alloys. For alloys 800H and 310, the as received and ground specimens show much smaller mass changes than the annealed and polished specimens. The opposite is true, however, for the HNSS specimens with the as received, abraded specimens showing higher rates and amounts of mass gain and then loss.

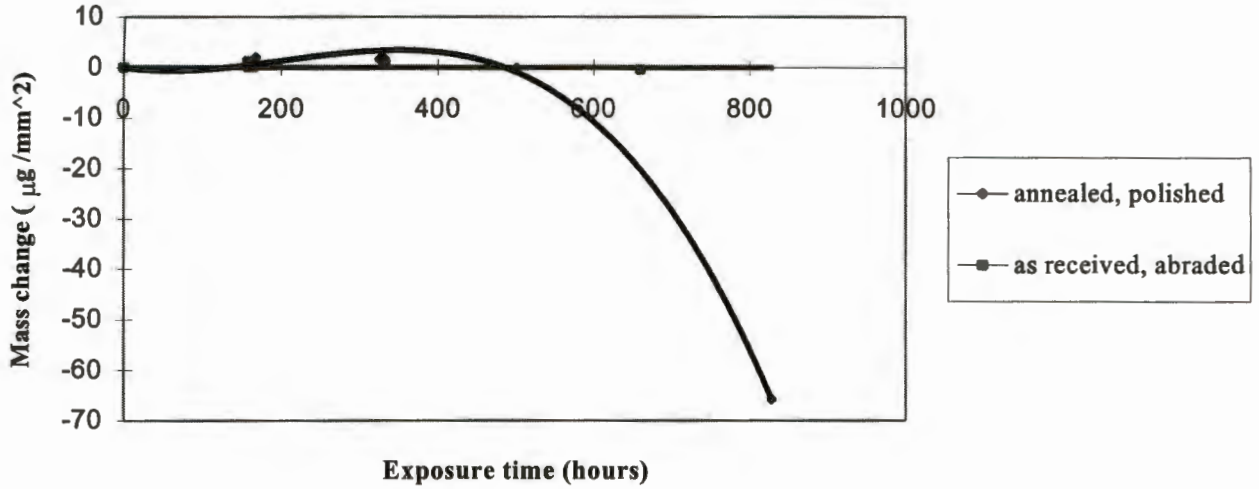


a)

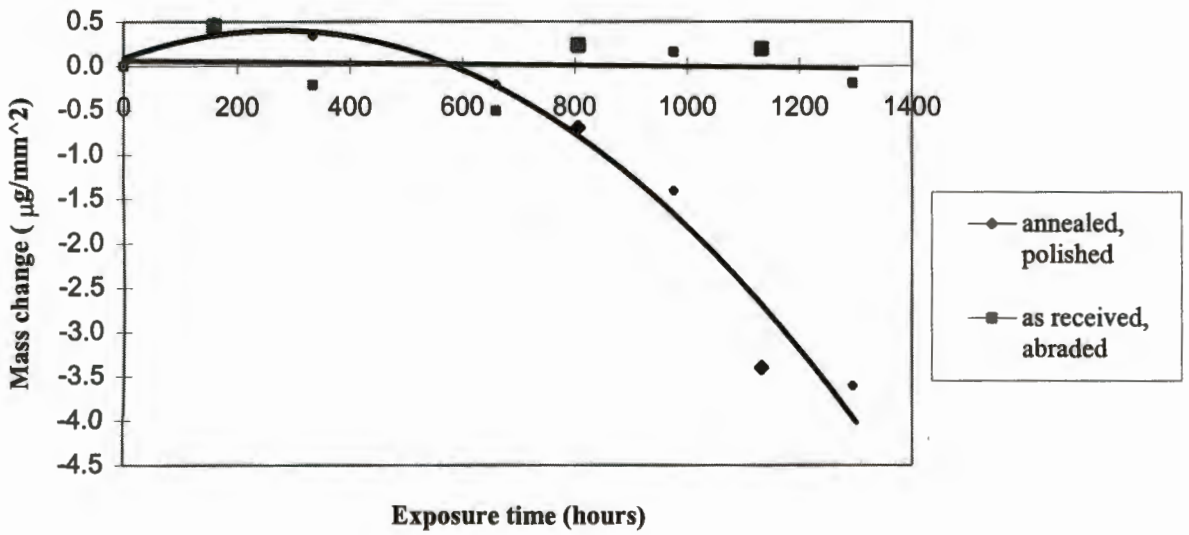


b)

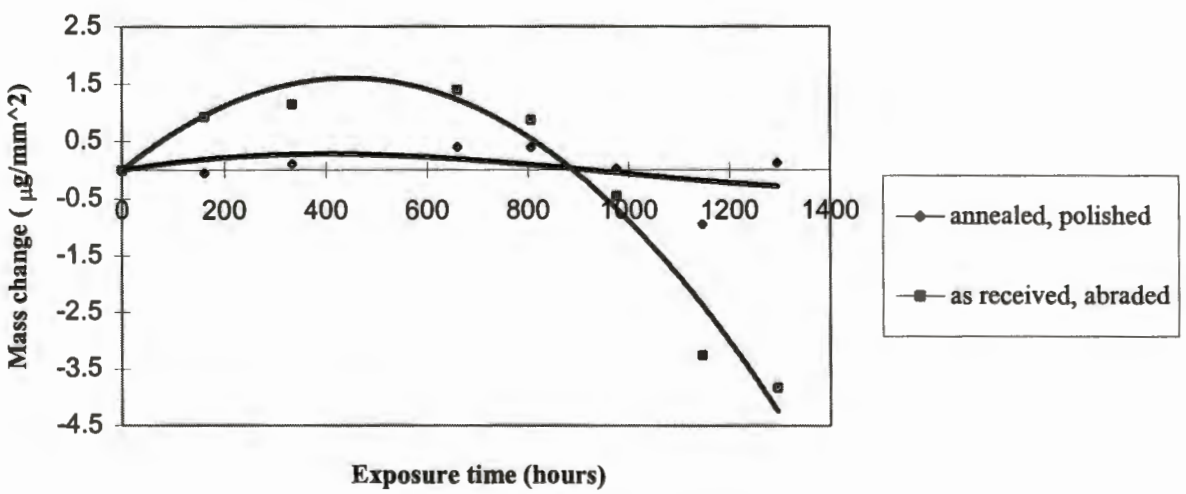


c)

**Figure 5-32 Specimen mass change curves for a) alloy 800H, b) AISI 310 and c) HNSS showing the difference in mass change for as received, abraded specimens and annealed, polished specimens.**

## 5.2.4 Metallographic examinations of specimen taper sections

**Annealed, polished alloy 800H specimens**

Internal carburisation of the 800H specimens occurred during the first week of exposure. The extent of carburisation, visible as the dark areas in Figure 5-33, was revealed by electrolytic etching in oxalic acid. The carburised areas are located mainly at the corners of the specimen. This corresponds with the location of the carbon protrusion, shown in Figure 5-10a, which grew from the lower corner of the same sample.

Figure 5-34 shows a carburised region near the hole that was drilled to suspend the specimen. These micrographs show the loss of material through the formation of a pit at the surface of the hole. The etching has revealed the presence of a heavily carburised band at the surface of the pit . Below this band is a region of carburisation in which fine carbides have precipitated. This region extends inwards along the grain and twin boundaries and slip lines, indicating preferential carbide precipitation along these zones. Beneath this inner carburised layer is a region in which large needle-like carbides have precipitated along preferred crystal planes. These precipitates become sparser with increasing depth into the specimen as the unaffected matrix is reached.

SEM micrographs of the area shown in Figure 5-34 illustrate these regions more clearly (Figure 5-35). Visible in these micrographs are regions of homogeneous chromium carbide precipitation within the grains. The grain boundaries are characterised by large chromium carbides surrounded on either side by regions of chromium-depleted matrix. These denuded zones have been heavily carburised, resulting in the possible precipitation of iron carbides, which signify the onset of metal dusting. The similarity in appearance of the grain boundary and surface regions indicates that metal dusting has proceeded preferentially at the surface and along the grain boundaries.

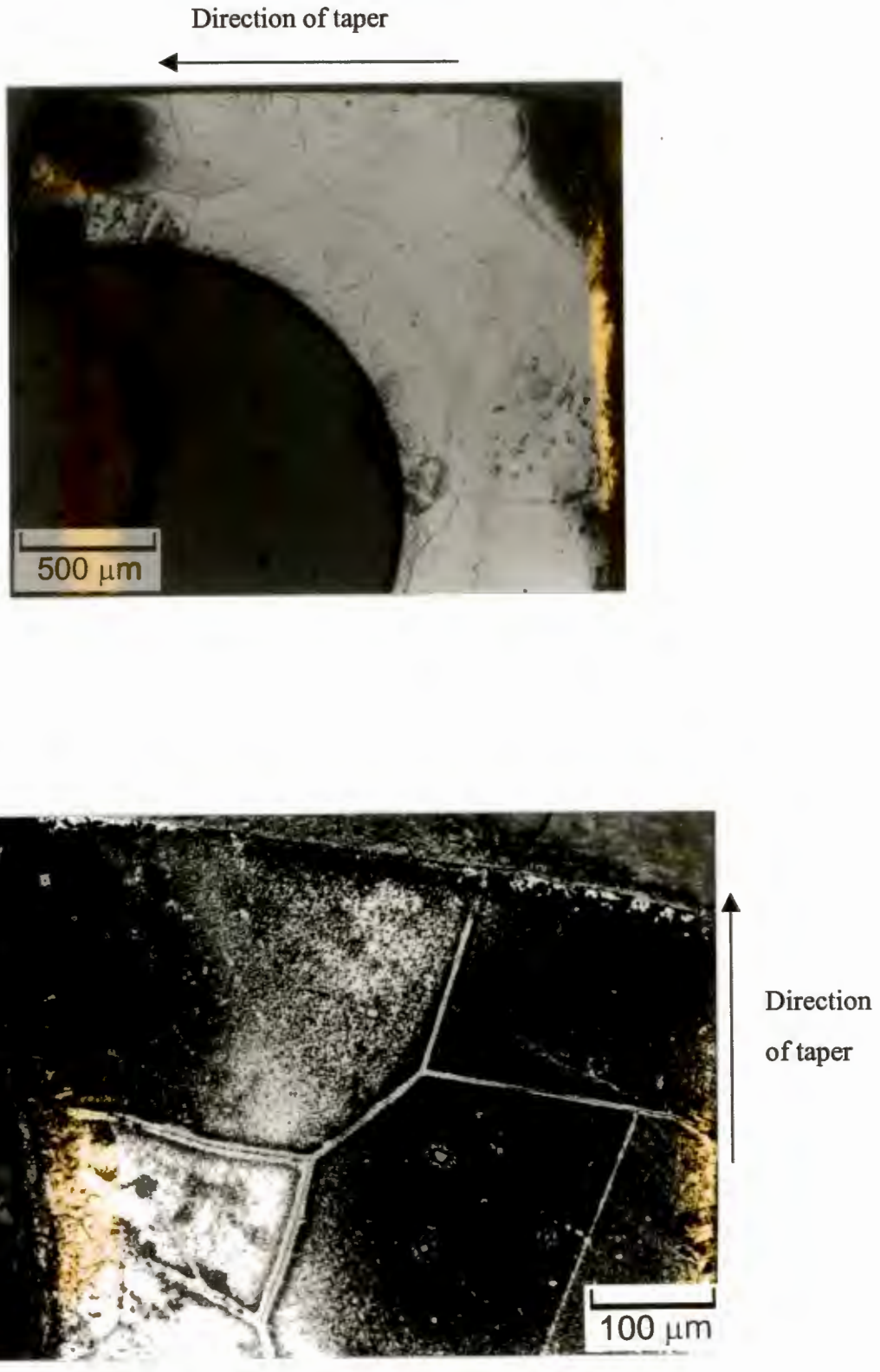


**Figure 5-33 Two views of a taper section of an annealed, polished alloy 800H specimen after 1 week. Carburisation has resulted in carbide precipitation at the corners of the specimen. Etched in oxalic acid.**

a)

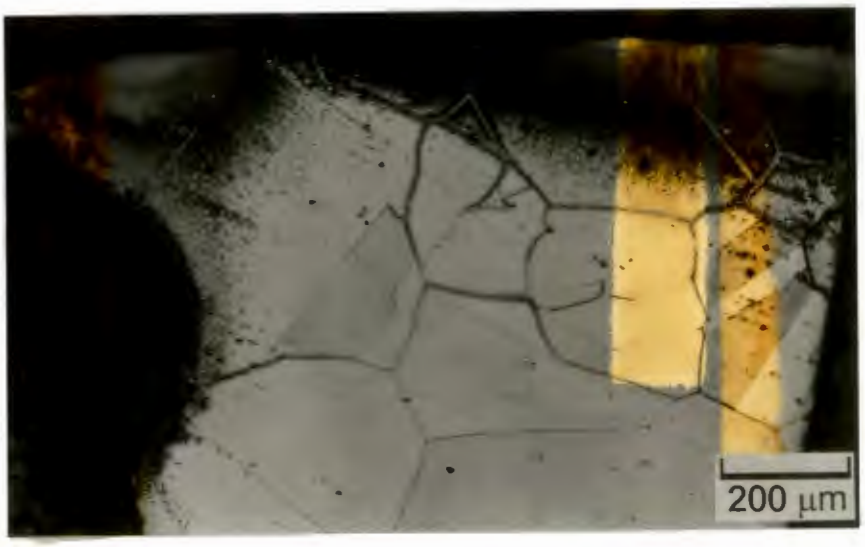


b)

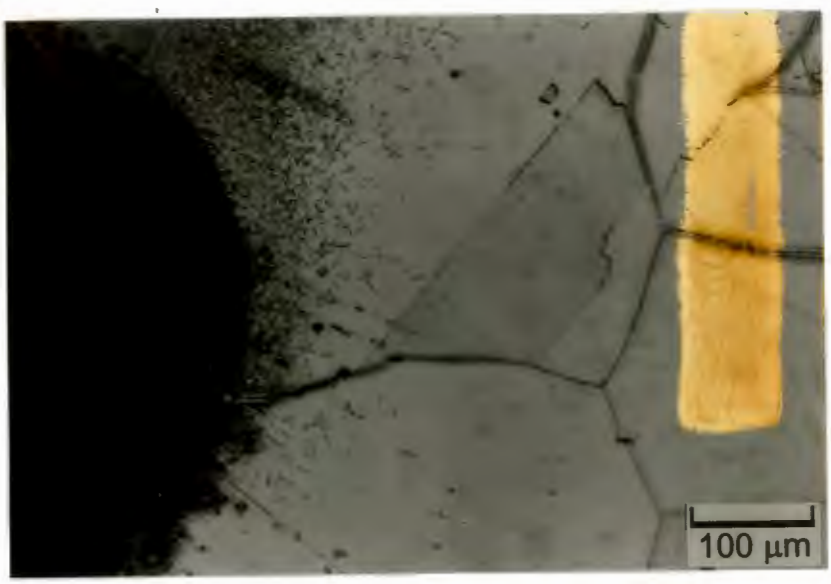


**Figure 5-34 Taper section through a pit on an annealed, polished 800H specimen after two weeks' exposure. Figure b) shows regions of metal degradation and carburisation surrounding the pit. Etched in oxalic acid.**

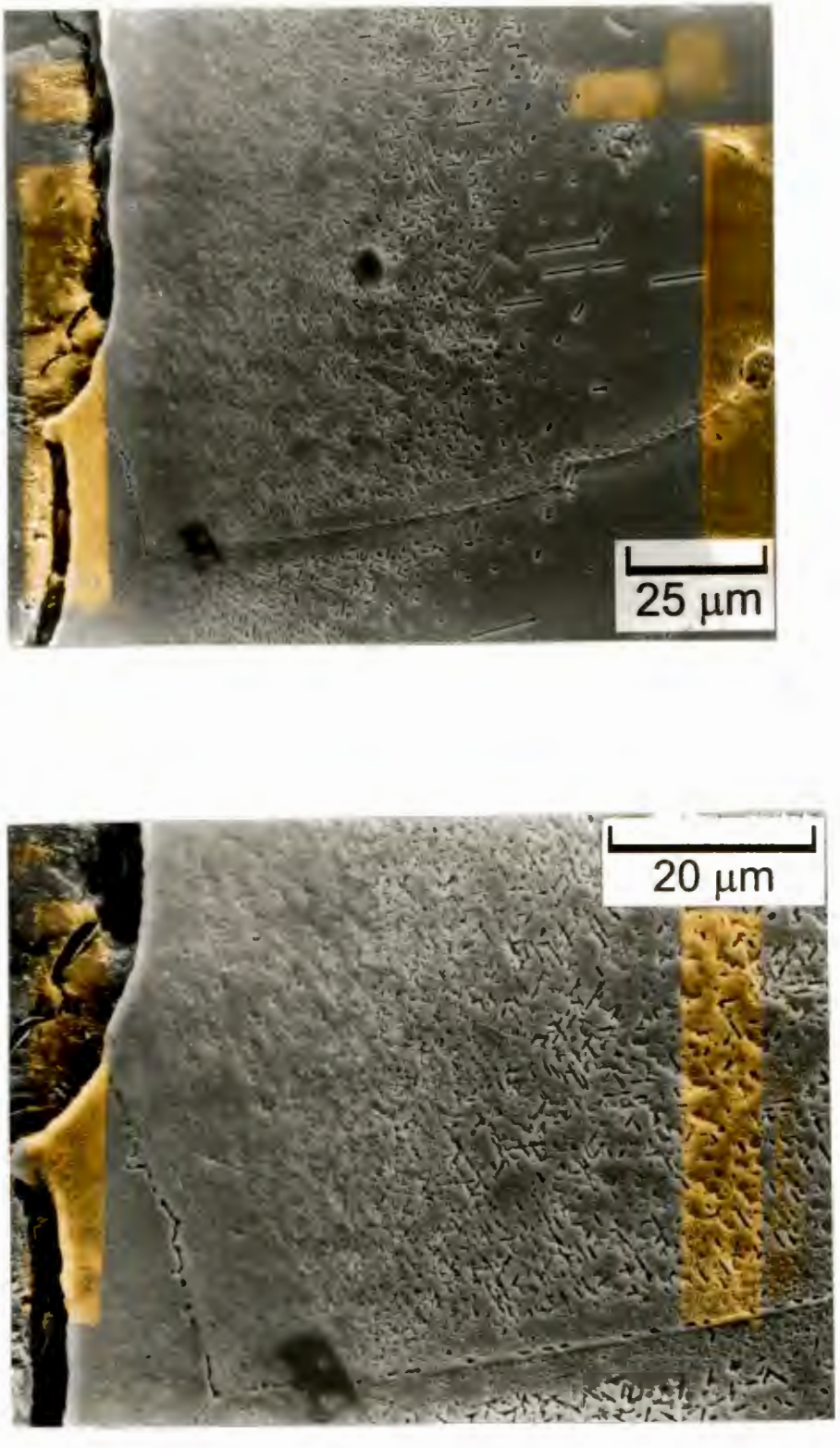


**Figure 5-35 Regions of chromium carbide precipitation and metal degradation beneath a pit at the surface of an alloy 800H specimen after 2 weeks' exposure.**

The results of microhardness measurements through a carburised and pitted region are shown in Figure 5-36. The hardness increases in the region of carbide precipitation and then decreases in the region where the alloy has become supersaturated with carbon and has started to disintegrate.

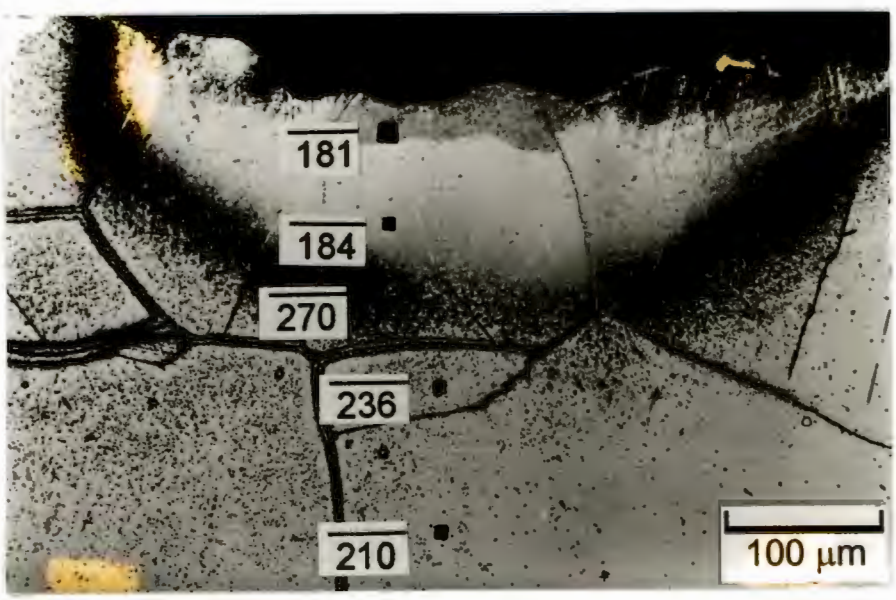


**Figure 5-36 Microhardness values (Vickers hardness) at various points in the carburised region beneath a pit in alloy 800H. The specimen was tested in the annealed and polished condition for 5 weeks.**

A taper section of a specimen exposed for five weeks, shown in Figure 5-37, indicates the increase in extent of carbide precipitation when compared with the specimen in Figure 5-33. Figure 5-38 shows pitting damage and carburisation along crystal planes at the lower edge of the specimen.

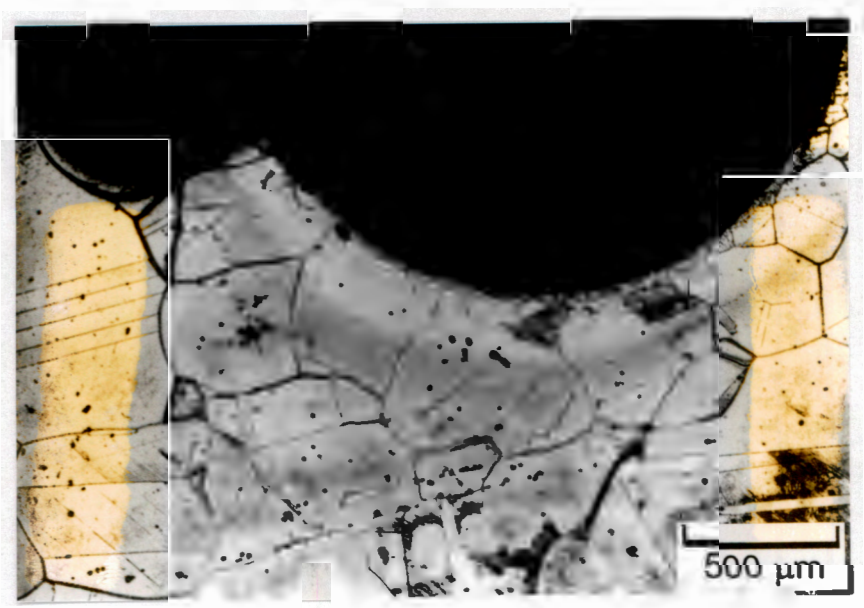


**Figure 5-37 Taper section showing carbide precipitation at the surface and near the support hole of an annealed, polished alloy 800H specimen exposed for 5 weeks.**


**Figure 5-38 Inhomogeneous precipitation of carbides along dislocations at the lower edge of an annealed, polished 800H specimen (5 weeks).**

The effectiveness of an oxide scale in preventing carburisation and metal dusting is illustrated in the series of micrographs shown in Figure 5-39. The area photographed is the region surrounding the hole drilled into the specimen for the supporting rod. Air-cooling of the specimen after the pre-test annealing treatment has resulted in the formation of a thick oxide scale at the surface. This scale was removed from the main surfaces of the specimen during the subsequent polishing. However, on the inside surface of the supporting hole the scale is left intact. This oxide layer is visible at the surface of the specimen in Figure 5-39 a. It is evident that carburisation and pitting of the specimen has occurred at the places where this scale has been damaged. Where the scale has remained intact the specimen shows no sign of carburisation.

A backscattered electron image of this region shows the increased carbon content of the zone immediately beneath the pit (Figure 5-40). Iron particles have separated from the matrix and can be seen in the carbon deposit. EDS analysis of the oxide layer showed that it was made up primarily of chromium but also included small amounts of titanium, silicon, aluminium and iron.

a)

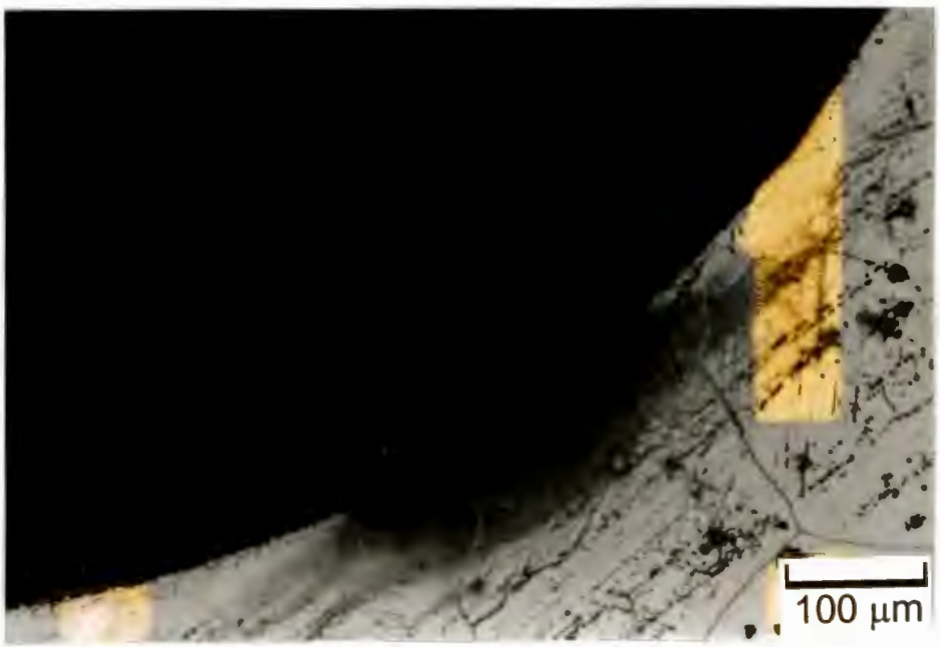


b)


**Figure 5-39 a) and b) Surface pit on an annealed and polished alloy 800H specimen after 4 weeks. No carbide precipitation has occurred where the oxide scale has remained intact.**

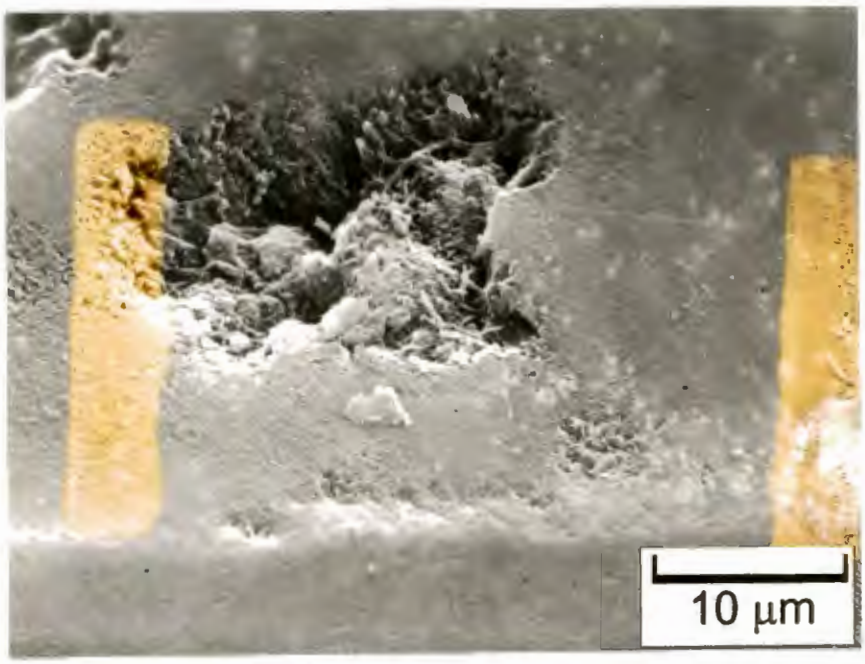


**Figure 5.39 c) Metal deterioration in a heavily carburised region of an annealed and polished 800H specimen after 4 weeks.**

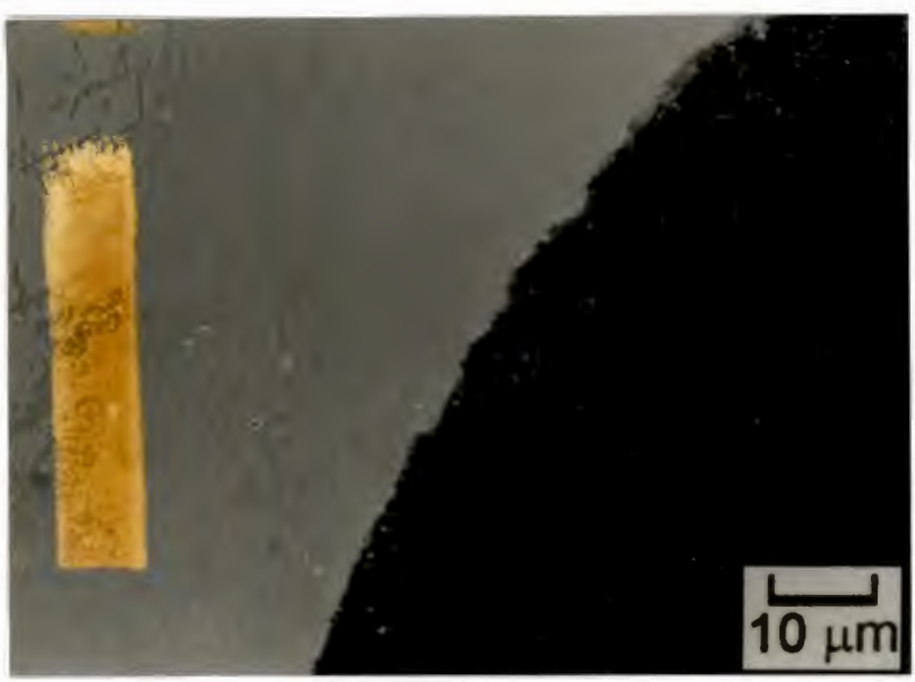


**Figure 5-40 Backscattered electron image of a pit at the surface of an annealed and polished 800H specimen. The dark region at the right of the micrograph is the carbon deposit. The bright spots in this region are iron particles, which have been removed from the specimen by metal dusting.**

**As received, abraded 800H specimens**

A taper section of an as received, abraded specimen is shown in Figure 5-41. The dark regions of carburisation, which are visible in the previous micrographs, are absent. There is also no evidence of surface damage by pit formation. A high density of grain boundaries and dislocations near the surface is visible.

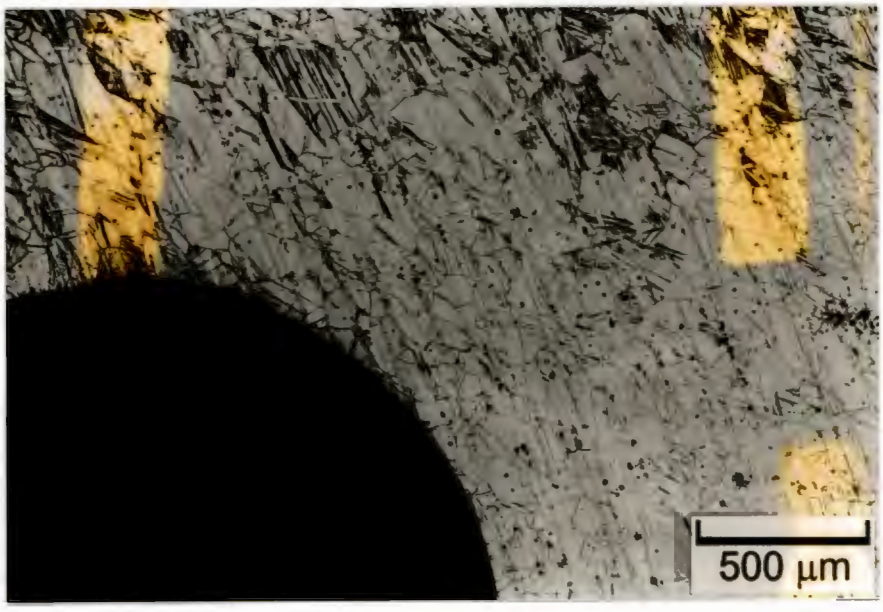


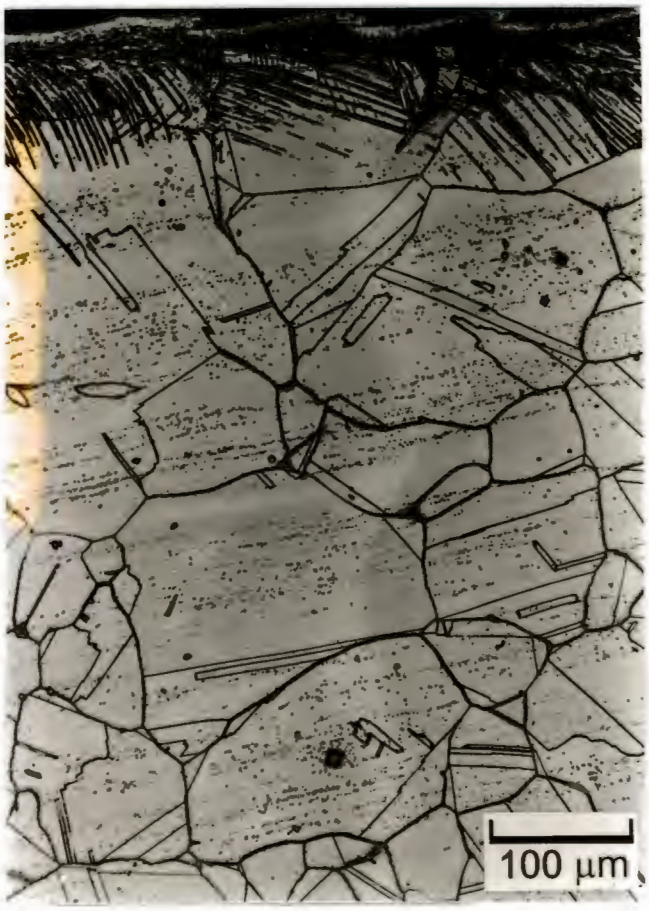


**Figure 5-41 Taper section of an as received, abraded 800H specimen after 4 weeks' exposure. Etched in oxalic acid.**

**Annealed, polished alloy 310 specimens**

Fifteen-degree taper sections of the 310 specimens show features of carburisation similar to those observed on the 800H specimens (Figure 5-42). However, the extent of carburisation is generally less than that in the 800H specimens. Carbides have again precipitated along dislocations and the grain boundary regions have been carburised more quickly than the surrounding matrix (Figure 5-42b).

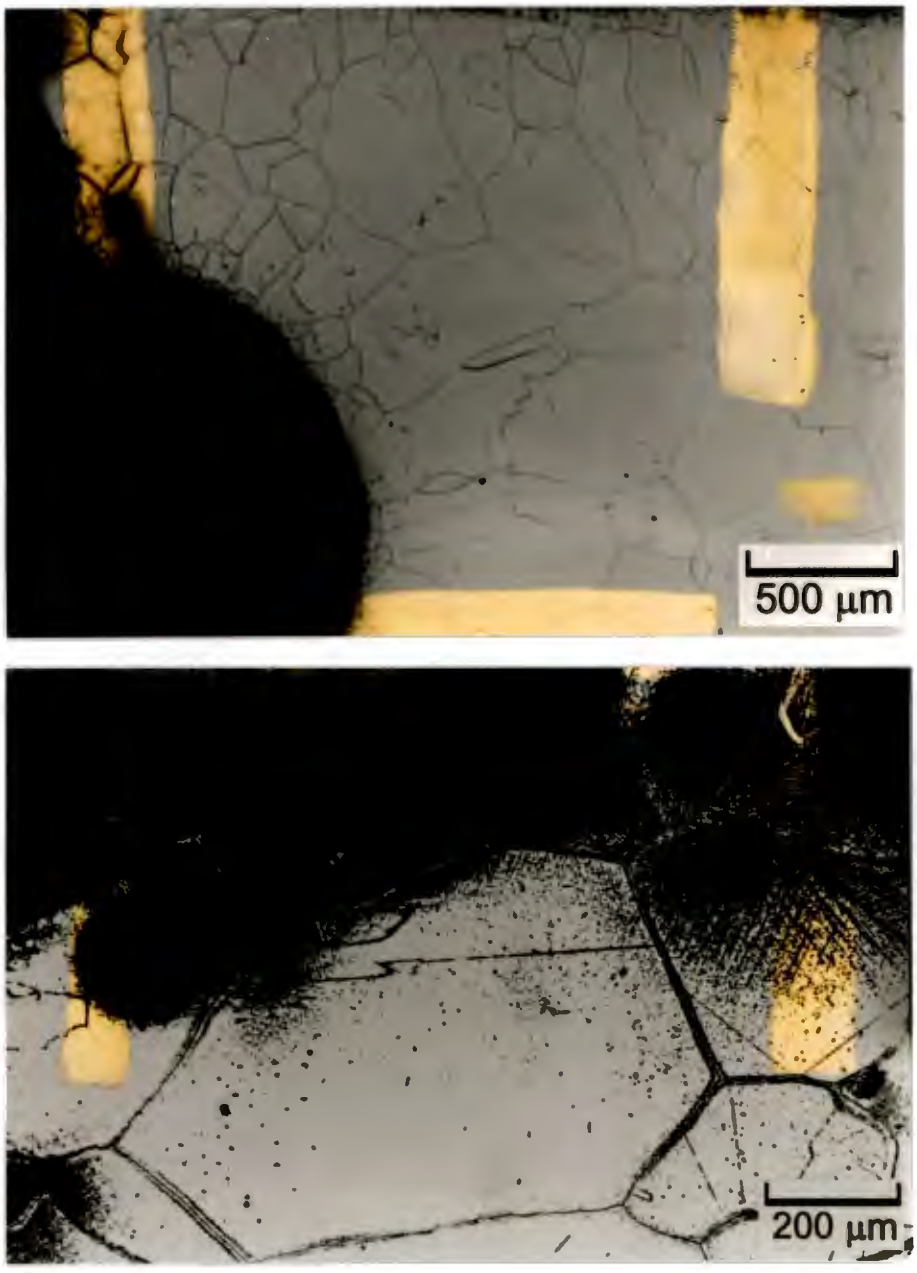


**Figure 5-42 Carburised regions of an annealed, polished 310 specimen after 2 weeks' exposure. Etched in oxalic acid.**

After seven weeks carburisation has still taken place in localised regions only (Figure 5-43). The three distinct areas of heavy carburisation, fine carbide precipitation and unaffected matrix are again visible. Figure 5-44 shows two optical micrographs of a pitted region before and after etching. The precipitation of carbides along the grain boundaries is visible even in an unetched condition.

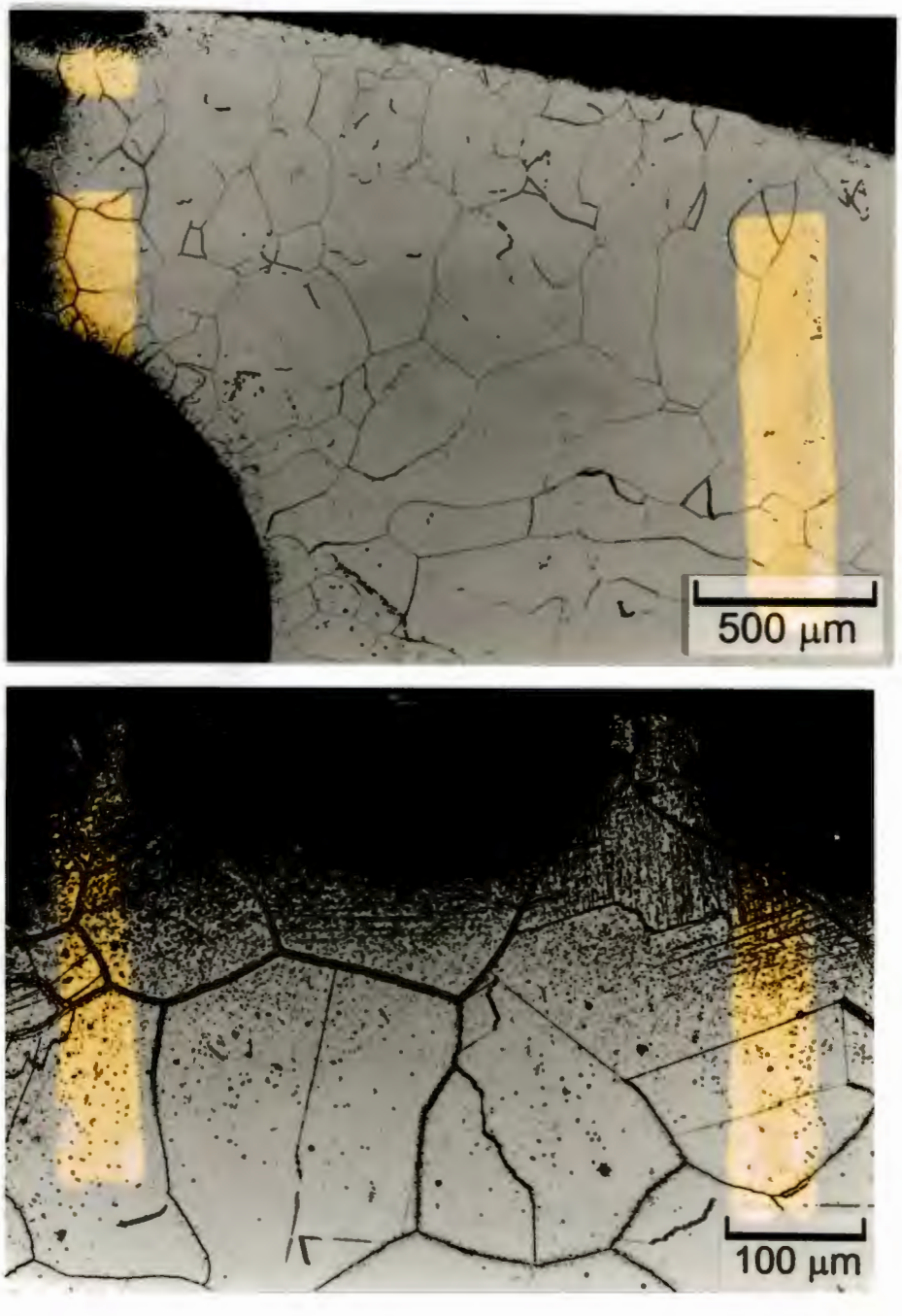


**Figure 5-43 Carburised regions of an annealed, polished alloy 310 specimen after 7 weeks' exposure. Etched in oxalic acid.**

a)

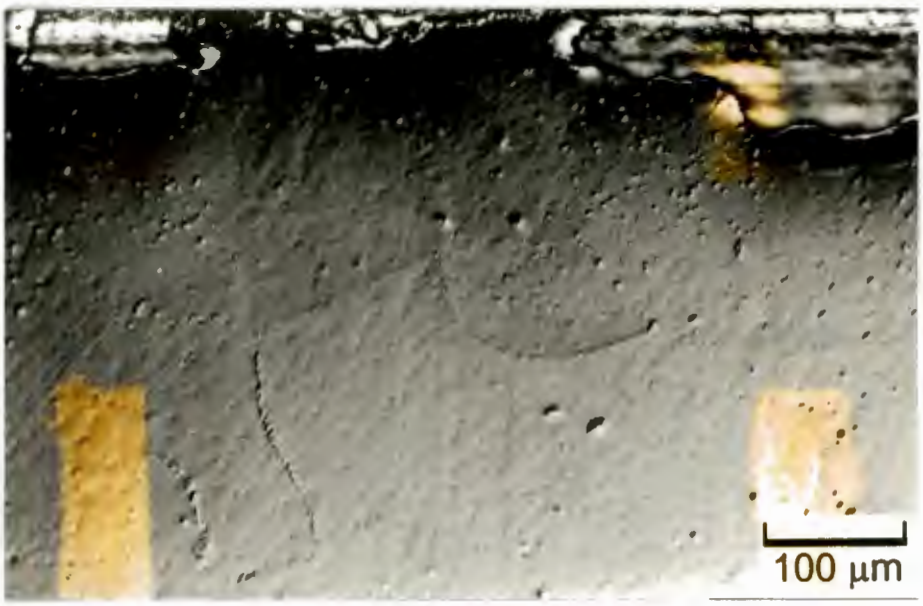


b)


**Figure 5-44 Pitted region of an annealed, polished 310 specimen after 7 weeks' exposure. a) Unetched taper section showing surface pitting and carbide precipitation along grain boundaries b) The same area after etching in oxalic acid.**

Figure 5-45 shows SEM micrographs of the region shown in Figure 5-44. In the outer region of less heavily carburised metal, the carbides are large and distinct. The density of these carbides increases in the direction of the pit until they become indistinct in the region of supersaturation and metal wastage.

a)

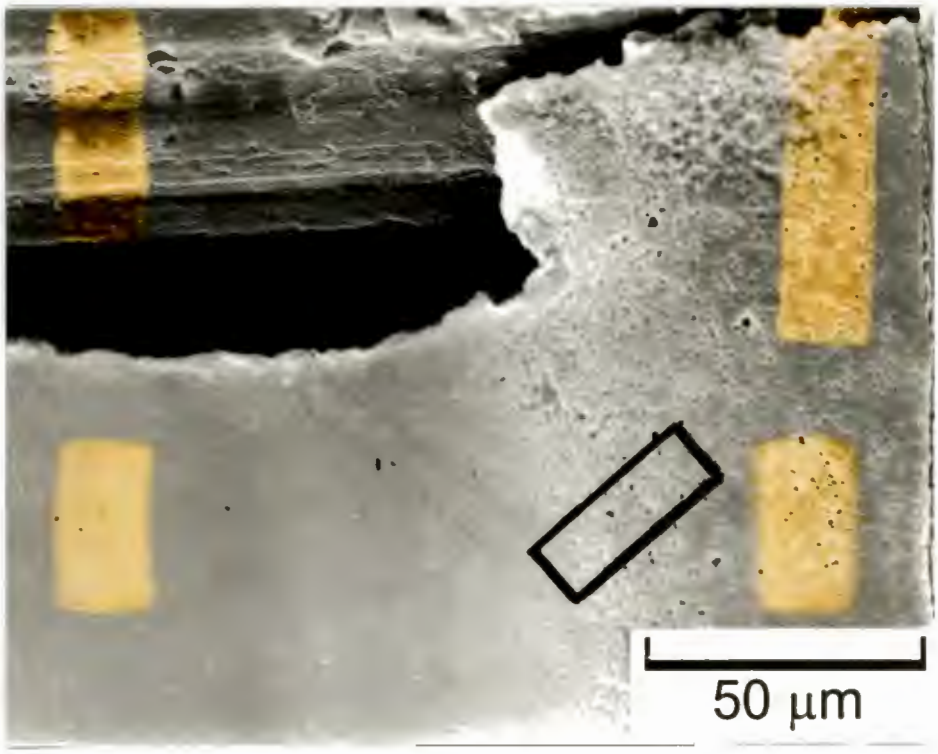



b)

**Figure 5-45 a) SEM micrograph showing the regions of carbide precipitation and metal deterioration near a pit on an annealed, polished 310 specimen after 7 weeks' exposure. Figure b) is a magnified view of the marked area in a)**

**As received, abraded 310 specimens**

Figure 5-46 shows taper sections of an as received, abraded 310 specimen after 3 weeks' exposure. As in the case of the 800H specimens, there is no evidence of internal carburisation or carbide formation. A high density of carbide-decorated twin and grain boundaries and dislocations near the surface is visible.

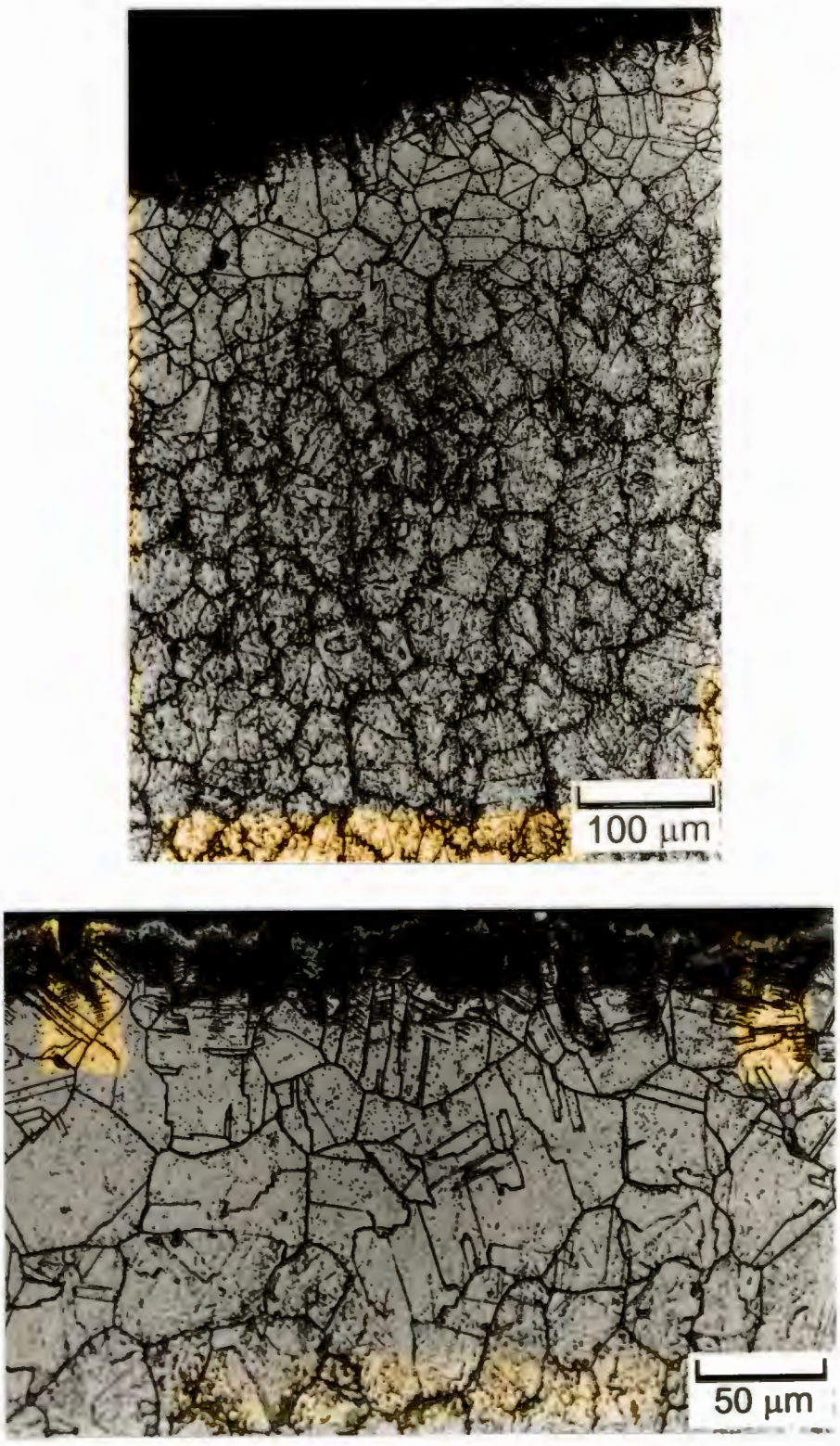


**Figure 5-46 Taper sections of an as received, abraded 310 specimen after 3 weeks' exposure. Etched in oxalic acid.**

**Annealed, polished HNSS specimens**

Taper sections of the HNSS specimens show a marked difference to the alloy 800H and 310 specimens. Carbon diffusion into this alloy has led to the precipitation of needle-shaped chromium nitrides ($Cr_2N$) or possibly carbo-nitrides ($Cr_2(CN)$), initially along the grain boundaries and then within the inner grains of the specimen (Figure 5-47). After two weeks this zone of precipitation has become more developed and is surrounded by an unetched band adjacent to the surface (Figure 5-48).

The region of precipitation gradually extends towards the edges of the specimen and, by the end of 6 weeks, is close to the specimen surface (Figure 5-49). At this stage, two forms of precipitate are visible. Regions of what is possibly $Cr_2N$ have formed near the grain boundaries in lamellae clusters, while needle-shaped $Cr_2(CN)$ precipitates have formed within the grains (Figure 5-50). A more detailed view of these precipitates is shown in the scanning electron micrograph of Figure 5-51.

A fifteen-degree taper section through an as received, abraded specimen is shown in Figure 5-52. The needle-shaped within-grain nitrides that are visible in Figure 5-50 are absent in these micrographs. Chromium nitride precipitation is exclusively in the form of lamellae clusters along the grain boundaries.

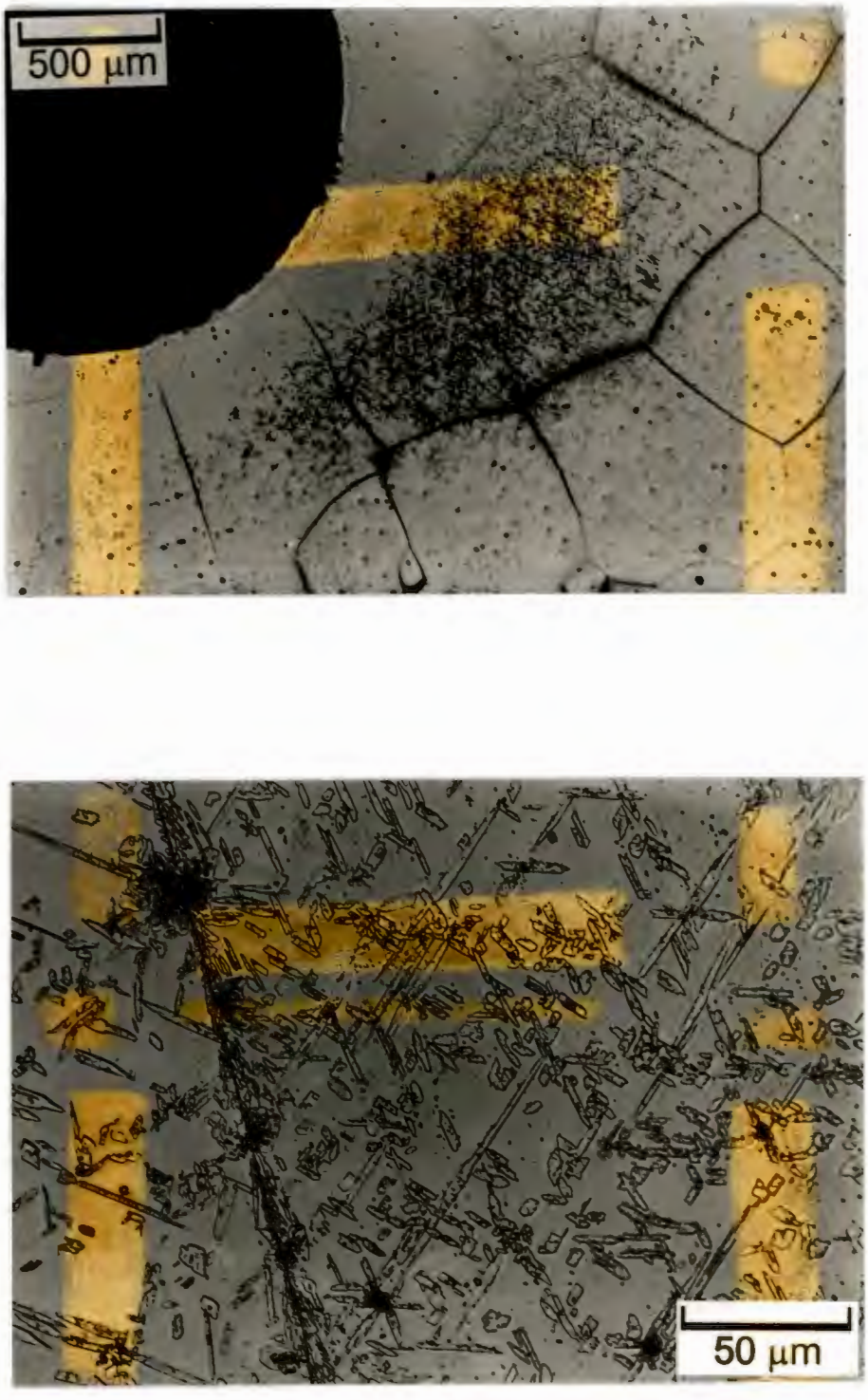


**Figure 5-47 Chromium nitride precipitates in the inner region of an annealed, polished HNSS specimen after one week's exposure.**

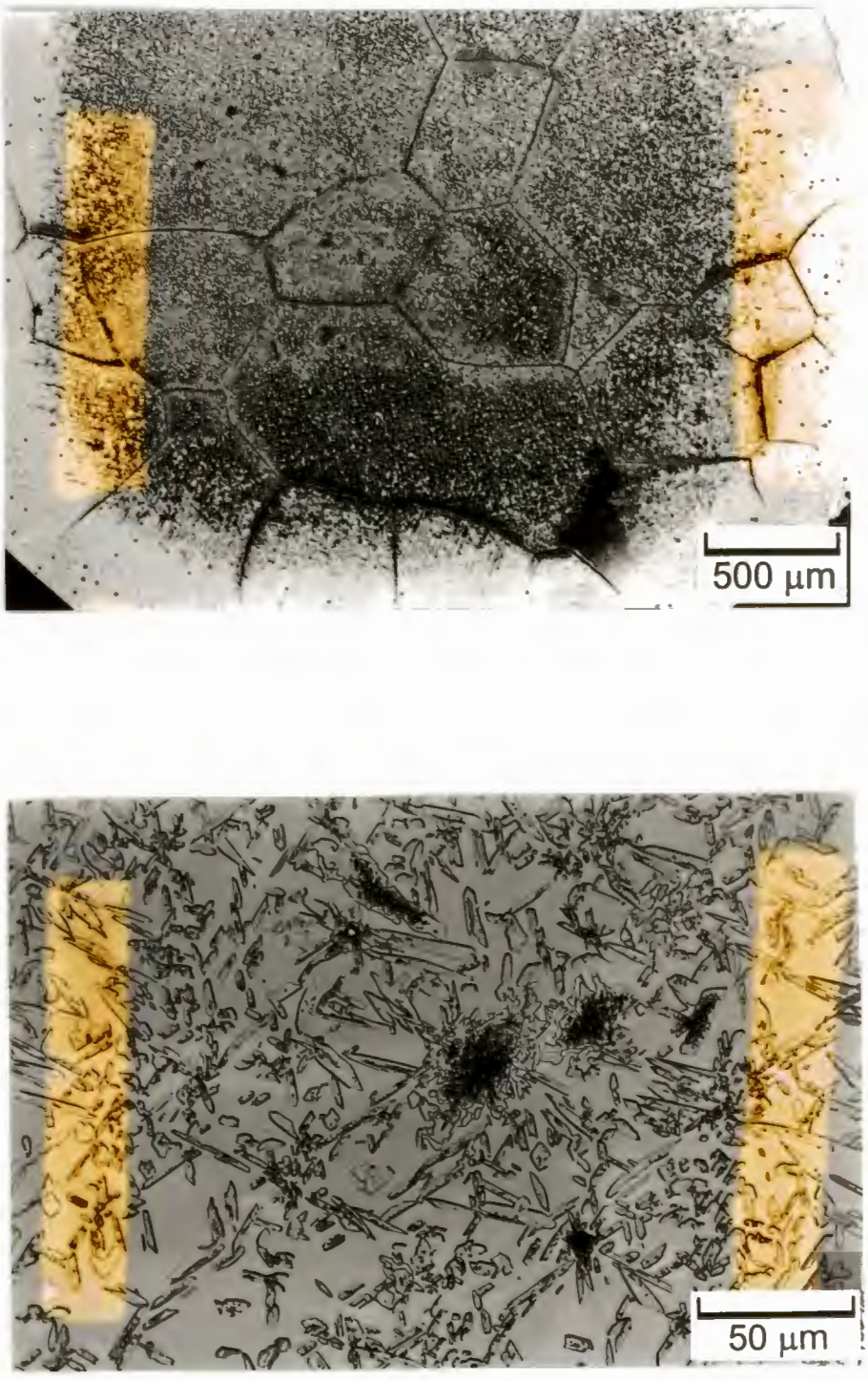


**Figure 5-48 Chromium nitride precipitates in an annealed, polished HNSS specimen after two weeks' exposure. Etched in oxalic acid.**

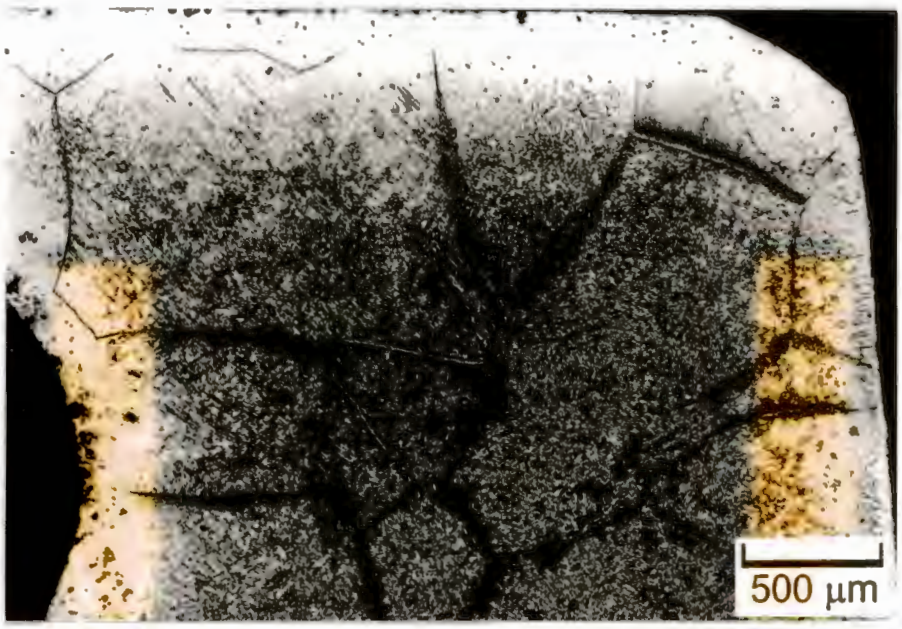


**Figure 5-49 Expanded region of chromium nitride precipitation in an annealed, polished HNSS specimen after 6 weeks' exposure.**

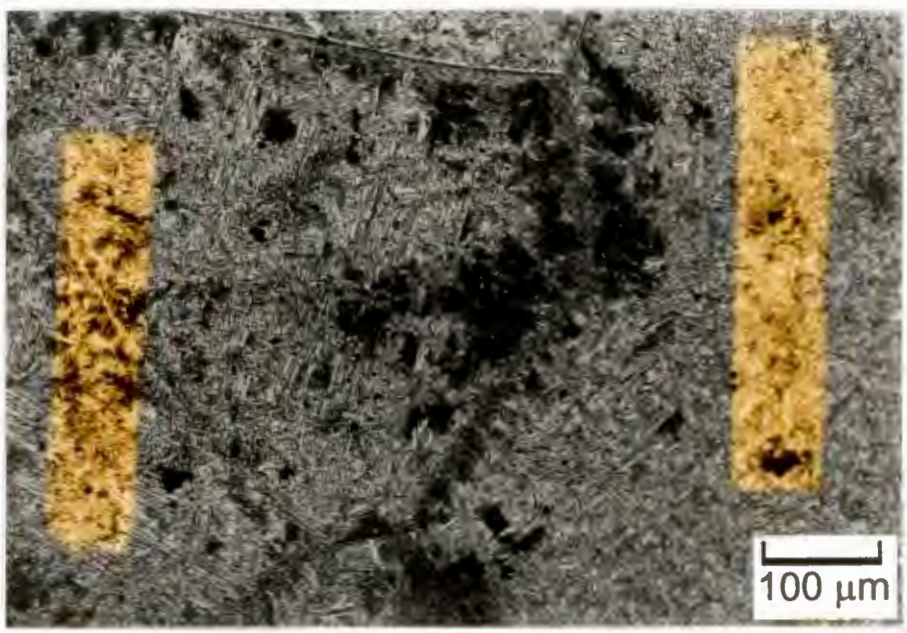


**Figure 5-50 Chromium nitride precipitates near the centre of an annealed, polished HNSS specimen after 6 weeks' exposure to the $H_2$-CO-$H_2O$ atmosphere.**

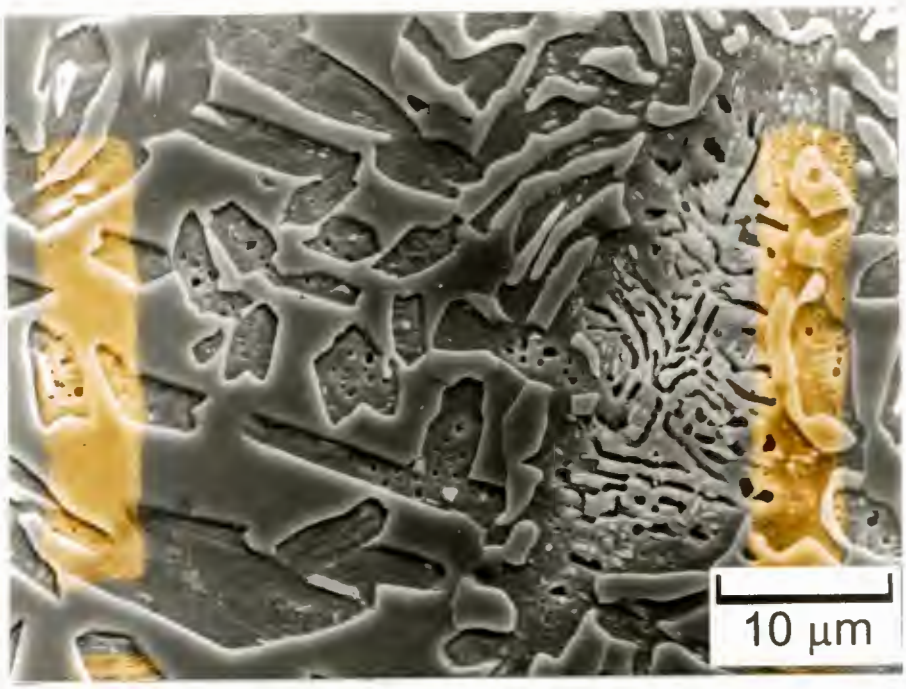


**Figure 5-51 Scanning electron micrograph of lamellae and needle precipitates in an annealed, polished HNSS specimen after 6 weeks in the $H_2$, CO, $H_2O$ atmosphere.**

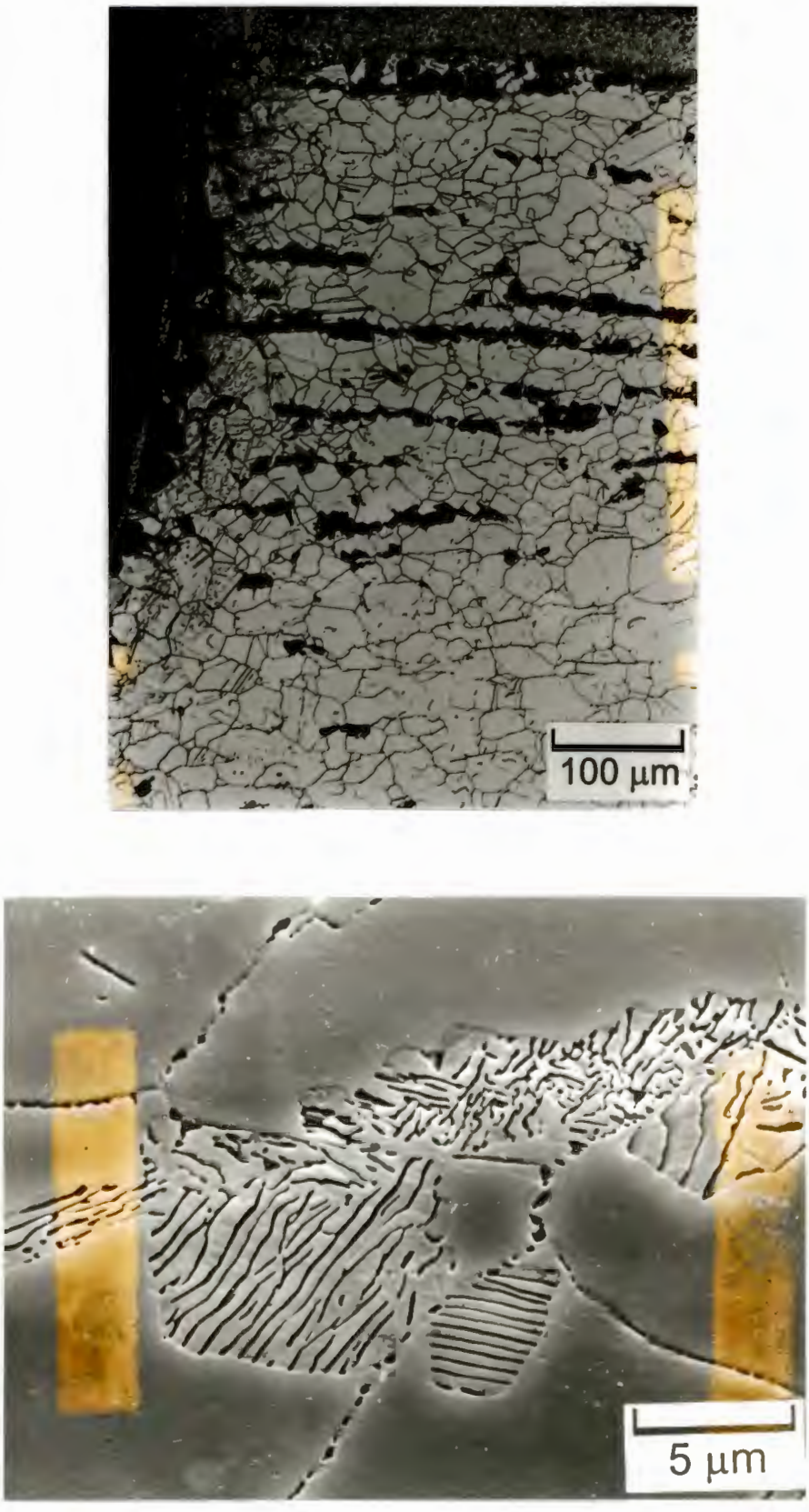


**Figure 5-52 Chromium nitride precipitates in an as received, abraded HNSS specimen after three weeks' exposure in the $H_2$, CO, $H_2O$ atmosphere.**

A one-week exposure of annealed, polished HNSS specimens in a $H_2/H_2O$ mixture resulted in the formation of precipitate clusters (Figure 5-53) similar to those visible in Figure 5-52. The absence of CO in this gas atmosphere has resulted in the absence of the within-grain needle precipitates (see Figure 5-47) that were formed in the normal carburising $H_2/CO/H_2O$ atmosphere.

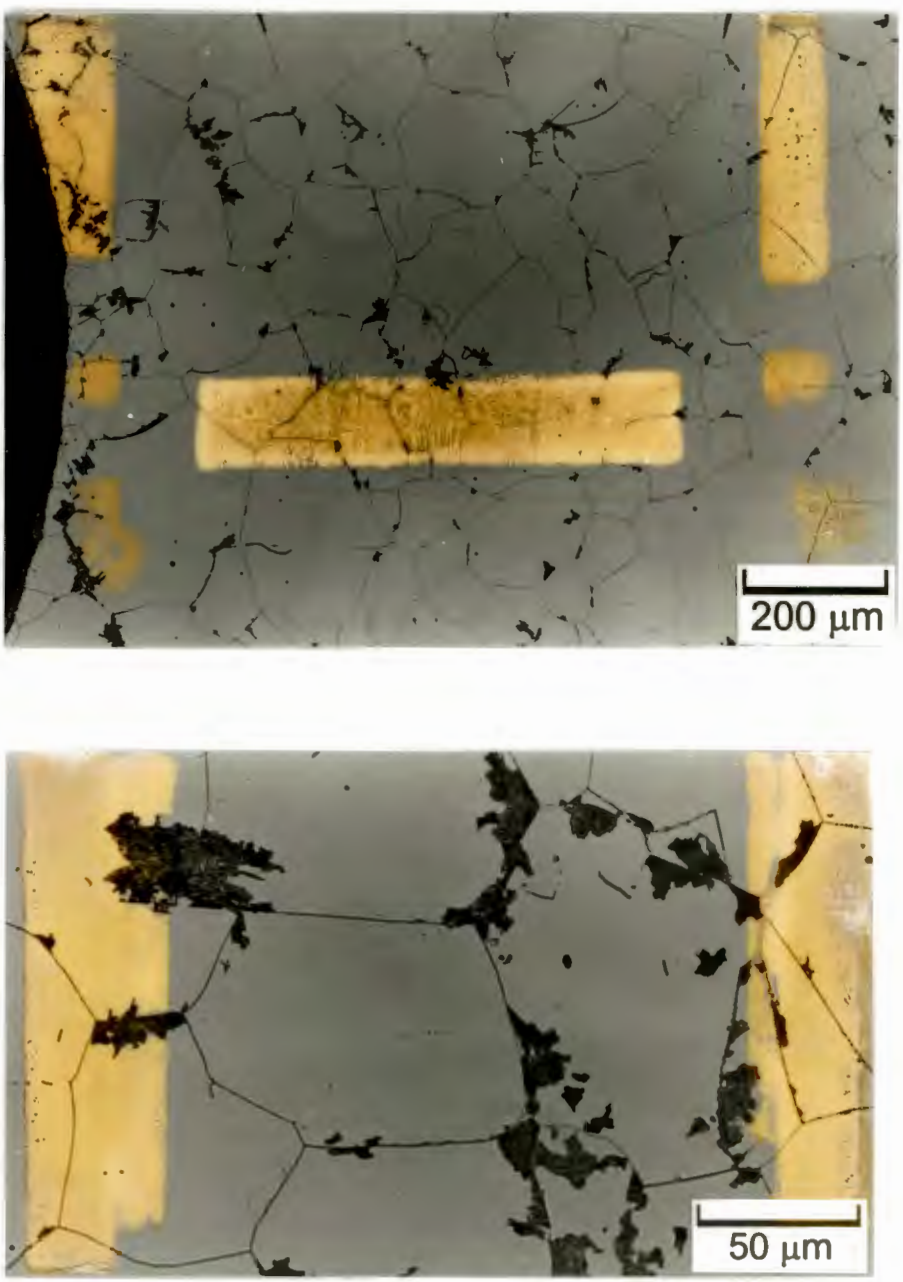


**Figure 5-53 Chromium nitride precipitation in an annealed, polished HNSS specimen after one week exposure in the $H_2/H_2O$ atmosphere.**

## 5.3 Effect of heat treatment, surface roughness and passivation on metal dusting resistance of alloy 800H

The effects of the four combinations of heat treatment and surface roughness preparations on resistance to metal dusting are summarised in Table 5-1. The preparations are listed in order of resistance to metal dusting attack. There was generally little difference in performance between the passivated and depassivated specimens.

| Resistance to metal dusting | Heat treatment | Surface condition |
|---|---|---|
| 1 | As received | Abraded |
| 2 | Annealed | Abraded |
| 3 | Annealed | Polished |
| 4 | As received | Polished |

**Table 5-1 Effect of heat treatment and surface preparation on the resistance to metal dusting of Incoloy 800H. Condition 1 is the most resistant, while condition 4 is the least resistant.**

### 5.3.1 Effect of passivation on the resistance of 800H to metal dusting

The effect on mass-loss of passivating and depassivating the specimens is illustrated by the mass change curves in Figure 5-54 a-d. For three of the different heat treatment and surface conditions the passivated specimens suffered slightly less loss in mass than the passivated specimens. The exception to this was the annealed and ground condition. However, these differences are small when compared with the effect of heat treatment and surface roughness. No noticeable effect of passivation on the amount of carbon deposited on the specimens was observed.

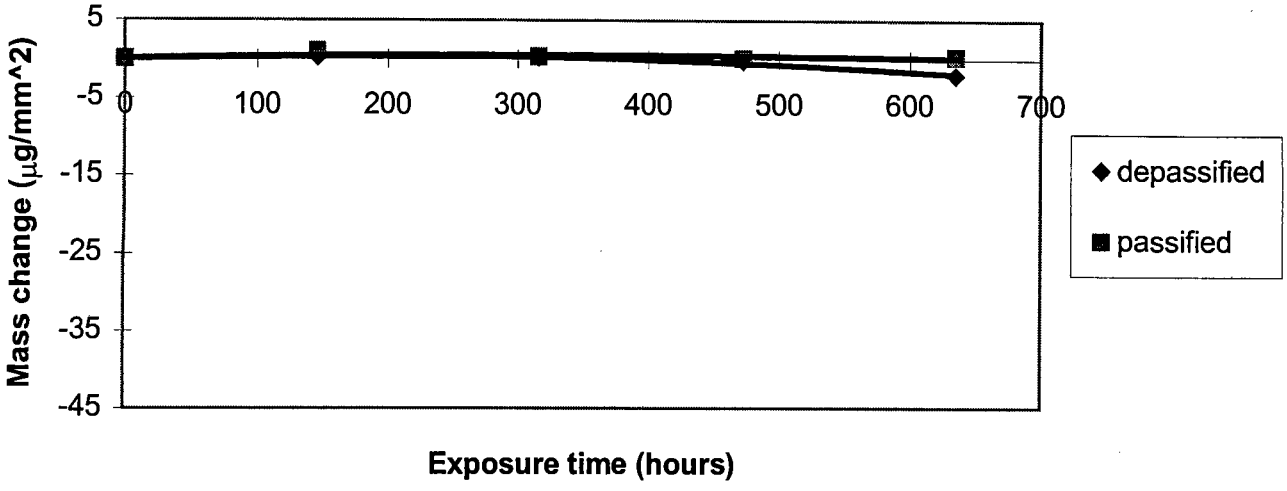


**Figure 5-54 a) as received, abraded specimens**

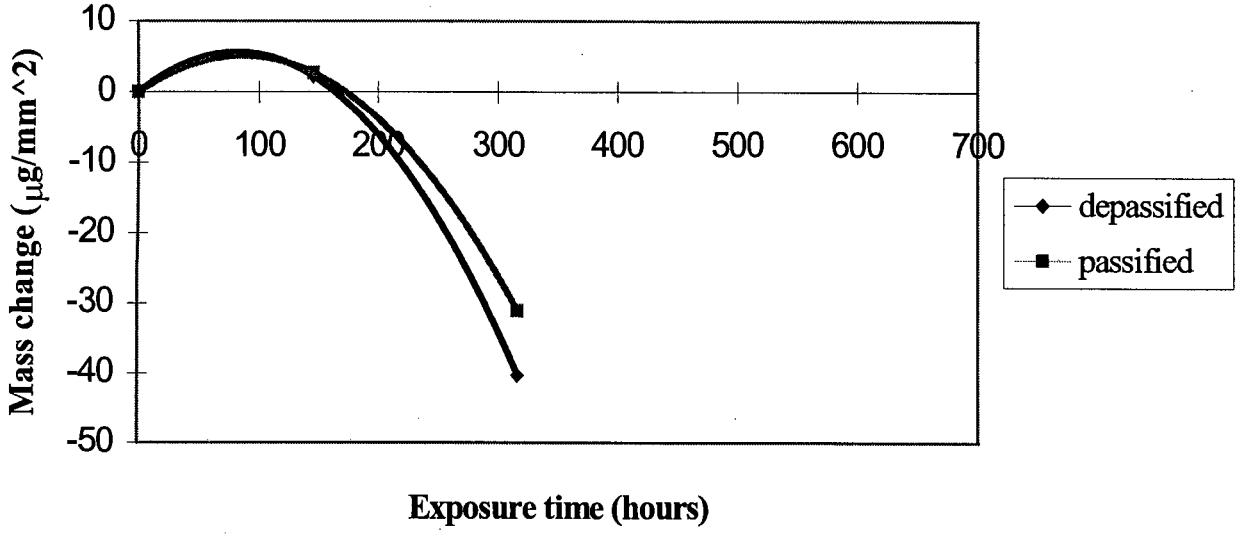


**Figure 5-54 b) annealed, abraded specimens**

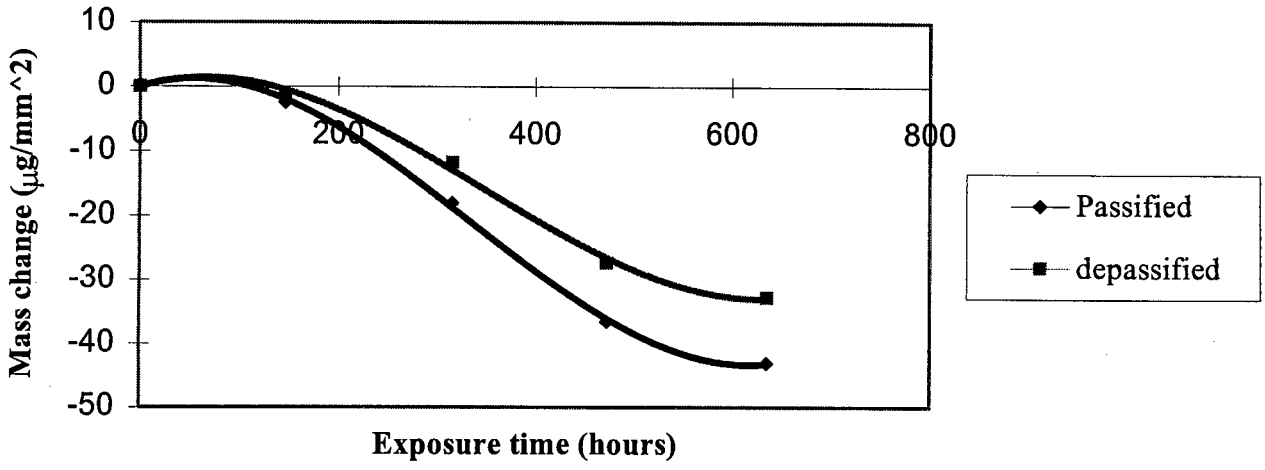


**Figure 5-54 c) annealed, polished specimens**

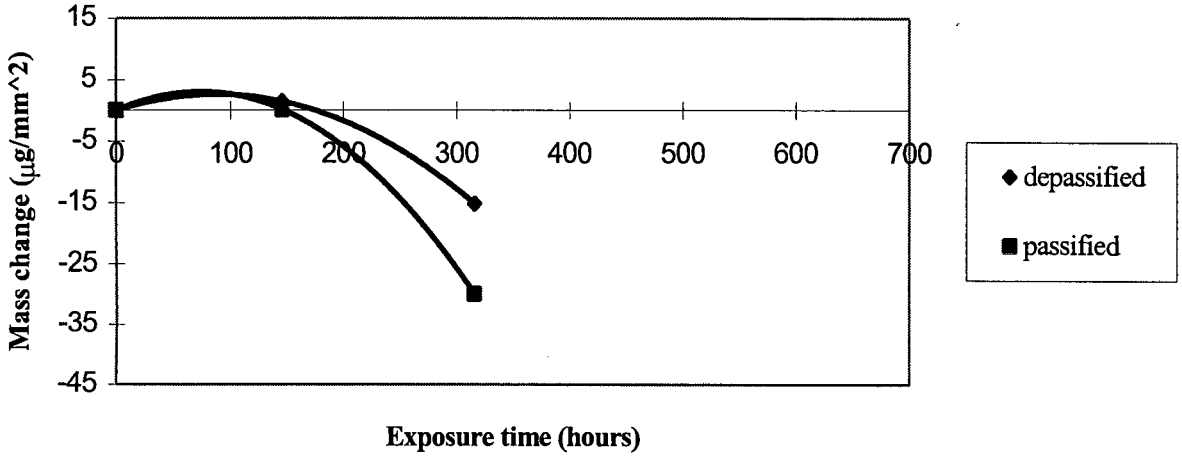


**Figure 5-54 d) as received polished specimens**

**Figure 5-54 Mass change curves showing the effect of passivation and depassivation of alloy 800H specimens for each of the four heat treatment and surface roughness conditions.**

### 5.3.2 Effect of heat treatment and surface preparation on carbon deposition on alloys 800H, 310 and HNSS

The extent of carbon deposition and pitting on the specimens is indicated in Figure 5-56. None of the specimens suffered any carbon deposition after the first week. Carbon protrusions and a thick surface covering were present after the second week of testing on all four of the polished specimens (Figure 5-57). The two annealed, abraded specimens were free of deposit on their two main surfaces. However, the region surrounding the mounting hole, particularly in the crevice formed along the contact area with the ceramic rod, suffered from heavy carbon deposition and protrusion growth. The as received, abraded specimens were free of carbon deposits throughout the test series. The contrast in amounts of deposition observed after the second exposure is apparent in a photograph taken of the specimens while still on the test rack (Figure 5-55). The as received, abraded specimens are free of deposition while the others are completely covered by a heavy deposit.

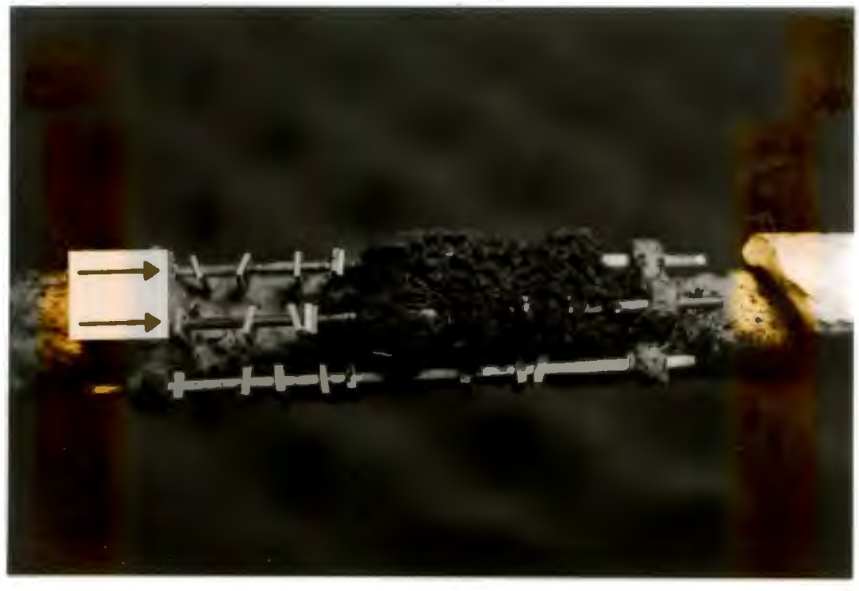

**Figure 5-55 Carbon deposition on alloy 800H specimens after the second week of exposure. The carbon-free specimens on the left of the two upper racks (as indicated by arrows) were tested in an as received and abraded condition. Specimens in an annealed and polished condition are entirely covered by a carbon deposit (right).**

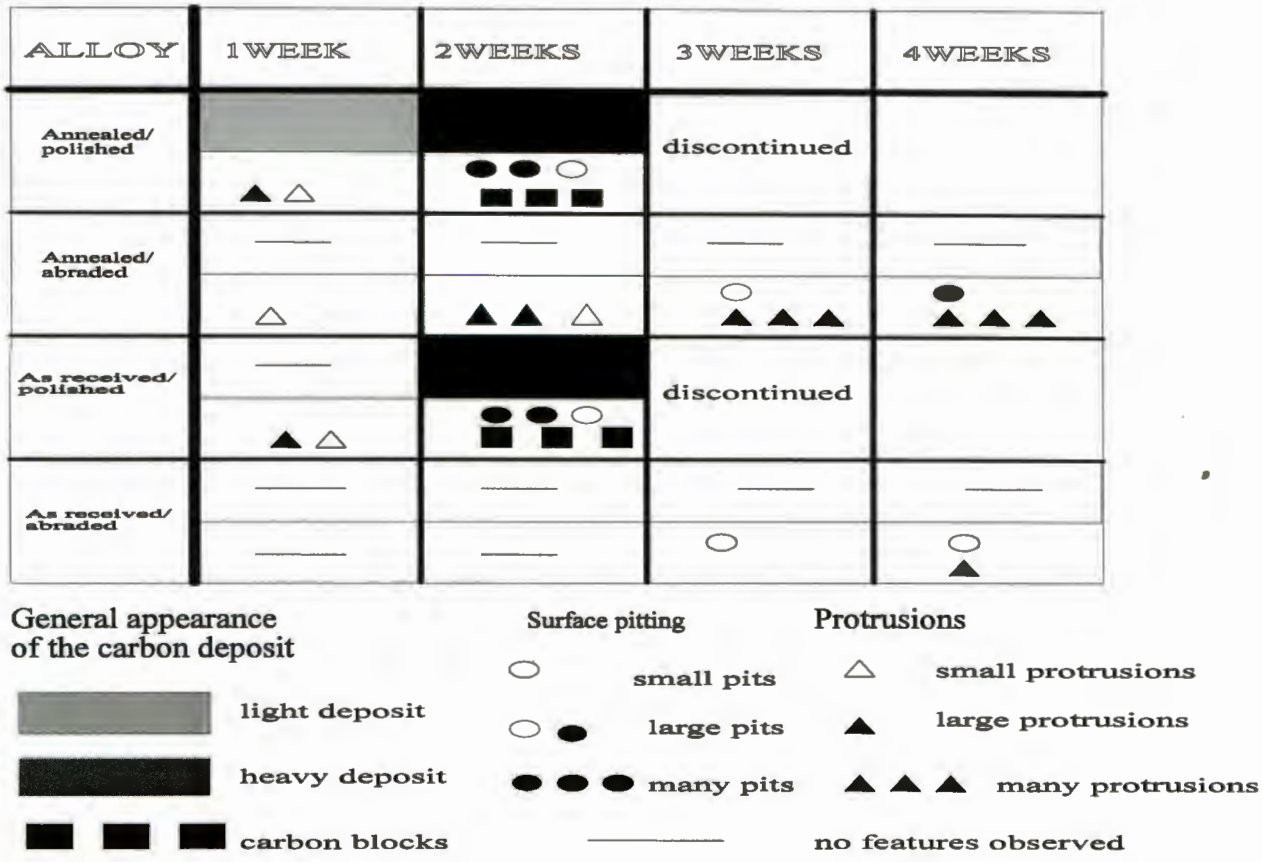


**Figure 5-56 Extent of carbon deposition and severity of pitting on alloy 800H specimens of different preparations.**

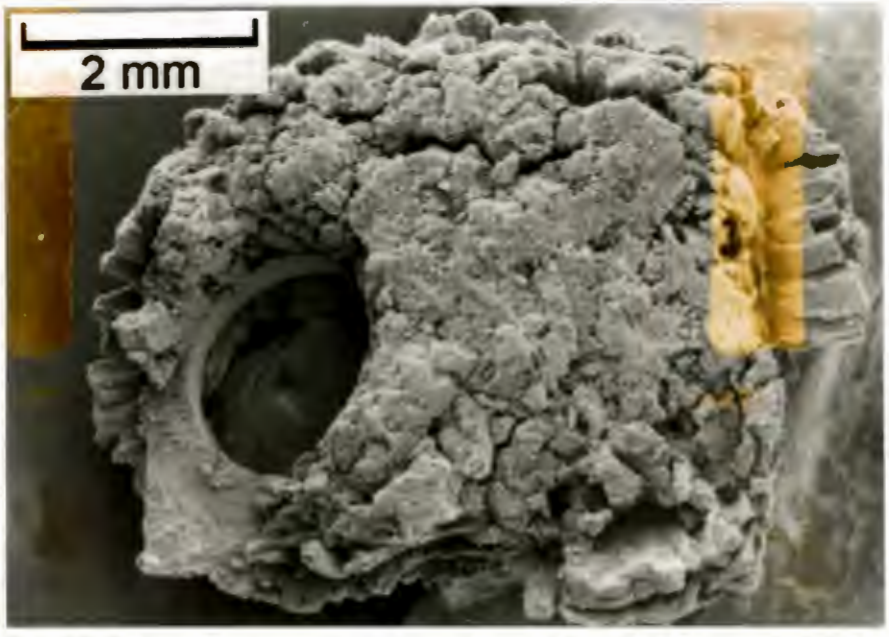


**Figure 5-57 Carbon deposition on an as received, polished 800H specimen after the second week of exposure.**

### 5.3.3 Effect of heat treatment and surface preparation on specimen mass changes

The mass loss curves shown in Figure 5-58 illustrate the effect of the four different specimen preparations on the specimen mass changes. The as received, abraded specimens showed a negligible change in mass compared to the other three conditions. The annealed, abraded specimens performed better than the two polished conditions. There appears to be little effect of heat treatment, and specifically grain size, on mass loss for the polished specimens.

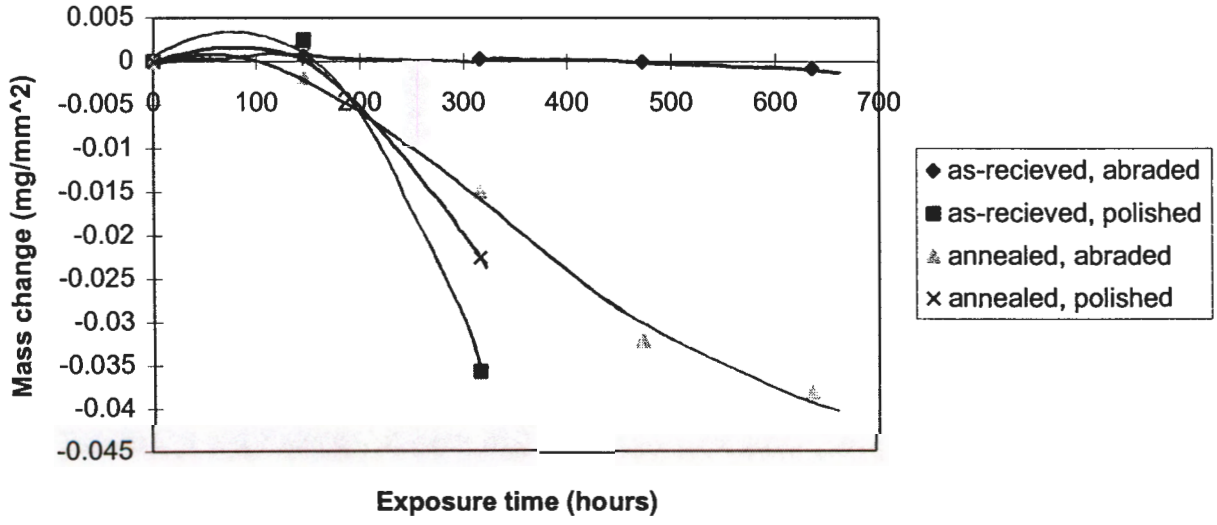


**Figure 5-58 Mass change curves for the four heat treatment and surface roughness preparations. All specimens were passivated.**

### 5.3.4 Metallographic examinations of the metal dusted specimens

Fifteen-degree taper sections of the samples were prepared in order to gauge the effect of heat treatment and surface roughness on the extent to which the alloys were carburised.

**Metal dusting features on annealed, polished specimens**

The taper section shown in Figure 5-59 reveals carburisation of the specimen from both main faces as well as from the support hole. Pitting along the lower side and at the hole has already developed after two weeks.


**Figure 5-59 Carburised and pitted regions of an annealed, polished 800H specimen after two weeks' exposure. Etched in oxalic acid.**

**Metal dusting features on annealed, abraded specimens**

The annealed, abraded specimens showed signs of pitting and carburisation only at the surface of the support hole (Figure 5-60). This corresponds with the observation of carbon deposition only at the interface of the support rod and the specimen. In other areas carburisation has occurred along the grain boundaries, but not in the surrounding matrix.

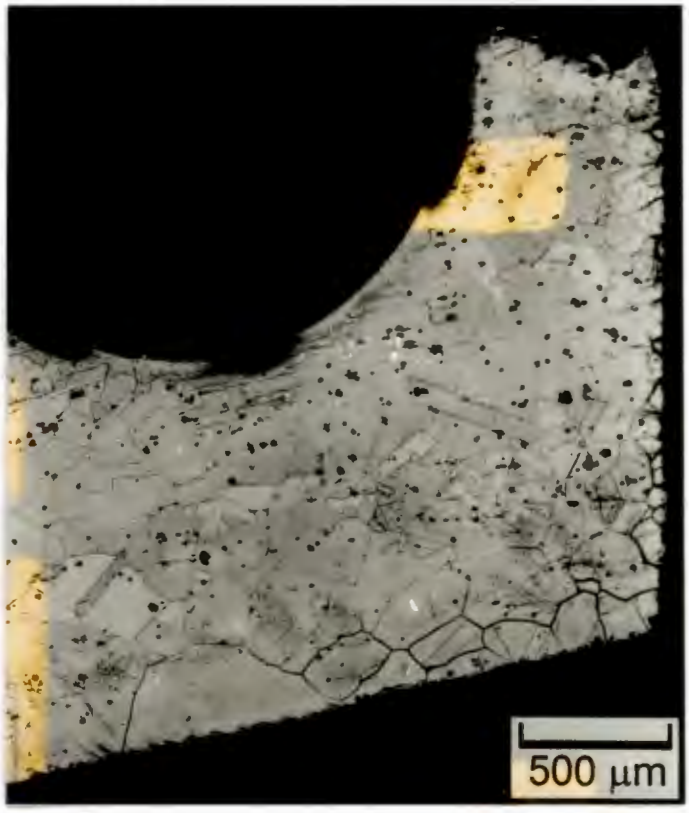


**Figure 5-60 Taper section of an as received, abraded 800H specimen after four weeks' exposure. Etched in oxalic acid.**

**Metal dusting features on as received, polished specimens**

These samples have suffered internal carburisation and pitting after 2 weeks' exposure (Figure 5-61). The surface at the hole is unaffected.

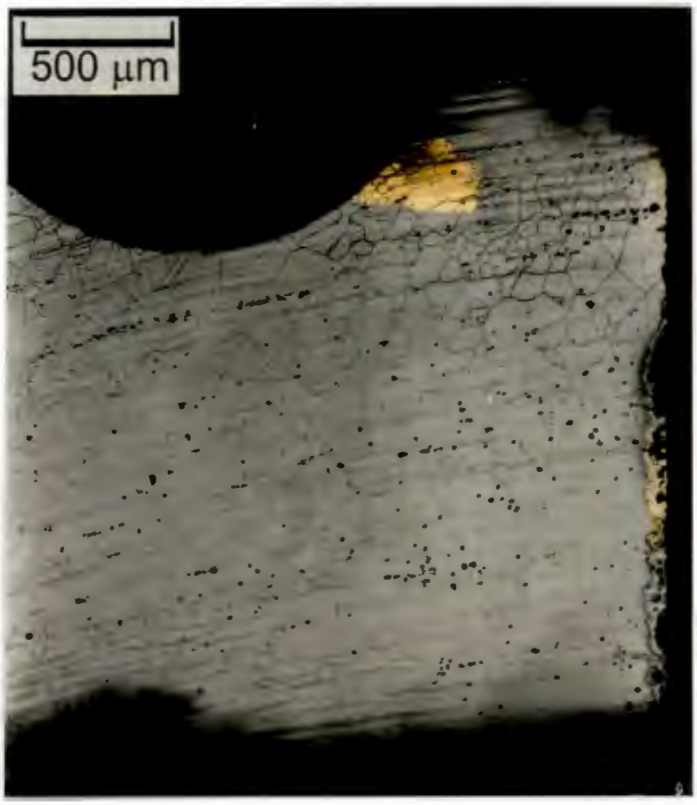


**Figure 5-61 Taper section of an as received, polished 800H specimen after two weeks' exposure. Etched in oxalic acid.**

**Metal dusting features on as received, abraded specimens**

Specimens tested in as received, abraded condition show no signs of carburisation or pitting at the surface regions, even after four weeks' exposure (Figure 5-62).

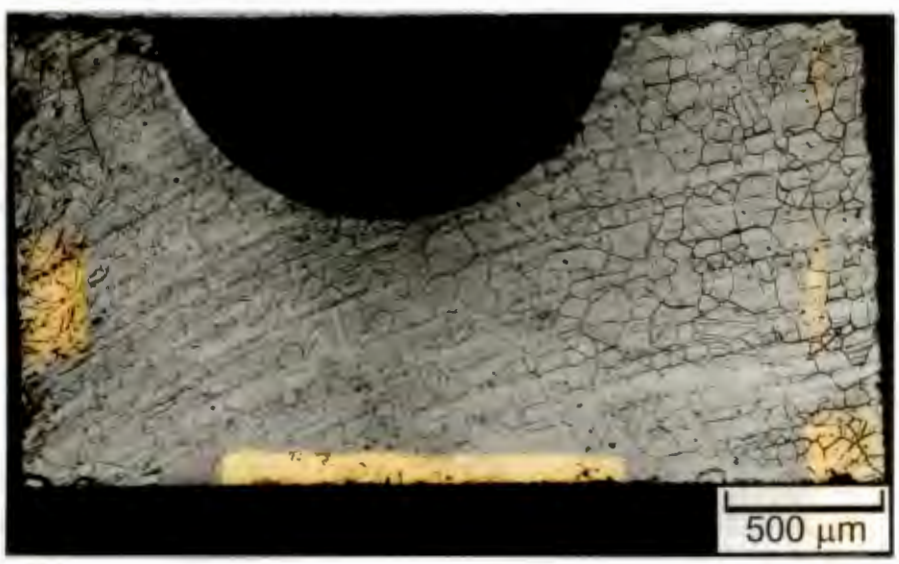


**Figure 5-62 Taper section of an as received, abraded 800H specimen after four weeks' exposure. Etched in oxalic acid.**

# 6. Discussion of results

## 6.1 Exposures of CrMo and as received 310 specimens

The aim of the first series of exposures of as received and polished CrMo and 310 specimens was to establish the occurrence of metal dusting in the simulation furnace. The results of this test series are discussed in the following section.

### 6.1.1 CrMo specimens

The results of the exposures of the CrMo specimens to the carburising environment show that the essential features of metal dusting are present in the corroded samples and in the carbon deposit.

The large amounts of carbon deposition indicate a strong tendency for the furnace atmosphere to transfer carbon to the samples. The two-degree taper sections that reveal regions of dense carbide precipitation show that carbon diffusion into the matrix has occurred. The surface carbide layer (Figure 5-6), while not fully characterised in this project, bears a close similarity to micrographs of similar alloys produced by Grabke *et al.* [17] (Figure 2-3). The constant rate of mass loss of the specimens shows that some form of metal wastage has taken place. The presence of metal particles in the carbon deposit corresponds with the predictions of the metal dusting mechanism and thus indicates that this mechanism is responsible for the metal wastage.

The uniform attack and subsequent thinning of the specimens can be attributed to the absence of a protective oxide layer on the surface of the specimen. The content of 1.25% Cr is well below the value of 12-18% recommended for chromia stability in ferritic steels [34]. This provides the carbon with uninhibited and uniform access to the alloy interior, resulting in evenly distributed metal dusting attack.

The large metal particles observed in the stereo light microscope and the SEM have a similar composition to the parent alloy and are thus probably metal grains that have been displaced from the sample. These surface grains may have been worked loose by the volume changes associated with large scale carbide precipitation along the boundary of the grain. This phenomenon was observed by Le Francois and Hoyt [26] and more recently by Nolan *et al* [13].

The above results, which compare well to previous work done on similar low alloy steels [19], show that metal dusting can be simulated in the carburising furnace that was built as a part of this project. In addition, the constant rate of specimen mass loss and the consistent formation of large amounts of metal dusting corrosion products shows that the furnace is able to produce a consistently severe metal dusting environment.

### 6.1.2 AISI 310 specimens

The strong resistance to carburisation and metal dusting of the 310 specimens contrasts sharply to the CrMo specimens.

The lack of any significant carburisation, surface deposits or mass change of the 310 specimens can be attributed to a stable surface chromia layer that prevents the inward diffusion of carbon into the matrix. The high chromium content (25 wt%) allows the alloy to maintain this layer even in the reducing test conditions.

Two other factors contributed to the good resistance of these specimens in this series of exposures. The first was the short total exposure period of just 100 hours. This

## 6.2 Exposures of alloy 800H, 310 and HNSS specimens

The results of the second test series involving the exposure of three high-alloy steels to a carburising environment in the metal dusting furnace are discussed in the following section.

### 6.2.1 Corrosion of annealed and polished alloy 800H, AISI 310 and HNSS specimens

In the course of the carburisation exposures, specimens of alloy 800H and 310 showed the carbon deposition, matrix carburisation and metal wastage associated with metal dusting corrosion. Taper sections such as those shown in Figure 5-34 show that carbon penetration has caused extensive carbide precipitation and ultimately pitting due to metal loss into a carbonaceous deposit. The low microhardness values measured in these regions indicate breakdown of the metal structure and subsequent loss in alloy integrity (Figure 5-36). These features compare well with those observed in earlier metal dusting research under similar conditions [12] [19]. The absence of any of these features on the HNSS specimens over the first six weeks shows a high initial resistance of this alloy to carburisation and metal dusting.

The highly localised nature of the metal dusting attack on these alloys is in contrast to the uniform metal thinning of the low-alloy CrMo specimens. This difference can be explained by the presence of protective oxide layers, which prevent carbon diffusion into the alloy [34]. The stability of these oxides is aided by the high levels of oxide-forming elements such as chromium and silicon in these alloys. Localised carburisation leading to protrusion growth and pitting can only take place where defects have formed in the oxide layers.

The tendency for protrusions to grow at the corners of the specimens is expected, since there is the highest ratio of surface area to volume at these points. Protrusion growth at the corners also indicates that the oxide layer is most vulnerable to cracking in these areas. The more evenly distributed carburisation of the specimens in later weeks indicates a gradual decrease in the alloy's ability to form a protective oxide layer. This is due to depletion of oxide-forming elements such as chromium, as they are tied up in $M_{23}C_6$ and $M_7C_3$ carbides [25]. The high resistance of the as received, abraded samples, which can repair damage to their protective oxide layers more easily due to the increased diffusivity of chromium, is further testimony to the effectiveness of oxide layers in preventing metal dusting.

**The effect of alloying elements on the different resistance's to metal dusting of alloy 800H and AISI 310.**

Resistance of alloys 800 and 310 can be gauged by the amount of pitting and carbon deposition shown in Figure 5-9. However, the best comparison is probably found in the specimen mass loss curves. On these curves the alloy 800H specimens show by far the highest rate and amount of mass increase, as well as the highest amount of mass loss. This indicates higher rates of carburisation and metal wastage than in the other two alloys. Since the grain size and surface roughness of the three alloys were similar and all alloys were tested simultaneously in the furnace, the most obvious remaining factor is the difference in the alloying contents.

An analysis of the alloy compositions shows that alloy 800 has lower weight percentages of most of the oxide-forming elements. This difference is shown in Table 6-1. The main effect of this difference is a lower ability of alloy 800H to form a protective oxide layer on the surface due to lower activities of these elements - particularly Cr and Si. The long-term resistance will also be reduced, since it will take a shorter time for the chromium in alloy 800H to be tied up in carbides.

The higher nickel content of alloy 800H further reduces its oxide-forming ability by reducing the chromium diffusivity though the matrix. This effect was cited by Richardson [8] as being a major reason why alloy 800H should perform poorly in metal dusting environments. The only oxide-forming element present in higher quantities in alloy 800H is aluminium.

| Oxide-forming element | Alloy 800H | AISI 310 | HNSS |
|---|---|---|---|
| Chromium | 21 | 26 | 18.1 |
| Silicon | 0.5 | 1.5 | 0.004 |
| Aluminium | 3.8 | - | 0.022 |
| Manganese | - | 2.0 | 10 |
| Titanium | 0.38 | - | 0.003 |

**Table 6-1 Comparative weight percentages of the main oxide-forming elements in alloy 800H , AISI 310 and HNSS [53].**

The ratio of iron to nickel in alloy 310 (Fe:Ni = 2.7:1) is closer than that of alloy 800 (Fe:Ni = 1.5:1) to the optimum ratio of 4:1 for metal dusting resistance found by Schnaas and Grabke [25]. In addition, the amount of silicon in 310 (1.5%) is closer to the ideal content of 2-2.5% suggested by Steinkusch [48] for good carburisation resistance.

On the basis of these alloying differences, it is reasonable to expect that Incoloy 800H would be more susceptible to metal dusting than AISI 310. However, the relatively high susceptibility of both of these alloys to metal dusting suggests that neither alloy is satisfactory for long term use in metal dusting environments. This is despite the fact that these alloys were tested in conditions of increased susceptibility to metal dusting i.e. with larger grains, less cold work in the matrix and a deformation-free surface. The specimens of these alloys tested in an as received condition showed a relatively good resistance to metal dusting. However, the continued resistance of these specimens over longer exposure periods is questionable, since the effect of the specimen sensitisation is to slow the rate of chromium diffusion to the surface. The effectiveness of this treatment would be diminished over a longer exposure time.

**The effect of alloying elements on the high initial resistance to metal dusting of high nitrogen stainless steel**

The good resistance of the HNSS specimens to metal dusting during the first seven weeks must be due mainly to its alloying composition. Although the chromium content is lower than that of the two other alloys at 18.1 %, it is still high enough for good oxide formability [19]. Levels of the other oxide-forming elements silicon, aluminium and titanium are very low when compared to those in alloy 800H and 310.

These deficiencies should result in an increased amount of carbon penetration and carburisation. It is difficult to compare the extent of matrix carburisation with alloy 800H and 310 due to the different forms of precipitation. A comparison of the mass change curves in Figure 5-31 shows that the amount of mass increase for the HNSS specimens is lower than that of the other two alloys. There are two possible reasons for this good carburisation resistance. The high level of manganese (10 %) allows the

alloy to form a MnO layer at the surface of the specimen. This layer was observed in the form of a green tinge on the surfaces of the specimens and, according to Grabke *et al.* [34], should suppress metal dusting for some time. The second reason may lie in the sulphur content of 0.044%. The presence of sulphur, either as $H_2S$ in the atmosphere or in solution in the alloy is known to retard metal dusting by poisoning active sites for carbon deposition [12]. The high resistance of these specimens to carbon deposition for most of the exposure period could be partly attributed to the sulphur in this alloy.

There is not much written in the literature about the role of nitrogen in preventing or retarding metal dusting. The main feature of HNSS is its nitrogen content of 0.5 %. This nitrogen exists in solid solution in the alloy and has been observed to cause fine precipitation of intragranular $Cr_2(CN)$ carbo-nitrides during carburisation [30].

Due to the limitations of this project, a detailed analysis of the $Cr_2N$-like precipitates shown in Figures 5.47, 5.48, 5.49, 5.50, 5.51, 5.52 and 5.53 could not be carried out. The possibility that these were chromium carbo-nitrides was tested by eliminating the diffusion of carbon into the specimens. This was done in two ways. The first was by exposing as received, abraded specimens which were able to form stable protective chromia layers preventing carbon penetration into the alloy matrix. The second was by exposing the specimens to a gas mixture from which the CO had been removed. In both cases the only precipitates that formed in the specimens were lamellae clusters, presumably of $Cr_2N$, near the grain boundaries (Figure 5-52 and Figure 5-53). The needle-shaped intragranular precipitates were therefore only formed when carbon was able to diffuse into the alloy. This leads to the conclusion that the needle phase consists of $Cr_2(CN)$ precipitates.

It is not clear why the precipitation of these carbo-nitrides should start in the centre of the specimens and progress towards the surface. Since carbon is diffusing inwards from the surface, it would be expected that the opposite progression should occur. It is possible that precipitation is in fact taking place near the specimen edges, but is not visible due to etching effects.

It is recommended that further studies on the precipitation in this alloy be carried out in order to characterise the type of precipitates that form with exposure to the carburising environment used in this project. This work could possibly involve the use of TEM analysis in order to gain an understanding of the good initial resistance of this alloy to metal dusting.

The contribution of nitrogen in this high-nitrogen stainless steel to its good initial resistance to metal dusting lies in its ability to tie up the penetrating carbon in $Cr_2(CN)$. The main benefit of the formation of these carbo-nitrides over the normal $M_{23}C_6$ and $M_7C_3$ carbides is that the chromium is tied up at a lower rate, due to the different stoichiometry of the three compounds. This leaves more chromium free to maintain the chromia layer at the surface, which prevents carbon penetration. The extended availability of chromium also delays the formation of $Fe_3C$, since this carbide can only form once the chromium is tied up [40]. $Fe_3C$ is the necessary intermediate in metal dusting [42], since chromium carbides are not destabilised by the drop in carbon activity caused by graphite deposition (see section 2.2.3).

Increased nitrogen content should extend the duration of this protection, as long as there is free chromium for $Cr_2(CN)$ formation. However, the presence of nitrogen in an alloy should only delay the onset of metal dusting. If carbon can diffuse into the alloy the nitrogen will eventually become depleted. This will lead to the formation of meta-stable $Fe_3C$ and metal dusting will start. The beneficial effect of nitrogen in this project appeared to decrease after about nine weeks in the carburising furnace, when the start of pitting on the surface of the HNSS specimens was observed (Figure 5-28).

### 6.2.2 Effect of surface preparation, heat treatment and passivation on the resistance to metal dusting of alloy 800H, 310 and HNSS

The results of the third test series show that metal dusting resistance is greatly increased by abrading the surface and annealing to enlarge the grain size and reduce the amount of cold work in the matrix. Surface passivation was marginally effective in some cases only.

The effect of surface roughness had the greatest level of influence on the resistance to metal dusting of alloy 800H. The large amount of near-surface deformation increases the diffusivity of the alloy close to the surface. This is due to the presence of dislocations in this area. While this will increase the rate of carbon diffusion into the alloy, a more significant effect is that the rate of chromium diffusion to the surface is also increased. This improves the stability of the surface chromia layer and its ability to repair defects such as cracks. If an effective barrier to carbon diffusion is formed, the effect of higher diffusivity of carbon caused by a rough surface is cancelled out.

Heat treatment of the alloys also has an effect on an alloy's ability to maintain a stable oxide layer at the surface. The as received samples have relatively small grains and a high density of dislocations and vacancies in the matrix due to cold work. The heat treatment given the annealed specimens has enlarged the grain size and reduced the amount of dislocations and vacancies in the matrix.

In the case of the as received specimens the smaller grains and hence the higher density of grain boundaries - which act as fast diffusion paths for carbon and chromium - will reduce metal dusting. It seems reasonable that the effect of increasing the surface roughness will be greater than that of decreasing the grain size. The average diameter of the grains is reduced only by a factor of about two after annealing at 1200 °C for five hours. This will approximately double the density of grain boundaries near the surface. Abrading the surface with 80-grit SiC paper

introduces a far higher amount of near-surface dislocations than there are at the surface of the polished specimens.

The higher amount of cold work in the matrices of the as received specimens is confirmed by the significantly higher bulk Vickers hardness values in these samples than in the annealed specimens (see
Table 4-3). The high dislocation and vacancy density associated with this cold work would again increase the rate of chromium diffusion to the surface, thus improving resistance to metal dusting.

The dislocations in the as received samples also act as nucleation sites for carbide precipitates. Thus, the greater density of dislocations in the as received samples leads to an increased rate of chromium carbide formation. The effect of this is to reduce the alloy's resistance to metal dusting, since chromium will be tied up faster in carbides than in an annealed specimen with fewer nucleation sites. Again, however, if the integrity of the chromia layer at the surface is maintained, carbon penetration will be prevented and the effect of the higher density of nucleation sites will be diminished.

It is therefore expected that specimens having small grains, more cold work and an abraded surface will be the most resistant to metal dusting. This was confirmed during the exposures when all of the as received, abraded specimens were largely free of carbon deposition after four weeks' exposure. These specimens also showed significantly lower rates of pitting and mass loss than the annealed, abraded specimens. Again, however, it should be remembered that these measures should only delay the onset of metal dusting. It is unlikely that any oxide film will be defect-free and completely impervious to carbon penetration. If carbon can enter the matrix, chromium will eventually become depleted in the alloy and the effect of increased chromium diffusion will be gradually reduced to zero.

It seems, then, that an effective approach to long term resistance to metal dusting will include more than the combination of these delaying measures. Alterations to the

process environment such as addition of $H_2S$ and steam as well as the right combination of alloys such as chromium, silicon and nickel, are essential.
A few possible approaches to alloy selection for metal dusting resistance are discussed in the next section.

## 6.3 Suggested alloy design and treatment techniques for improved metal dusting resistance

The best approach to finding a solution to the metal dusting problem will involve an alloy designed for maximum resistance to caburisation. It is likely that even the most resistant alloy will succumb to carburisation over time. It is thus important that additional measures, such as applying coatings and preparing the component with the optimum surface treatments, are carried out. A few possibilities for each of these approaches are explored here.

### 6.3.1 Alloy design for metal dusting resistance

An alloy that will be used in a high temperature carburising environment such as that found in a methane reformer must meet a number of performance requirements. These include creep and oxidation resistance, good formability and weldability and carburisation resistance. The alloy should also be as cheap as possible to produce.

The majority of the alloys used in petrochemical environments are iron-based austenitic stainless steels containing 18 % or more chromium and other alloying elements such as nickel, silicon and manganese. These alloys generally meet the above requirements, but all have proven susceptible to metal dusting.

A study of the literature pertaining to the effect of alloying elements as well as alloys that have performed well in metal dusting environments has been used to propose an

alloy design - presented in Table 6-2 - that may yield good resistance to metal dusting. The results of the exposures conducted in this project have also been taken into account.

| Element | Proposed Alloy (wt %) |
|---|---|
| Fe | 47 |
| Cr | 25 |
| Ni | 12 |
| Mn | 9 |
| Al | 4.5 |
| Si | 2 |
| N | 0.5 |

**Table 6-2 Composition of a proposed alloy for metal dusting resistance.**

This composition takes into account factors such as the optimum iron:nickel ratio of 4:1 suggested by Schnaas *et al.* [25], as well as the optimum silicon and aluminium levels for carburisation resistance determined by Steinkusch [48] and Lai [46] respectively. The alloy is austenitic which, although less resistant than a similar ferritic alloy, should have the necessary weldability and creep resistance. The manganese content should contribute to the formation of a protective oxide scale as was the case for the resistant Chromanite alloy exposed in this project. The nitrogen content of 0.5 % should provide good toughness and resistance to metal dusting through the precipitation of chromium nitrides and carbo-nitrides.

### 6.3.2 Surface preparation and heat treatments for metal dusting resistance

The results of the exposures conducted in this study concur with the literature that the matrix with the greatest intrinsic resistance to carburisation is characterised by small

grains, a large amount of cold work and near-surface deformation. Components should therefore be made from cold-rolled material where possible. This process will ensure a high dislocation density in the matrix. Components that must be cast should be given a surface treatment such as shot-peening or sandblasting in order to introduce some cold work into the surface of the material. Post-welding and -casting heat treatments should focus on obtaining the smallest grain size that is practical.

### 6.3.3 Possibilities for further testing

The good resistance of the high-nitrogen steel, Chromanite, to metal dusting suggests that further testing of this type of alloy is necessary. A model alloy such as Fe-18Cr-9Mn containing varying amounts of nitrogen up to the solubility limit of 1% should be exposed and evaluated. Also, the effect of increasing the chromium and manganese contents should be studied.

Other aspects worthy of further study are the effects of aluminising and nitriding a model alloy such as Fe-20Cr-7Ni on metal dusting resistance. Aluminising has been shown to retard carbon penetration and metal dusting through the formation of a stable aluminium-oxide layer [4][55]. Nitriding the surface of an alloy could increase carburisation resistance through the formation of a thick, protective layer of chromium nitride at the surface.

The prevention of metal dusting through surface coatings has not been considered in this thesis. Plasma-sprayed coatings such as 50Cr-50Ni offer good possibilities for the control of metal dusting. Another approach is the use of self-sealing ceramic coatings, which may be effective barriers to carbon penetration that leads to metal dusting [56]. The role of coatings to improve the resistance of components such as boiler tube sheets is important and warrants further investigation.

The effects of modifying the furnace atmosphere on the rate of metal dusting should also be investigated. Varying the water vapour content and $H_2/CO$ ratio as well as the

addition of gases such as $H_2S$ will influence the severity of metal dusting attack and are thus possibilities for further work.

# 7. Conclusions and Recommendations

Analysis of the specimens that were exposed to the carburising atmosphere leads to the following conclusions:

- the furnace that was designed and built for this project is able to produce a consistent metal dusting environment
- of the four alloys exposed in the furnace, the most susceptible alloy to metal dusting was the low-alloy CrMo steel. This is due to its inability to form a protective oxide scale, leading to even carburisation and metal loss
- of the three high-alloy steels, alloy 800H showed the highest susceptibility to metal dusting. This is largely due to its high nickel content and low iron/nickel ratio. The better performance of AISI 310 stainless steel is due to its higher chromium and silicon content and iron/nickel ratio of 2.7
- the most resistant alloy to metal dusting was the high nitrogen stainless steel - Chromanite. Its good performance can be attributed to its high manganese and sulphur contents which prevent carburisation, and its high level of nitrogen which reduces the rate of chromium depletion
- the resistance to metal dusting of the specimens was greatly improved by abrading the surface of the specimens. This works by facilitating the formation of surface oxide layers
- the effect of enlarging the specimen grain size was also beneficial in increasing metal dusting resistance, though to a lesser extent than abrading the surface.

It is expected that this initial work will be used in further studies on metal dusting of engineering alloys. For this purpose, the following recommendations regarding the modification of the metal dusting rig are made:

- modifications of the element winding configuration to produce a longer constant-temperature test section should be considered
- a facility to vary the water-vapour content of the gas mixture should be incorporated in the design.

Areas of further research into metal dusting resistance should include:

- study of the interactions of nitrogen with chromium and carbon in a carburisation environment with particular regard to the precipitation of chromium nitrides and carbo-nitrides
- fabrication and evaluation of the long term resistance of a Fe-25Cr-12Ni-9Mn-4.5Al-2Si-0.5N alloy
- evaluation of the effect of increasing the nitrogen, chromium and manganese contents in a model Fe-18Cr-9Mn alloy
- evaluation of the effect of aluminising and nitriding on metal dusting resistance of components
- evaluation of thermal-sprayed and self-sealing ceramic coatings for alloy protection.

# References

[1] Prange, F.A. (1959) Corrosion 15 (12), 619

[2] Eberle, F., Wylie, R.D. (1959) Corrosion 15, 622

[3] Hoyt, W.B., Caughey, R.H. (1959) Corrosion 15, 627

[4] Gommans, R.J., Huurdeman, T.L. (1994) Paper No. 3b presented at the AIChE Ammonia Safety Symposium, Vancouver

[5] Lai, G.Y. (1990) High Temperature Corrosion of Engineering Alloys, pp. 47-72, American Society for Metals International, USA

[6] Holland, M.L., De Bruyn, H.J. (1996) International Journal of Pressure Vessels and Piping 66, 125

[7] Hochman, R.F., Burson J.H. (1966) Proceedings of 31st Midyear Meeting of API Division of Refining, Houston, 331

[8] Richardson, J.A. (1993) Nitrogen, 205, 49

[9] Dejaeger, J., Guns, L., Korkhaus, J. (1994) Paper number 3a presented at the AIChE Ammonia Safety Symposium, Vancouver

[10] Grosch, J. (1991) In Quenching and Carburising: Proceedings of the 3rd International Seminar of the International Federation for Heat Treatment, p.227, Institute of Materials. London: The Alden Press

[11] Perkins, R.A. (1979) Proceedings of the Petten International Conference on Behaviour of High Temperature Alloys in Aggressive Environments, I. Kirman, J.B. Marriot, M. Merz, P.R. Sahm, D.P. Whittle, eds., The Metals Society, London, 617

[12] Hochman, R.F. (1976) Proceedings of Symposium on Properties of High-Temperature Alloys, Z.A. Foroulis and F.S Pettit, eds, The Electrochemical Society, Princeton, NJ, 715

[13] Nolan, P.J., Banks, P., Lister, S.K. (1980) Proceedings of the Petten International Conference on Behaviour of High-Temperature Alloys in Aggressive Environments, The Metals Society, London, 705

[14] Grabke H.J., Wolf, I. (1986) Materials Science and Engineering 87, 23

[15] Grabke, H.J., Tauber, G. (1975) Archiv Eisenhuttenwes. 46, 215

[16] Natesan, K., Kassner, T.F. (1973) Metall. Trans. 4, 2557

[17] Grabke, H.J (1995) Solid State Phenomena 41,3

[18] Baker, R.T.K., Yates, D.J.C., Dumesic, J.A. (1982) Coke Formation on Metal Surfaces, L.F. Albright and R.T.K. Baker, eds, American Chemical Society, New York, 1

[19] Nava Paz, J.C, Grabke, H.J. (1993) Oxidation of Metals 39 (5,6), 437

[20] Kock, A.J.H.M., De Bokx, P.K., Boellaard, E., Klop, W., Geus, J.W. (1985) Journal of Catalysis, 96, 468

[21] Baker, R.T.K., Barber, M.A., Feates, F.S., Harris, P.S., Waite, R.J. (1972) Journal of Catalysis, 26, 51

[22] Rostrup-Nielsen, J.R. (1984) J.R. Anderson and M. Boudart, eds, Catalysis Science and Technology, 5, 77

[23] Sacco, A., Caulmare, J.C. (1982) Coke Formation on Metal Surfaces, L.F. Albright and R.T.K. Baker, eds, American Chemical Society, New York, 177

[24] Fast, J.D. (1976) Gases in Metals, 2nd ed., vol.2, p.142. Surrey:MacMillan

[25] Schnaas, A., Grabke, H.J. (1978) Werkstoffe und Korrosion 29, 635

[26] Lefrancois, P.A., Hoyt, W.B. (1959) Corrosion 15, 627

[27] Hochman, R.F. (1972) Proceedings of 5th Int. Cong. on Metallic Corrosion, NACE, Houston, 258

[28] Hemmings, P.L., Perkins, R.A. (1977) Report FP-539, Electric Power Research Institute, California

[29] Harrison, J.M., Norton, J.F., Derricott, R.T., Marriot, J.B. (1979) Werkst. Korros. 30, 785

[30] Demel, O., Degisher, H.P. (1980) Proceedings of the Petten International Conference on Behaviour of High-Temperature Alloys in Aggressive Environments, The Metals Society, London, 649

[31] Truman, J.E. (1992) Constitution and Properties of Stainless Steels, R.W. Cahn, P. Haasen, E.J. Kramer, eds, vol. 7, pp.538,569. VCH, Germany

[32] Briant, C.L., Mulford, R.A., Hall, E.L. (1982) Corrosion 38 (9), 468

[33] Kikutchi, M., Masanori, K., Choi, S. (1991) Materials Science and Engineering 146, 131

[34] Grabke, H.J., Krajak, R., Muller-Lorenz, E.M (1993) Werkstoffe und Korrosion 44, 89

[35] Perkins, R.A., Coons, W.C., Radd, F.J. (1976) Proceedings of the 1976 Fall Meeting of the Electrochemical Society, The Electrochemical Society. Cited by Lai, G.Y. in High Temperature Corrosion of Engineering Alloys (1990) pp. 47-72, American Society for Metals International, USA

[36] Materials and Components (1995) Electric Power Research Institute Newsletter No. 118, p.1

[37] Lai, G.Y. (1985) J. Met. 37 (7), 14

[38] Hofer, J.E., Sterling, E., McCartney, J.T. (1955) Journal of Physical Chemistry 59, 1153

[39] Ratliff, T.R. (1968) Ph.D. Thesis, Georgia Institute of Technology

[40] Grabke, H.J., Krajak, R., Muller-Lorenz, E.M, Strauss, S., Werkstoffe und Korrosion, in press

[41] Grabke, H.J., Bracho-Troconis, C.B., Muller-Lorenz, E.M (1994) Werkstoffe und Korrosion 45, 215

[42] Pippel, E., Woltersdorf, J., Grabke, H.J., Strauss, S. (1995) Steel Research 66, 217

[43] Grabke, H.J., Krajak, R., Nava Paz, J.C. (1993) Corrosion Science 35 (5-8), 1141

[44] Van den Bruck, U., Schillmoller, C.M. (1985) presented at Corrosion/85, NACE, Houston

[45] Mason, J.F., Moran, J.J., Skinner, E.N. (1960) Corrosion 16, 593t

[46] Lai, G.Y. (1985) Proceedings of the TMS-AIME Symposium, M.F. Rothman, ed.,The Metallurgical Society of AIME, 551

[47] Stringer, J. (1979) Proceedings of the Petten International Conference on Behaviour of High-Temperature Alloys in Aggressive Environments, I. Kirman, J.B. Marriot, M. Merz, P.R. Sahm, D.P. Whittle, eds., The Metals Society, London, 739

[48] Steinkusch, W. (1980) Behaviour of High-Temperature Alloys in Aggressive Environments, The Metals Society, London, 83

[49] Steinkusch, W (1977) Werkstoffe und Korrosion 28, 1

[50] Dawes, C., Trauter, D.F. (1974) Metals Tech. 1, 397

[51] Goldstein, J.T., Moren, A.E. (1978) Met. Trans. 9A (11), 1515

[52] Steel, C., Engel, W. (1981) AFS Int. Cast Metals Journal, 28

[53] Mills, K. ed. (1973) ASM Metals Handbook, vol. 9, 9th Edition, ASM, Ohio

[54] Guidelines for Methods of Testing and Research in High Temperature Corrosion - a Working Party Report, H.J. Grabke, D.B. Meadowcroft, eds, European Federation of Corrosion No. 14, Institute of Materials, 1995.

[55] McGill, W.A., Weinbaum, M.J. (1979) Metal Progress, 115, 26

[56] Perugini, G (1983) Thin Solid Films, 108, 415